Title	Formulation for Shear Force-Relative Displacement Relationship of L-shape Shear Connector in Steel-Concrete Composite Structures
Author(s)	ROS, Soty
Citation	高知工科大学，博士論文.
Date of issue	2011-09
URL	http://hdl.handle.net/10173/779
Rights	
Text version	author

Formulation for Shear Force-Relative Displacement Relationship of L-shape Shear Connector in Steel-Concrete Composite Structures

ROS Soty

A dissertation submitted to
Kochi University of Technology
in partial fulfillment of the requirements for the degree of

Doctor of Engineering

Department of Infrastructure Systems Engineering
Graduate School of Engineering
Kochi University of Technology
Kochi, Japan

August 2011

ACKNOLEDGEMENTS

I would like to express my deepest gratitude with full respect to my supervisor, Professor Doctor Hiroshi Shima for his endorsement giving me numerous of creative suggestions and guidance on my research work. I am greatly indebted to him that cannot be described in words for his enduring patience and continuous encouragement throughout my study. Without him this research work would have not yet been achieved.

My grateful thanks also go to all members of my thesis supervising committee, Prof. Nobumitsu Fujisawa, Prof. Yoshiro Kai, Prof. Masataka Takagi, and Assoc. Prof. Masahiro Ouchi for their valuable comments on my thesis. By means of their comments the scope of my work has been enhanced.

My gratitude goes to Mr. Hideo Miyazi for his helpful technical instructions during my experimental work. My gratitude also extends the members of concrete laboratory of Infrastructure Systems Engineering Department for their helpful assistances during the experimental work.

Special thanks are due to all members of IRC, International Relationship Center for their helpful support for all administration works during my study. With their helps I feel like home living and working here.

Finally, I would like to dedicate this thesis to my wife, NUON Puthearene for her full support and encouragement for every day life, and to my first son, ROS Sotypiseth born on 3rd August, 2011. The dedications also go to my family for their guidance and supports through all difficult times.

ABSTRACT

Partial interaction between steel and concrete has become a challenge in more rational design and more economical construction of steel-concrete composite structures. According to the design specifications for hybrid structures of JSCE 2009, the formulation of shear force and slip relationship of headed stud, plate shape, and block dowel shear connectors have already been proposed. However, that of L-shape shear connector has not yet been identified. Therefore, this study was conducted to formulate the relationship between shear force and relative displacement relationship of L-shape shear connector in steel-concrete composite structures.

The investigation has been made through the experiments and compared with the FEM analyses. Beam type specimens in which the shear connectors were installed to be subjected to strut compressive force were constructed and tested. Concrete strength, size of shear connector, and strut angle are the main parameters which were typically selected by means FEM analyses conducted during the experimental planning.

Consequently, different failure modes of L-shape shear connectors, split failure, shear failure/concrete crush were identified. The possibility of split failure mode and shear failure/concrete crush mode were found to be controlled by the strut angle and the thickness to height ratio of the shear connector. Moreover, there exists a critical strut angle separating the two different failure modes. Accordingly, an equation to predict the critical strut angle was developed and it was a function of thickness to height ratio of the shear connector.

Furthermore, the ultimate shear force of L-shape shear connector calculated by means of the design specifications for hybrid structures of JSCE 2009 was found to be too conservative when the strut angles were small. Accordingly, the formulas to predict the ultimate shear capacity of L-shape shear connector at split failure and at shear failure/concrete crush were developed and proposed. The equations were found to be functions of thickness to height ratio of the shear connector, the height and with width of the shear connector, the concrete strength, and the strut angle. The applicable ranges of the formulas were proposed for the strut angle between 20 to 45 degrees.

More importantly, the relationships between shear force and relative displacement of L-shape shear connector can be represented by a unique enveloped curve by normalizing shear force by the ultimate shear force and the relative displacement by the height of the shear connector. The

unique enveloped curve was observed regardless of concrete strengths, sizes of shear connectors and strut angles. Hence, a unique formula to predict the shear force-relative displacement relationship of L-shape shear connector subjected to strut compressive force was developed and proposed. Meanwhile, the ultimate relative displacements of L-shape shear connectors were found approximately 0.02 times the height of the shear connector.

TABLE OF CONTENTS

LIST OF TABLES

LIST OF FIGURES

CHAPTER I

INTRODUCTION

I.1Background

Steel-concrete composite structure has been popular in advance concrete construction technology in these recent years. This kind of structure has been widely used instead of the conventional reinforced concrete structure in many purposes including buildings, bridges, retaining walls, as well as underground structures. It has been becoming under high demand for civil engineer societies due to its high durability and constructability.

One of the most important components in steel-concrete composite structure is the shear connector. It has been known to be a structure component used to mechanically connect steel with concrete and it plays a vital role in the composite structure. It prevents the separation at steel-concrete interface and transfers shear force, delamination force, and bearing force from steel to concrete and vice versa [1]. The monolithic behavior of steel-concrete composite structure is highly influenced by the performance of the shear connector. Accordingly, several researches have been conducted to examine the mechanical properties of the shear connector to fulfill the needs of civil engineers in the designing work. Most recently, in 2006, Japanese Society of Civil Engineers has developed a guideline for performance verification of steel-concrete composite structures in which the equations to design the shear capacity of the shear connectors were introduced.

However, the focuses of civil engineers' point of view are not only the stability and the constructability, but also the economy and the rationality. Therefore, many researchers have been trying to develop a design method which meets the present demands. Similarly, this research was conducted to propose a rational design model for L-shape shear connector which is recently used in the steel-concrete composite structures. Not only the shear resisting capacity of the shear connector itself, but also its partial interaction mechanisms represented by shear force-slip relationships are included in this study. The propose equations were developed by means of experimentations and FEM analyses. Moreover, the applicable ranges of the proposed equations were also introduced.

Prior to the experimental program, the properties of steel-concrete composite structures and the existing shear connectors used in practices are briefly described in the following subchapters.

I.2 Steel-Concrete Composite Structures

Steel-concrete composite structure is a structural member, which is composed of steel and concrete behaving as a monolithic member. The components of the structure generally consist of steel, concrete, stiffener, shear connector, shear reinforcing steel plate and diaphragm. The definitions and the functions of these components in the structure are available in the Guidelines for Performance Verification for Hybrid Structures of JSCE 2006 [1]. According to the guidelines, the performance of the structure is highly influenced by the presence of these components. For instant, it has been confirmed that the monolithic behavior of steel-concrete composite structure is highly influenced by the performance of the shear connector.

Fig.I.1 illustrates a typical steel-concrete sandwich slab given by JSCE 2006 [1]. The core concrete was sandwiched by the steel skin plate, while the steel and concrete were connected each other by shear connectors. Steel-concrete composite members could be used as slab, beam, and column. Meanwhile, the typical sections of composite columns are given in **Fig.I.2**.

The design shear capacity of steel-concrete composite beam, slap, column, and shear connectors are available in the Design Specifications for Steel-Concrete Composite Structure of JSCE 2009[2] as well as in the Design Code for Steel-Concrete Sandwich Structures, JSCE 1992[3].

In the design of steel-concrete composite structures, the mechanical properties of the shear connectors are always concerned. The following subchapter presents the details of the shear connectors most recently used in practice.

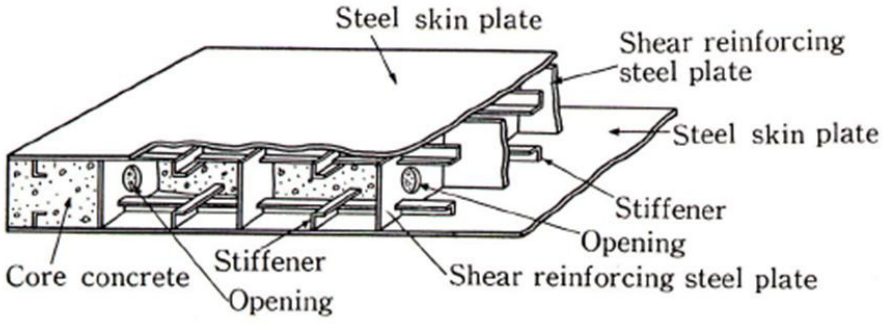

Figure I.1 Steel-concrete sandwich slab (JSCE 2006 [1])

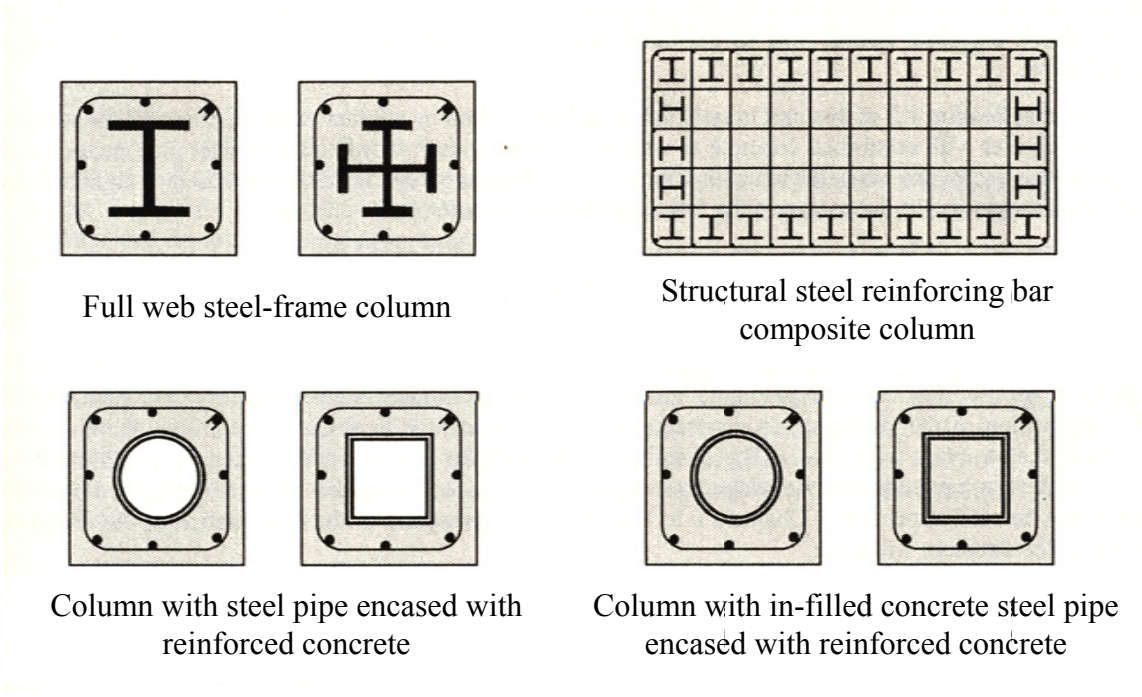

Figure I.2 Various sectional types of composite column (JSCE 2006 [1])

I.3 Shear Connectors

There are several types of shear connector used in the composite structures such as headed stud shear connector, plate shape shear connector, block dowel shear connector, channel shear connector, and L-shape shear connector. The illustrations of these shear connectors are given in **Fig.I.3**.

Headed stud shear connector is widely used to connector the shape steel (I-shape or H-shape steel) with the concrete slab forming the composite beam. It has been also used to connect steel plate and concrete for road bridges. Moreover, in bridge structures, if the space between the main girders is large, the shear connectors located at the slab-girder connector are subjected to pull-out force due to the rotational deformation of the floor slab. Meanwhile, the level of pull-out force depends on the locations and the weight of the wheels. According to Sakai et al [4][5], the shear capacity of the head stud shear connector decreased approximately 25% with the presence of pull-out out force. Furthermore, with the presence of repeated loads of the vehicle wheels, shear connectors will be also subjected to fatigue loads and it is ineligible in the design for road bridge structures.

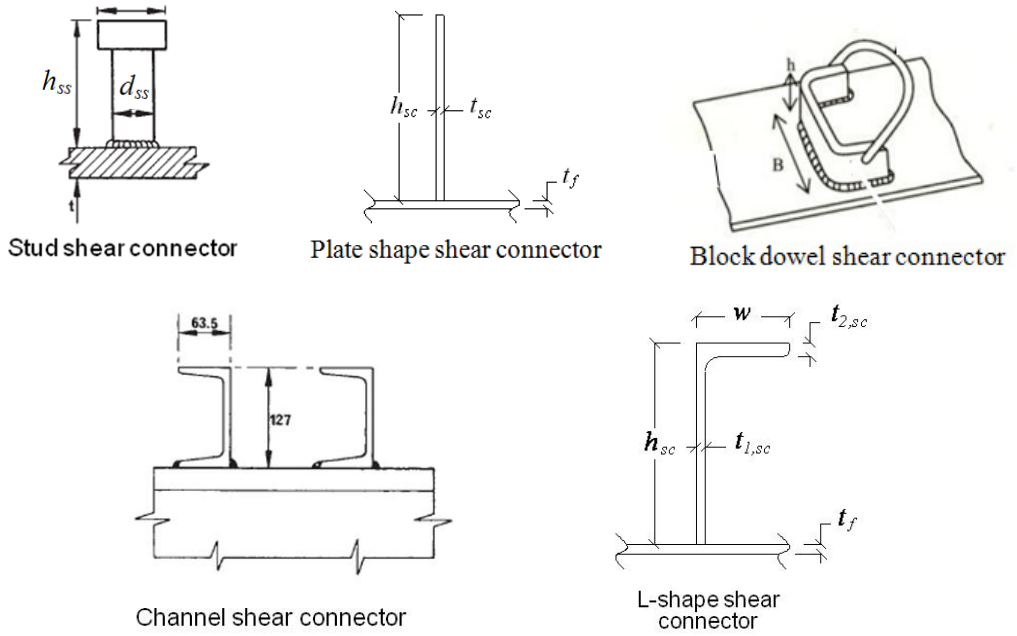

Figure I.3 Various types of shear connector

Additionally, other types of shear connector including plate shape shear connector, L-shape shear connector, and channel shear connector are usually used in the steel-concrete sandwich slab for tunneling constructions, floor slab for bridge constructions, dam wall constructions, and so on. They became popular due to their high strength durability and easy-installing process. The shear connectors are used not only to transfer shear in steel-concrete interface, but also to prevent the buckling of the steel skin plate during service life. On the other hand, the block dowel shear connector is usually used in railway bridges.

According to the design code of steel-concrete sandwich structure of JSCE 1992 [3], in order to assure the full interaction between steel and concrete, the numbers of shear connector used can be determined by dividing the total shear force by the individual shear capacity of the shear connector as given in Eq.I.1.

$$\gamma_i \frac{H_d}{\sum_{i=1}^{N_{sc}} V_{scdi}} \leq 1.0 \qquad \text{Eq. I. 1}$$

Where:

H_d : design value for shear force per unit width transferred between skin plate and core concrete at portion $L = t_f \sigma_f$;

γ_i : structure factor;

V_{scdi} : design value for shear transfer capacity of individual shear connector per unit width;

N_{sc} : total number of shear connectors per unit width at portion L;

L : portion between maximum flexural moment and zero flexural moment section;

t_f : thickness of steel skin plate at maximum flexural moment;

σ_f : tensile stress in steel skin plate at maximum flexural moment section $\left(= f_{yd}(M_d/M_{ud})\right)$;

M_d : Design value for flexural moment at maximum flexural moment section;

M_{ud} : Design value for flexural capacity of maximum flexural moment section.

I.4 Statement of Problems

Usually, in design of steel-concrete composite structures, plane remain plane assumption has been applied for conservative purpose. However, partial interaction between steel and concrete has been becoming highly demanded due to more rational and more economical respectively in the design and in the construction. The partial interaction mechanisms of the shear connector are explained by the relationships between shear force and slip. Consequently, several types of test methods for shear connectors were developed and the existing research results are summarized in the following subchapter. It has been observed that the formulas for shear force-slip relationship of some types of shear connectors namely Plate shape, Headed Stud, and Block Dowel shear connectors have been formulated and proposed. However, the study of L-shape shear connector is quite limited and the formula to predict its shear force-slip displacement relationship has not yet been identified.

I.5 Purpose of Research

This study was conducted to examine the partial interaction mechanisms of L-shape shear connector in steel-concrete composite structure by taking into account the effects of concrete strength, size of shear connector, and direction of the applied shear force. Again, the purpose of this study is to "***Formulate the relationship between shear force and slip of L-shape shear connector subjected to strut compressive force in steel-concrete composite structures***".

At the same time, the *ultimate shear capacity* and the *ultimate slip* of the shear connector are also required to fully understand the partial interaction mechanisms of the shear connector.

I.6 Research Design

In this study, L-shape shear connectors were examined by means of experimentation and FEM Analysis. A new beam type test method was developed and used for the experiment. Two series of beam type specimens were constructed and tested. The 1st test series consists of four specimens in which the shear connectors were designed to be subjected to strut compressive force with 45 degrees of strut direction. Concrete strength and size of shear connector are the main focus parameters. The equations to predict the shear force-relative displacement relationship and the ultimate shear force of the shear connector were formulated for the case that the strut angle is equal to 45 degrees. Subsequently, the 2nd test series specimens were tested to confirm the applicable ranges of the proposed equations found from the 1st test series. The selection of the main parameters was made with the help from the FEM analysis during the experimental planning which are the strut angle and the size of the shear connector. The results calculated by means of the proposed equations were compared with those of the 2nd test series specimens.

There are five chapters in this thesis which orderly introduced as followings:

Chapter I: This chapter introduces the steel-concrete composite structure and its components especially the shear connector. The usage and importance of the shear connector in the structure were explained. The purpose of research and the research design were described in this chapter.

Chapter II: This chapter describes the literature reviews which are related to the purpose this research. In this chapter, the existing test methods including push-out test method, direct pull-out test method, and steel-concrete sandwich beam test methods were described and their limitations were introduced. Moreover, the existing research results of shear force-slip relationship of the Headed stud, and Block dowel shear connector were also summarized and discussed. Accordingly, the absence and the importance of the study on L-shape shear connector were introduced.

Chapter III: This chapter describes in details about the experiments. Properties of steel, concrete, and shear connector were introduced. The originality and the details of beam type specimens are illustrated while the measurement and the equipment installations were also illustrated.

Chapter IV: This chapter shows, analyzes, and discusses all experimental results of both 1st and 2nd test series specimens. In this chapter, the shear resisting mechanisms of L-shape shear connector were identified. The formula for shear force-relative displacement relationship of L-

CHAPTER II

LITERATURE REVIEWS

II.1General

Partial interaction mechanisms of shear connector have been becoming high demand due to more rational in the design and more economical in the construction. That was the reason why several test methods for examining both the shear capacity and the partial interaction mechanisms of the shear connectors have been developed. Consequently, the mechanical properties of the shear connectors including shear resisting capacity and shear force-slip relationship have been identified. The following subchapters described the existing test methods as well as the existing research results of different types of shear connectors.

II.2 Existing Test Methods for Shear Connectors

II.2.1 Push-out Test Method

Push-out test is a popular test method to study the performances of shear connectors. The illustration of this test method is given in **Fig.II.1(a)**. The shear connectors are perpendicularly welded with the H-shape steel and connect the concrete with the steel as shown in the figure. When the load is applied by the hydraulic jack, the relative displacement between the steel and concrete can be measured by the displacement transducer, while the load magnitudes are detected by the load cell. More details illustration and explanation of this test method are available in the Euro-code II. This test method is applicable to study the partial interaction mechanisms of the shear connectors which are expressed by the shear force and slip relationships.

For instant, in 1986, Kiyomiya et al. [6] studied the behavior the shape steel shear connector by means of push-out test method and found that the relative slip between the steel and the concrete appeared even under load level. Meanwhile, the cracking loads were found approximately half of the maximum applied load. The failure mode of the specimens was shown in **Fig.II.1(b)**. Tensile fracture of shear connector, concrete crush, and shear failure of concrete were observed in their study. Consequently an equation to predict the load-carrying capacity of the angle, T-shape steel,

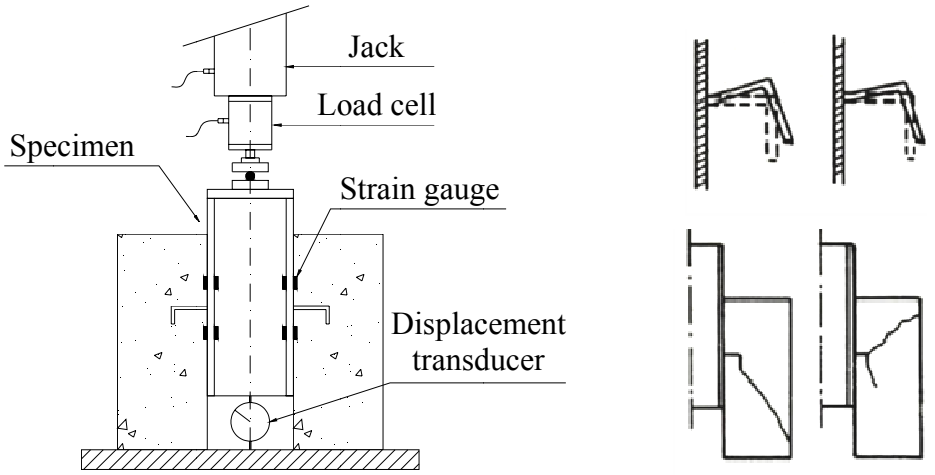

(a) Test Set-up (b) Failure mode, Kiyomiya et al. (1986)

Figure II.1 Push-out Test

and channel shear connector was developed by selecting the lower limit of the maximum shear force obtained from experimental results. Their equation is expressed as followings:

$$P = 75 \times \sqrt{t} \times w \times \sqrt{f_c'} \qquad \text{Eq.II.1}$$

Where:

t : Thickness of the shear connector (inches)

w : Length of channel (inches)

f_c' : Concrete compressive strength (psi)

Moreover, in 1993 Kimura et al. [7] presented the effects of test method on the ultimate strength of shape steel shear connector by means of the modified push-out test method. The core concrete was sandwiched by the two steel plates. The load was applied by pulling and pushing as shown in the figure. As a result, the shear capacity of the shear connector was found relatively low as compared to the results found by Kiyomiya et al. [6] due to large deformation of the steel plate found in the modified test method.

II.2.2 Direct Pull-out Test Method

The illustrations of direct pull-out test method are given in both **Fig.II.2(a)**, a single shear connector test and **Fig.II.3(a)**, a multiple shear connectors test. As shown in the figures, the concrete specimens are connected with the skin plate by the shear connectors. During the test, the pulling load was applied and the reacting load accordingly reacted. This test method is also applicable for examining the shear force and slip relationship of the shear connector that slip can be easily obtained from the relative displacement between the steel and the concrete.

In 1989, Ueda and Chin [8] used this test method to examine the shear resisting capacity of a single plate shape shear connector as illustrated in **Fig.II.2(a)**. The specimens were found to failed by the occurrence of crack in the concrete from the head of the shear connector as shown in **Fig.II.2(b)**. Also, punching shear was also found at failure of the shear connector. Consequently, a formula for predicting the shear capacity of the plate shape shear connector was developed by assuming that the punching shear strength of the concrete in front of the shear connector is equal to the bearing strength of the concrete block on which the load was applied through the steel plate. Meanwhile, the bearing strength of the concrete affected by thickness to height ratio of the shear connector and the ratio between the shear connector's thickness to that of the steel plate. However, the effect of shear connector spacing was not included.

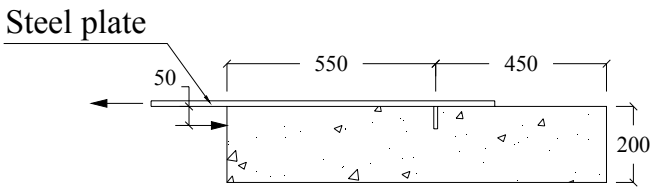

(a) Test Set-up

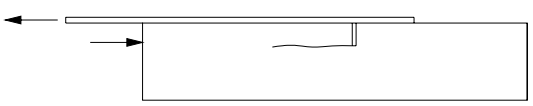

(b) Failure mode

Figure II.2 Direct Pull-out Test, Ueda and Chin (1989)

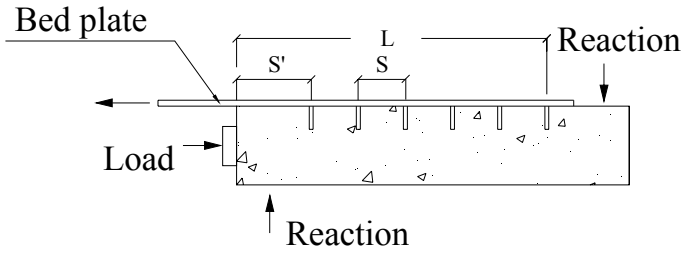

(a) Test Set-up

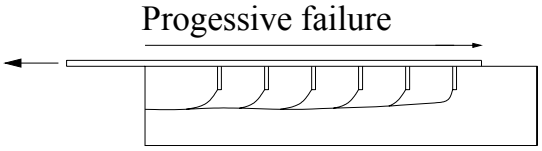

(b) Failure mode

Figure II.3 Direct Pull-out Test, Chuah et al. (1991)

Two years later, in 1991, Chuah et al. [9] examining the load-slip relationship of the plate shape shear connector by the direct pull-out test method with multiple shear connectors as illustrated in **Fig.II.3(a)**. Consequently progressive failure was observed which cracks appeared from the heads of the shear connectors and continuously propagated as shown in **Fig.II.3(b)**. Moreover, they found that the shear resisting capacity of the shear connector gradually reduced after the occurrence of crack in the concrete from the head of the shear connector. By means of their experimental results, the effect of shear connector spacing on the shear capacity of the shear connector was identified.

As a results, by combining the research results of both Ueda and Chin (1992) [10] and Chuah et al. (1991) [9], the formula to predict the shear capacity of plate shape shear connector was available in the Design Code of Steel-Concrete Sandwich Structure of JSCE in 1992 [3] and also in the Guidelines for performances verifications of steel-concrete hybrid structures in 2006 [1] and lately in the Design specifications for hybrid structures in 2009 [2]. The equation was also proposed to be applicable for the angle shape shear connector with the configurations illustrated in **Fig.II.4**.

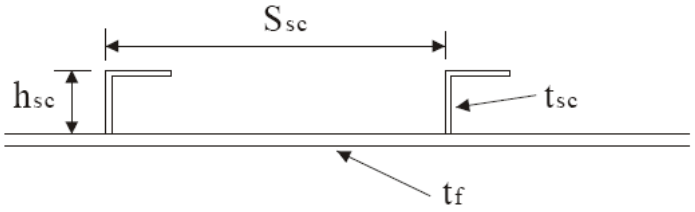

Figure II.4 Shape steel shear connector

The equation is expressed as followings:

$$V_{scd1} = \left(0.56 h_{sc} w_{sc} (f'_{cd})^{1/2} k_1 k_2 k_3\right) \quad \text{Eq.II.2}$$

But not greater than the tensile yield strength of the shear connector V_{scd2}.

$$V_{scd2} = 0.1 t_{sco} w_{sc} \left(f_{scyd}/\sqrt{3}\right)/\gamma_{b2} \quad \text{Eq.II.3}$$

Where:

$k_1 = 2.2(t_{sc}/h_{sc})^{2/3} \leq 1$

$k_2 = 0.4\left(t_f/t_{sc}\right)^{1/2} + 0.43 \leq 1$

$k_2 = ((S_{sc}/h_{sc})/10)^{1/2} \leq 1$

f'_{cd} : design value for compressive strength of concrete (N/mm^2);

h_{sc} : height of shear connector (cm);

w_{sc} : width in the direction normal to shear force of shear connector (cm);

t_{sco} : a lesser of thickness of shear connector considering welded part and thickness of shear connector itself (cm);

f_{scyd} : design value for tensile yield strength of shear connector (N/mm2);

t_{sc} : thickness of shear connector (cm);

S_{sc} : spacing in the direction of shear force of shear connectors (cm);

γ_{b1} : member factor which may be 1.3 generally;

γ_{b2} : member factor which may be 1.15 generally;

γ_c : material factor for calculation of f_c' which maybe 1.3 general;

γ_s : material factor for calculation of f_{scyd} which maybe 1.05 generally;

II.2.3 Steel-Concrete Sandwich Beam Test Method

Steel-concrete sandwich beam test has also been used to study the mechanical properties of the shear connector. The layout of steel-concrete sandwich beam is given in **Fig.II.5**. The concrete core is sandwiched by the steel skin plates, while the steel and the concrete were connected by the shear connector.

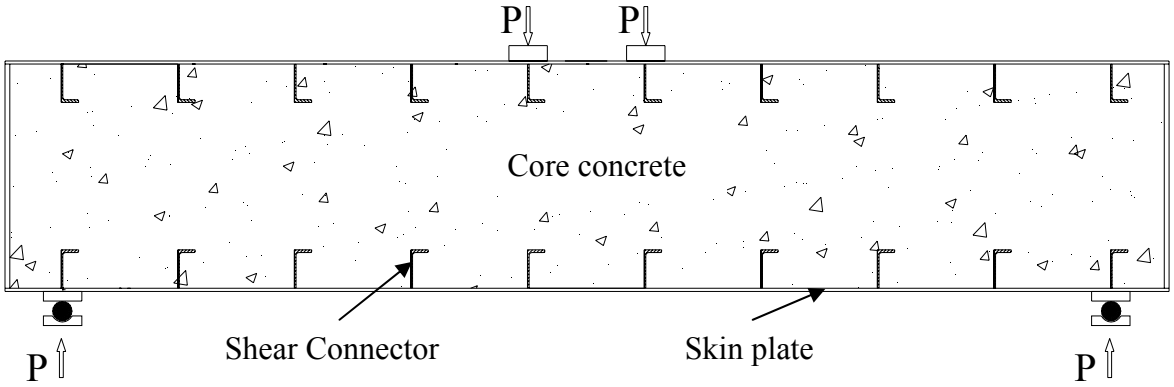

Figure II.5 Layout of steel-concrete sandwich beam test

In 1992, Makabe et al. [11] studied the mechanical properties of steel and concrete sandwich beam in which L-shape shear connectors were used. The behaviors of the L-shape shear connector in steel-concrete sandwich beam were also identified. By examining the strain distributions on the vertical part of the shear connector, the curvature was observed. Meanwhile, the head of the shear connector was found to have forward movement (opposite to the direction of shear force) under low load levels (0 – 100 kN) and have backward movement (the same the direction of shear force) under higher load levels (greater than 100 kN).

The same test method was used by Saidi et al. [12][13][14] to study the transferred shear force and relative displacement relationship of the shear connector including L-shape, T-shape and I-shape shear connector. A formula to predict the transferred shear force at a sudden decrease of the equivalent stiffness of the shear connector (Q_c) was proposed as expressed in Eq.II.4.

$$Q_c = (0.000216F'_{com} + 0.00542)f_c'^{0.5}\frac{b_{sc}t_c t_{sc}}{h_{sc}^{0.8}} \quad \text{Eq. II. 4}$$

Where:

F'_{com} : compressive force on the shear connector (kN);

f'_c : compressive strength of concrete (N/mm^2);

h_{sc} : height of shear connector (mm);

b_{sc} : width in the direction normal to shear force of shear connector (mm);

t_c : effective thickness of concrete surrounding the shear connector (mm);

t_{sc} : thickness of shear connector (mm);

Moreover, Saidi et al. [14] also proposed an equation, Eq.II.4 to predict the transferred shear force-relative displacement relationship in which the stiffness of the shear connector (*EI*), the slope (θ_o) and the modulus of the assumed foundation (*k*) were considered.

II.2.4 Limitations of Existing Test Method

a) Limitations of Push-out Test Method

The limitations can be derived from the configurations of the both push-out test method and the experimental results found in previous studies. Three considerable limitations were observed as followings:

(1) The thickness of the H-shape steel is too thick which may affect on both behaviors of the shear connectors as well as their shear resisting capacity. It has been clarified by Kimura et al. [7] that the shear capacity of the shear connectors reduces with the deformation of the attached steel plates.

(2) The direction of stress upon the shear connectors are only perpendicular ($\theta = 0^o$) which is different from the real structure that the stress direction changes according to the location of the applied load; for instant, the locations of the vehicles on the bridge deck.

(3) The ultimate state of the shear connectors cannot be observed. Based on previous studied, the shear resisting capacity of the shear connector can be obtained only until crack in the

concrete reached surface of the specimen [9] & [10]. It means that both the ultimate shear capacity and the ultimate slip of the shear connector cannot be identified.

b) Limitations of Direct Pull-out Test Method

Three limitations were also observed in this test method:

(1) The first limitation is similar to that of the Push-out test method that the directions of stress upon the shear connectors are only perpendicular ($\theta = 0^o$).

(2) Progressive failure would occur in case of multiple shear connectors are tested and the shear resisting ability of the shear connector gradually reduces after the occurrence of first crack from the head of the shear connector [9]. It means that the ultimate state of the shear connectors cannot be obtained.

c) Limitations of Steel-Concrete Sandwich Beam Test Method

Steel-concrete sandwich beam test method was also found to have some limitations that cannot be avoided.

(1) Steel-concrete sandwich beam was found to fail before the shear connector that the ultimate shear capacity and the ultimate slip of the shear connector cannot be obtained [12][13][14].

(2) The specimen will be too large in case of large size shear connector need to be tested. It would mean that this kind of test method seems to be inapplicable for large size shear connector. Additionally, the maximum size of L-shape shear connector used to be investigated by this test method was L140×40×5mm [14].

II.3 Existing Formulas of Shear Force-Slip Relationship of Shear Connectors

II.3.1 Headed Stud Shear Connector

The equation of shear force-slip relationship of headed stud shear connector with diameter of 19 mm and 9.5 mm were previously proposed by Ollgaard et al [15] and Chuah et al [9], respectively. Moreover, the most recent formula of shear force-slip relationship of headed stud shear connector was given by Shima and Watanabe in 2009 [16] and again was recommended by JSCE 2009 [2]. **Fig.II.6** gives the shear force-slip relationship of headed stud shear connector.

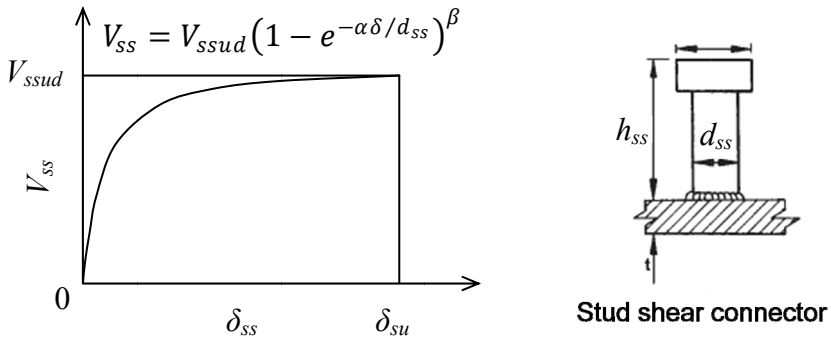

Figure II.6 Shear force-slip relationship of headed stud shear connector

It was confirmed that the relationship between shear force and slip of headed stud shear connector can be represented by the normalized curve in which the shear force was normalized by the ultimate shear capacity of the shear connector and the slip was normalized by the diameter of the stud. The equation was expressed as followings:

$$V_{ss} = V_{ssud}\left(1 - e^{-\alpha\delta/d_{ss}}\right)^{\beta} \quad \text{Eq. II. 5}$$

$$\alpha = 11.5\{1.1(\gamma - 1)^2 + 1\} f_c'/f_{co}' \quad \text{Eq. II. 6}$$

And V_{ssud} is the ultimate shear capacity of the headed stud shear connector which is the lower value between Eq.II.7 and Eq.II.8.

$$V_u = 31A_{ss}\sqrt{\frac{h_{ss}}{d_{ss}}f_c'} + 1000 \quad \text{Eq. II. 7}$$

$$V_u = 31A_{ss}f_{ss} \quad \text{Eq. II. 8}$$

Where:

A_{ss} : cross sectional area of stud (mm^2);

f_c' : compressive strength of concrete (N/mm^2);

f_y : tensile strength of stud (N/mm^2);

h_{ss} : height of stud (mm);

d_{ss} : diameter of stud (mm);

α & β: constant.

Additionally, the ultimate slip of the headed stud was found to vary from 0.3 to 0.4 times the diameter of the stud [16].

II.3.3 Block Dowel Shear Connector

The equation for shear force-slip relationship of block dowel shear connector was also recently proposed by JSCE 2009 [2], **Fig.II.7** whose equation is expressed in Eq.II.9. The equation is expressed as followings:

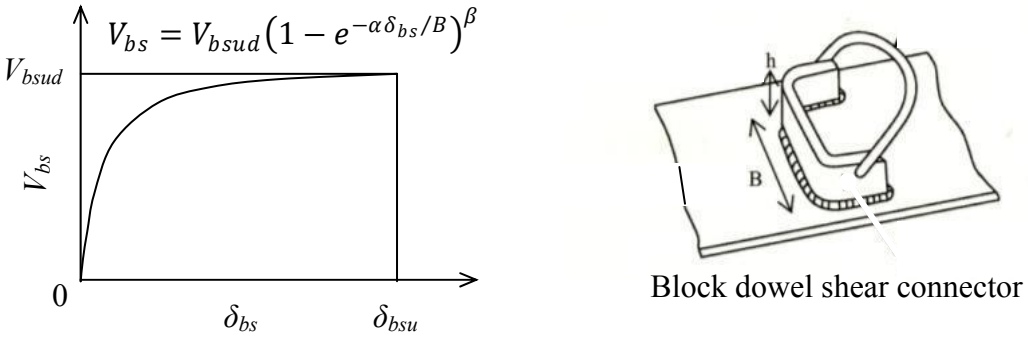

Figure II.7 Shear force-slip relationship of block dowel shear connector

$$V_{bs} = V_{bsud}\left(1 - e^{-\alpha\delta_{bs}/B}\right)^{\beta} \qquad \text{Eq. II. 9}$$

Where:

V_{bsud} : design shear strength of the shear connector (N), JSCE 2009 [2];

f_c' : compressive strength of concrete (N/mm^2);

δ_{bsu} : ultimate slip (mm);

δ_{bs} : slip (mm); and

α & β: constant.

As described above, the both shear resisting capacity and shear force-slip relationship of headed stud, plate shape, and block dowel shear connectors have already been identified. However, those of L-shape shear connector have not yet been confirmed. Therefore, this study was conducted to formulate both shear capacity and shear force-relative displacement relationship of L-shape shear connector subjected to strut compressive force in steel-concrete composite structures.

In terms of the existing test methods for the study of performance of shear connector, there are three main limitations including the ultimate state of the shear connector, stress distributions, and the large size L-shape shear connector. Fortunately, these limitations can be fulfilled by a new test method namely Beam Type Test Method which was recently initiated and used for the studying on the mechanical properties of L-shape shear connector subjected to strut compressive force [17][18][19][20][21][22][23][24]. The detail of this test method is described in the following chapter, Chapter III Experiment.

CHAPTER III

EXPERIMENT

III.1General

It is important that the performance of the shear connectors obtained from tested specimens are most similar to those in the real structures. It means that test method plays a vital role in the reliability and the applicability of the test results. In the real structures, shear connectors may resist against various directions of stresses depending on the locations of the applied loads. Therefore, the study of effects of stress directions on the performance of the shear connector is necessary. Unfortunately, according to the discussions over the limitations of previous studies in chapter II, large size L-shape shear connector and different stress directions on shear connector cannot be examined by the existing test methods. In order to fulfill these limitations, a new beam type test method has been initiated, constructed and tested. Advantageously, this test method was found to be applicable for the investigation of the effects of strut angle on the performances of large size L-shape shear connector subjected to strut compressive force in steel-concrete composite structures. This chapter describes every detail of the test method and the specimens used in this study.

III.2 Beam Type Test Method

III.2.1 Originality of Beam Type Specimens

Beam type specimens were constructed to replicate a part of a possible steel-concrete composite structures as illustrated in **Fig.III.1**. L-shape shear connectors with different directions to shear force were welded perpendicularly to the steel skin plate to resist against strut compressive force with strut direction θ. Meanwhile, there was only one shear connector in the shear span a. The values of strut angle could be adjusted by varying the values of the shear span a. Moreover, by considering the possible surrounding concrete around the shear connector in the real structure, the height of the specimen h was selected to be three times the height of the shear connector h_{sc}. In this test method, both shear connectors were located at the direct supports so that the strut and tied mechanism was carried by the shear connectors and the skin plate, respectively.

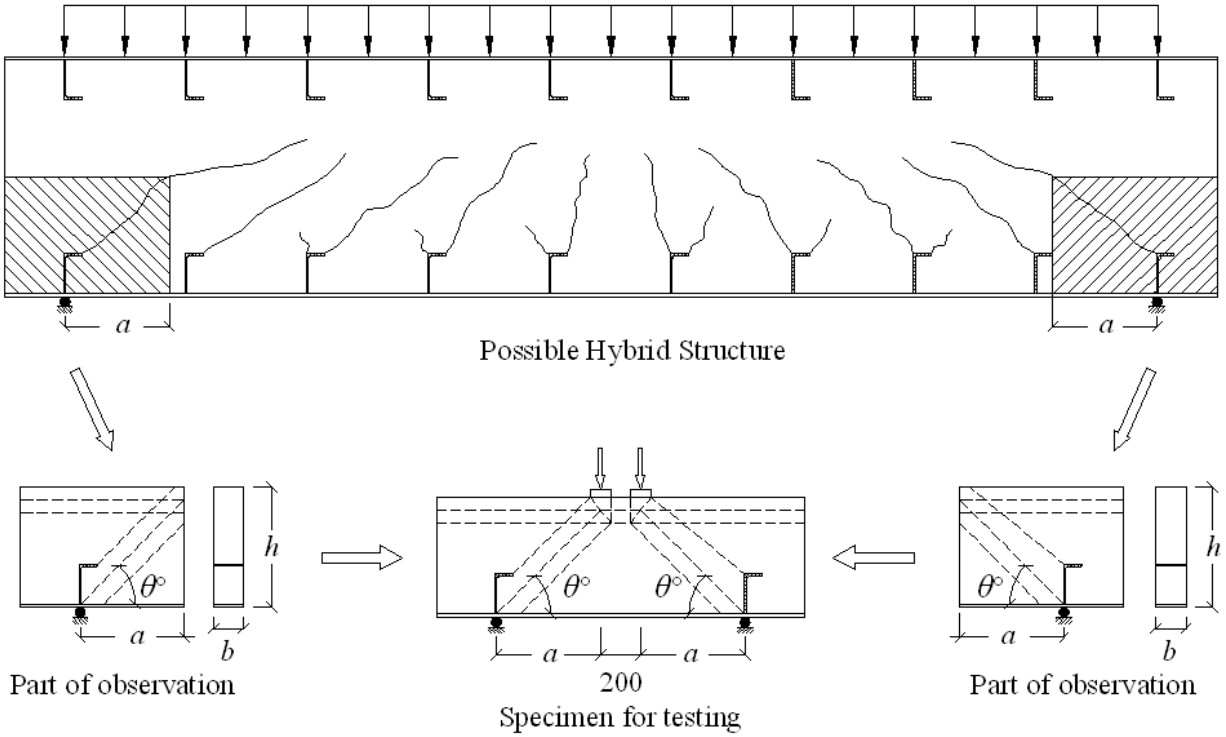

Figure III.1 Development of beam type specimen

More importantly, the other necessary parameters such as concrete strength f_c', size and mechanical properties of both shear connector and steel skin plate are carefully selected and pre-analyzed to assure that the shear connector fail before yielding of the steel skin plate.

III.2.2 Specimens

The beam type specimens were symbolized as S-height of specimen-height of shear connector-thickness of shear connector-concrete strength-strut angle (S-h-h_{sc}-t_{sc}-f_c'-θ). Two series of beam type specimens, 1st and 2nd test series specimens were constructed as listed in **Table III.1**. All specimens have the same width (b = 150mm) and different shear span depending on the wanted strut angle.

The 1st test series consist of four specimens designed to study the mechanical behaviors of the shear connector by taking the effects of the concrete strength and the size of the shear connector into account. S-600-200-9-25.3-45 and S-600-200-9-38-45 whose strut angle and size of shear connector are the same were constructed to study the effects of concrete strength. Meanwhile, the effects of the size of the shear connector were investigated on S-600-200-9-25.3-45, S-450-150-9-23.6, and S-300-100-9-25.1-45 whose concrete strength and strut angle are the same.

Moreover, the 2nd test series consisting of six specimens were specially designed after the analyses of the 1st test series' results and FEM analyses results. These specimens were constructed to study mainly the effect of strut angle and size of shear connector on the performances of the shear connectors. S-600-200-9-43-35 & S-600-200-9-43-30, S-450-150-9-43-30 & S-450-150-9-43-25, and S-300-100-9-41.5-25 & S-300-100-9-42.7-20 were constructed to examine the effects of strut angle when the thickness to height ratio of the shear connector $t_{1,sc}/h_{sc} = 0.045$, $t_{1,sc}/h_{sc} = 0.06$, and $t_{1,sc}/h_{sc} = 0.09$, respectively. **Fig.III.2** shows the detail of the specimens and the shear connectors. Additionally, a flexural crack initiator was inserted at mid span of the 2nd test series specimens in order to remove the flexural resistance of the concrete.

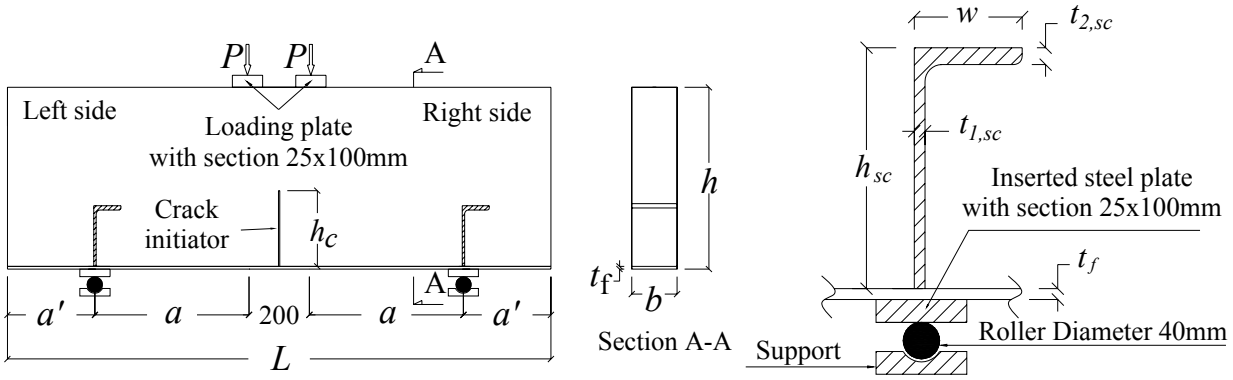

Figure III. 2 Detail of beam type specimen and shear connector

Table III. 1 Detail of specimens

Specimens	Sizes of Specimens (mm)							Sizes of shear connectors (mm)				Thick-ness of skin plate t_f (mm)	Concrete strength f_c' (N/mm^2)
	a	b	h	L	a'	θ	h_c	h_{sc}	w	$t_{1,sc}$	$t_{2,sc}$		
1st Test Series													
S-600-200-9-38.0-45	510	150	600	1800	300	45	-	200	90	9	14	9	38.0
S-600-200-9-25.3-45	510	150	600	1800	300	45	-	200	90	9	14	9	25.3
S-450-150-9-23.6-45	410	150	450	1500	250	45	-	150	75	9	14	9	23.6
S-300-100-9-25.1-45	290	150	300	1100	200	45	-	100	50	9	14	9	25.1
2nd Test Series													
S-600-200-9-43.0-30	950	150	600	2700	300	30	300	200	90	9	14	9	43.0
S-600-200-9-43.0-35	750	150	600	2300	300	35	300	200	90	9	14	9	43.0
S-450-150-9-43.0-25	850	150	450	2400	250	25	250	150	75	9	14	9	43.0
S-450-150-9-43.0-30	650	150	450	2000	250	30	250	150	75	9	14	9	43.0
S-300-100-9-42.7-20	650	150	300	1900	200	20	150	100	50	9	14	9	42.7
S-300-100-9-41.5-25	500	150	300	1600	200	25	150	100	50	9	14	9	41.5

III.2.3 Materials

a) Steel Properties

JIS G 3101 standard steels with grade SM490 and grade SS400 whose mechanical properties are given in **Table III.2** were used for the steel plate and the shear connector, respectively. The different grades of steels were purposefully selected to assure that shear connector fail before yielding of skin plate. Additionally, the activities of steel's tensile strength testing as well as stress-strain relationships of the steels are available **APPENDIX III.1**.

Table III. 2 Characteristics of steel

	Shear Connector	Skin Plate
Tensile yield strength f_y (N/mm^2)	352	370
Ultimate strength f_u (N/mm^2)	448	511
Modulus of elasticity E (kN/mm^2)	202	204

b) Concrete Product

The mix proportions of concrete were accordingly designed depending on the required strength of the concrete. The summary of the mix proportion are given in **Table III.3**. Normal Portland Cement was used to produce the concrete. Additionally, the minimum size and maximum size of aggregates are 5 mm and 20 mm respectively. Water Reduction Agent (WRA) and Air Entrance Agent (AEA) were also used in the concrete product. Moreover, the direction of concrete casting was perpendicular to the big face of the specimen in order to minimize the cavities around the shear connectors. The activities of concrete and form work are available in **APPEXDIX III.2**.

Table III. 3 Concrete mix proportions

Specimens	Slump (cm)	W/C (%)	s/a (%)	Unit weight (kg/m^3)					
				Water	Cement	Sand	Coarse Aggregate	WRA	AEA
S-600-200-9-38.0-45	18	46	40	175	378	695	1059	3.78	15.1
S-600-200-9-25.3-45 S-450-150-9-23.6-45 S-300-100-9-25.1-45	8	73	45	155	211	876	1070	2.11	8.4
2nd Test Series	18	54	48.8	175	342	520	921	2.5	1.62

III.2.4 Experimental Set-up

a) Stain gauge installation

Strain gauges were attached on both steel and concrete as shown in **Fig.III.3**. In both 1st and 2nd test series specimens, strain gauges with 30 mm length were attached on both sides of the concrete surface in order to measure strain development in the concrete in front of the shear connector with respect to shear force. The strain gauges L39, L41, and L43 were attached on the concrete surface of the opposite side of L40, L42, and L44, respectively. Moreover, strain gauges with 5 mm length were attached on both sides of the steel plate in front of the shear connector with the aims of measuring strain distribution in the steel plate. On the other hand, differently from 1st test series specimens, strain gauge L5-L6 were mounted on the shear connectors of 2nd test series specimens in order to examine the stress-strain conditions of the shear connector. Additionally, all strain gauges were attached left-right symmetrically in pairs in all specimens.

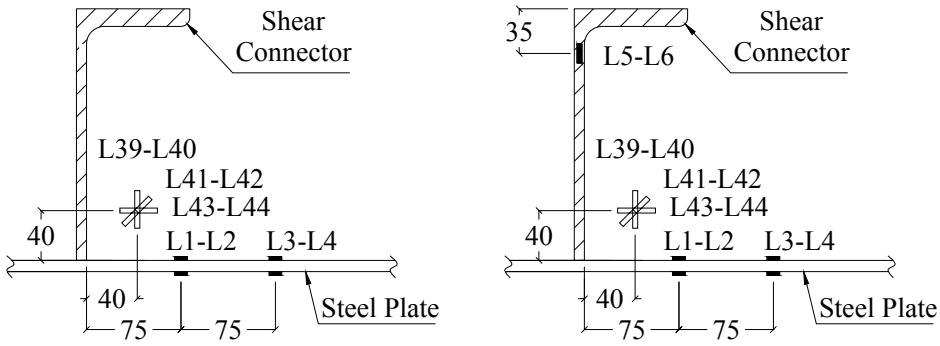

(a) 1st test series (Unit: mm) (b) 2nd test series (Unit: mm)

Figure III. 3 Locations of strain gauges of 1st test series specimens

b) Instrumentations for Relative Displacement Measurement

The relative displacements between head and toe of the shear connector were measured by two displacement transducers LD11 and LD12 for both 1st and 2nd test series specimens. The installations of the displacement transducers are illustrated in **Fig.III.4**. Two pins were welded perpendicularly to top of both sides of the shear connector. It means that the pins can freely move when the head of the shear connector displaces. Then the displacement transducers connected to the magnetic bases horizontally pointed against the pins in order to measure the displacement of the head of the shear connector. Meanwhile, the magnetic bases were attached on an extra inserted steel plate between the roller and the skin plate the specimen. The inserted steel plate and the

skin plate easily rotate as one on the roller. The horizontal displacements due to the rotation of the steel plates are also considered as the relative displacements of the shear connectors. By means of the installation mentioned above, the behaviors of the shear connectors in the specimens are reasonable identical to those in the real structures. The average values obtained from LD11 and L12 were determined as the relative displacement of the shear connector.

Moreover, the inserted steel plates were inserted for not only the magnetic base but also for the supported. However, the specimens were stable during the test even though the supports were modified. Additionally, displacement transducers were installed left-right symmetrically in pairs in all specimens.

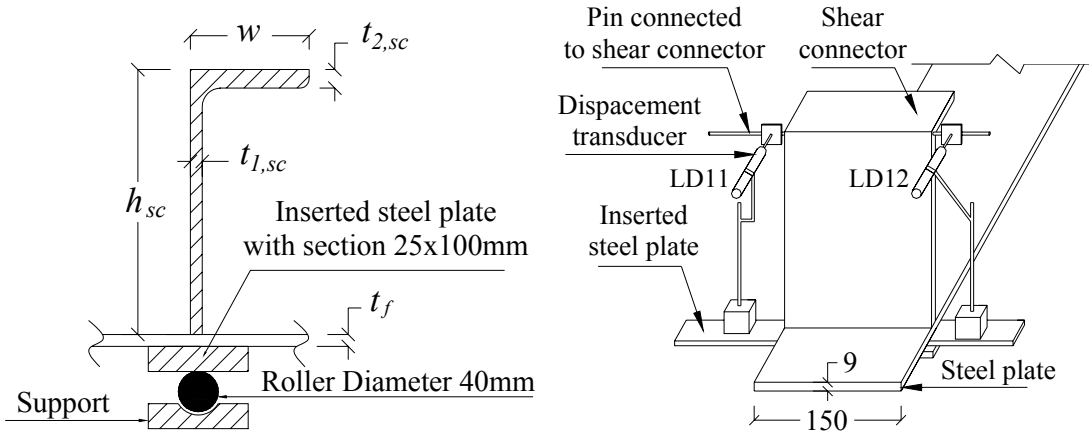

Figure III. 4 Detail of relative displacement measurement

c) Instrumentations for Slip Measurement

Concrete-skin plate slips in front of the shear connector were measured by means of four displacement transducers LD1-LD2 and LD3-LD4 for both 1st and 2nd test series specimens as illustrated in **Fig.III.4**. The displacement transducers which were connected with the magnetic bases were horizontally pointed against the angle plates which were attached on the concrete's surface. Meanwhile, the magnetic bases were attached with the bottom of the skin plate. When the concrete and the skin plate of the specimen relatively displaced due to applied load the displacement transducers detected the horizontal relative displacement between skin plate and concrete called as concrete-skin plate slip. The average values obtained from the displacement transducers LD1 to LD4 were determined as the slip. Also, displacement transducers were installed left-right symmetrically in pairs in all specimens.

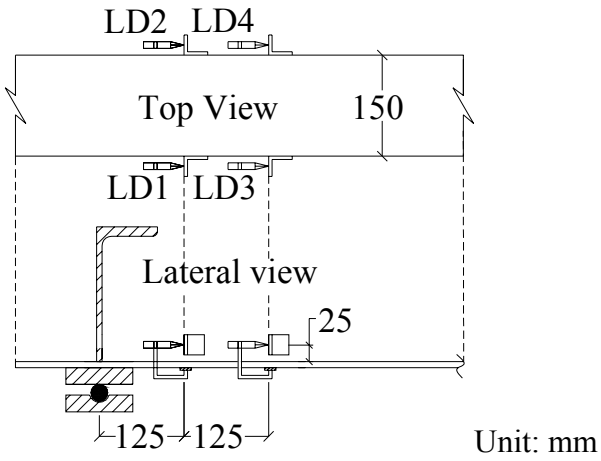

Figure III. 5 Detail of concrete-skin plate slip measurement

d) Experimental Set-up

The experimental work was conducted by a symmetric two-point loading system on the simply supported beam type specimen as illustrated in **Fig.III.6**. A hydraulic jack and an electrical load cell were used to apply the load and to measure the load, respectively. The hydraulic jack was fixed with a strong steel frame. Meanwhile, the support reacted against a strong steel beam which was laid on a thick steel plate. The load was applied until the shear connector fail.

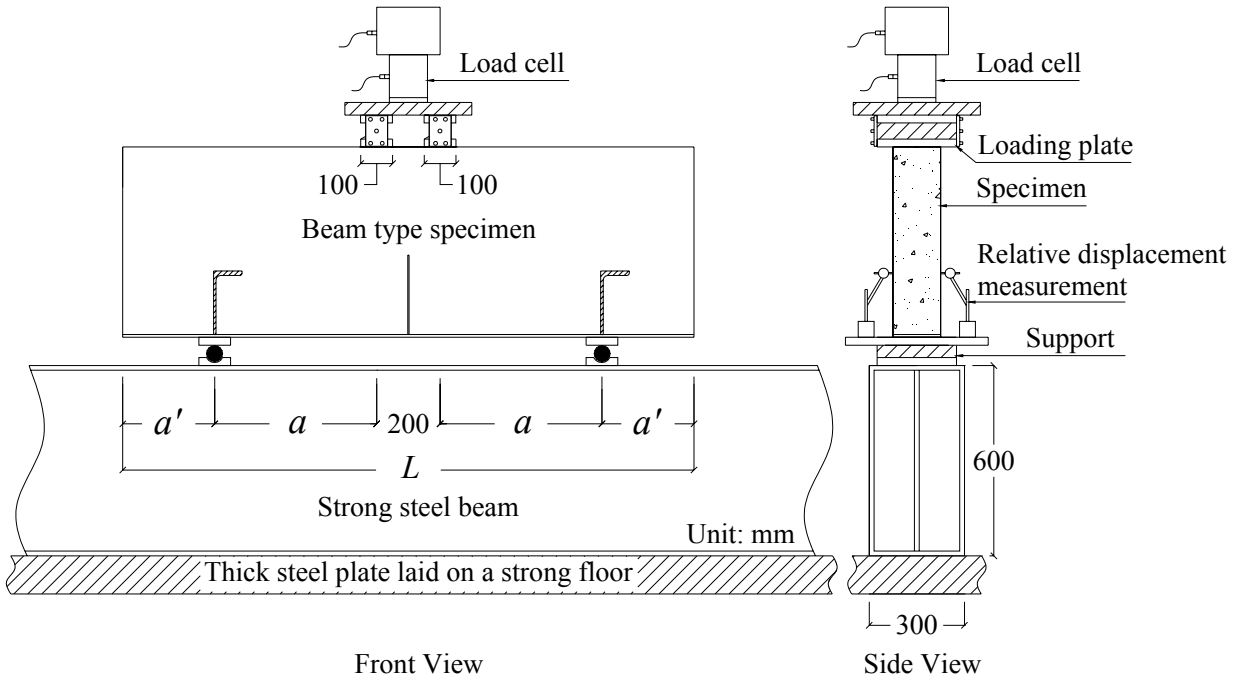

Figure III. 6 Experimental set-up

CHAPTER IV

EXPERIMENTAL RESULTS, ANALYSES, AND DISCUSSIONS

IV.1 L-Shape Shear Connector under Strut Compressive Force with Strut Angle of 45 Degrees (1st Test Series Specimens)

IV.1.1 General

The performance of L-shape shear connector subjected to strut compressive force with strut angle of 45 degrees ($\theta = 45^o$) were examined by 1st test series specimens that consisted of four beam type specimens. As described in chapter III, they were designed to study the effects of size of shear connector and concrete strength on the mechanical behavior of the shear connector especially the shear force-relative displacement relationship. Since all specimens failed on the left side, this study focused on the left side shear connectors. Therefore, this chapter accordingly describes and discussed every detail of the results of 1st test series specimens and FEM analyses.

IV.1.2 Failure Mode of L-Shape Shear Connectors ($\boldsymbol{\theta = 45^o}$)

All specimens failed when splitting crack occurred (split failure) in the concrete from the toe of the shear connector to the loading point. No break of L-shape shear connector and also no sign of yielding of skin plate were observed. Three stages of cracking in the concrete were observed before failure. Firstly, flexural crack took place at mid span and propagated almost vertically to the upper compression zone. Secondly, first diagonal crack occurred in the concrete starting from the head of the shear connector to the loading point. Finally, at failure, splitting crack appeared in the concrete starting from the toe of the shear connector forming an angle of approximately 45^o with the member's horizontal axis. It was found that all specimens have almost the same crack patterns, **Fig.IV.1.1**. The conditions of the specimens at failures are available in **APPENDIX IV.1**.

During the experiment, load *P* still could be applied on the specimens even though a diagonal crack already took place in the concrete starting from the head of the shear connector. However, the specimens could not resist against any more load when splitting crack occurred. Therefore, it

can be said that L-shape shear connector subjected to strut compressive force failed by failure of concrete block in front of the shear connector or failed by splitting crack occurrence.

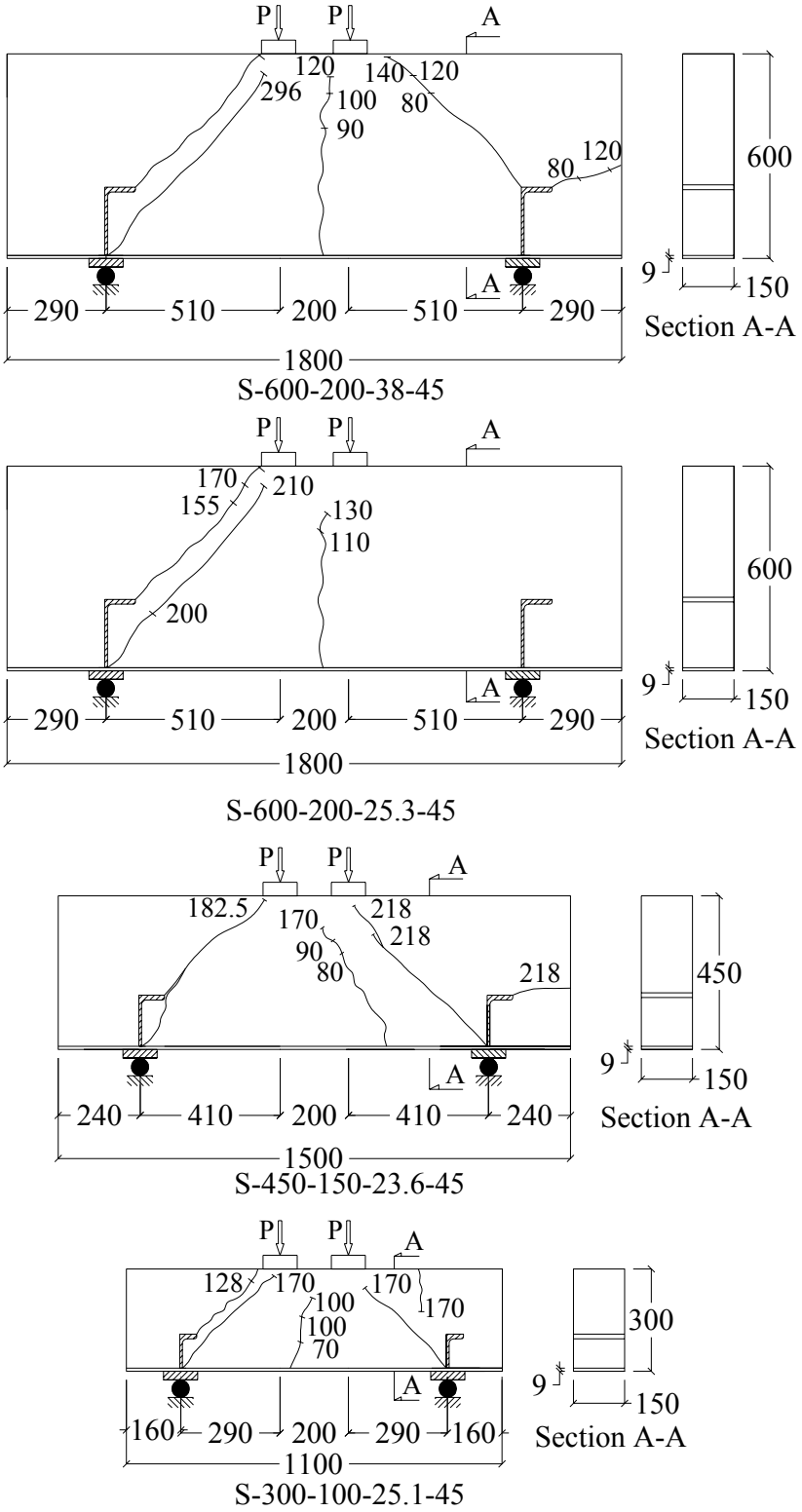

Figure IV.1. 1 Crack patterns of 1st test series specimens

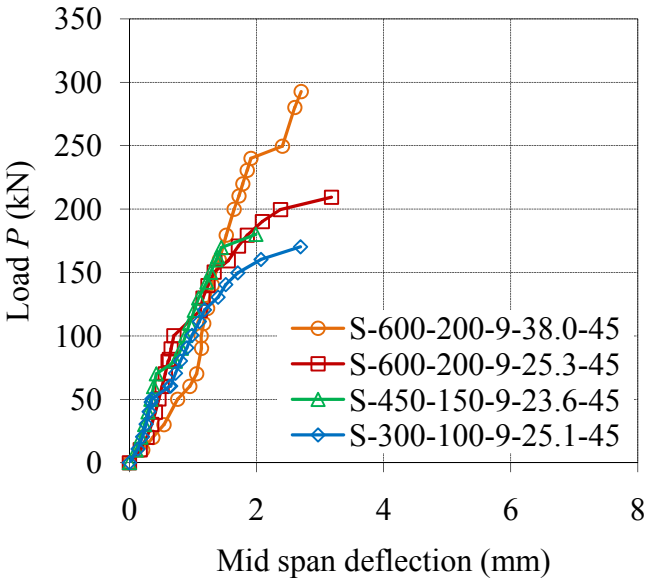

Figure IV.1. 2 Load-mid span deflection relationships of 1st test series specimens

Furthermore, load-mid span deflection relationships of the specimens were also observed. As illustrated in **Fig.IV.1.2**, at the early stage the curves of the relationships are almost the same. The effect of concrete strength on load-mid span deflection relationships can be observed between S-600-200-9-38-45 and S-600-200-9-25.3-45 that with the same size of shear connector and the same strut angle, both specimens failed at similar values of deflection but the specimen with higher concrete strength failed at higher load levels. Additionally, since S-600-200-9-25.3-45, S-450-150-9-23.6-45, and S-300-100-9-25.1-45 behaved similarly until failure, the effect of size of shear connector on the relationships cannot be identified.

IV.1.3 Ultimate Shear Force of Shear Connector Failed in Split Failure Mode($\theta = 45^o$)

a) Critical Factor Controlling Ultimate Shear Force of L-shape Shear Connector

The behavior of the shear connector and the surrounding concrete at failure indicated the most critical factor controlling ultimate shear force of L-shape shear connector subjected to strut compressive force. As illustrated in the previous subchapter, shear connector were found to lose its shear resistance ability when splitting crack took place in the concrete in front of the shear connector. Therefore, the observations were made on the behavior of concrete where splitting crack occurred.

The development of the principal tensile strain in the concrete at which splitting crack took place may illustrate the behaviors of the concrete. The strain values obtained from LD39 to LD44 were used to calculate the principal tensile strain perpendicular to the splitting crack direction. As shown in **Fig.IV.3** splitting crack took place when the principal tensile strains in the concrete reached approximately 210μ, simultaneously, ultimate shear forces of the shear connectors were observed. Therefore, it can be said that splitting crack occurrence in the concrete in front of the shear connector controlled the ultimate shear force of L-shape shear connector subjected to strut compressive force.

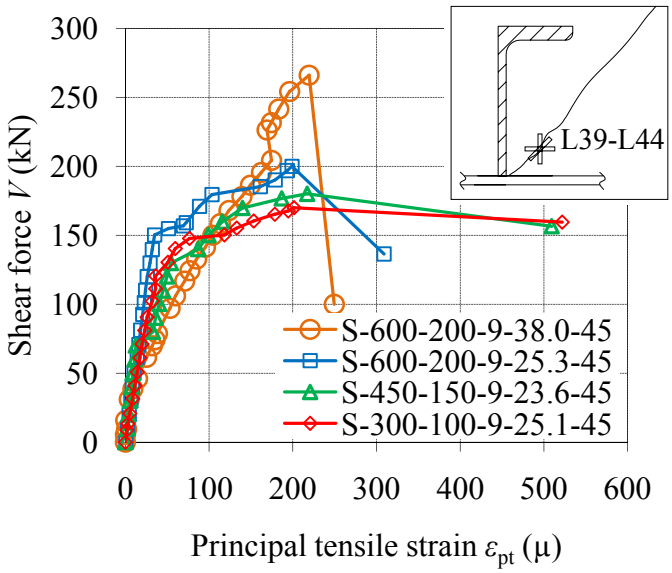

Figure IV.1.3 Shear force and principal tensile strain relationship

Furthermore, the behaviors of the shear connector can be illustrated in **Fig.IV.1.4**. The experimental results showed that after crack took place from the head of the shear connector, the strain in concrete in front of the shear connector transformed to principal direction and splitting crack occurred when the principal tensile stress σ_t exited the tensile strength of the concrete f_t. Simultaneously, splitting crack appeared along the strut compressive axis perpendicular to the direction of the principal stress.

Additionally, splitting crack could take place unless there was a release of principal tensile stress which was controlled by the relative displacement of shear connector. As shown in **Fig.IV.1.4** split failure occurred when the value of the relative displacement of the shear connector δ reached its ultimate value δ_u. Therefore, it can be said that the relative displacement of the shear

connector indirectly controlled the ultimate shear force of the shear connector; meanwhile, the tensile strength of the concrete directly determined the ultimate shear force of the shear connector subjected to strut compressive force.

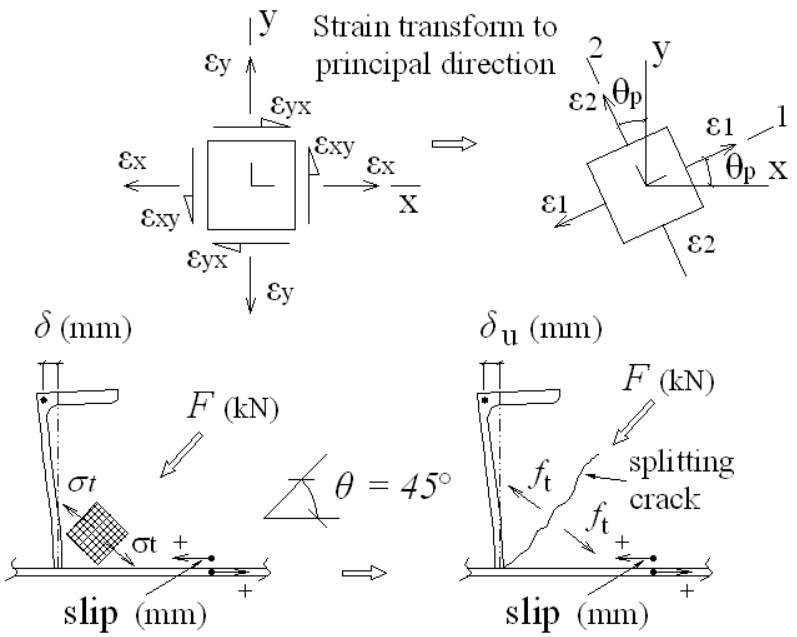

(a) after crack from head of shear connector (b) at splitting crack occurrence

Figure IV.1.4 L-shape shear connector before and at split failure

b) Ultimate Shear Force of L-shape Shear Connector

Shear force V was calculated by multiplying stress σ_s in the steel plate in front of the shear connector by the area of the steel plate A_s $(A_s = t_f \times b)$. Meanwhile, the stress was calculated by means of the stress-strain relationship of the steel skin plate, $(\sigma_s = E_s \varepsilon_s)$ whose strain values were obtained from the strain gauges LD1-LD4. Since there were no sign of the steel skin plate yielding until failure of the shear connector, the stress-strain relationship of the steel skin plate can be used to calculate the ultimate shear force of the shear connector V_u. The relationships between load *P* and strain in the skin plate are given in **APPENDIX IV.2**.

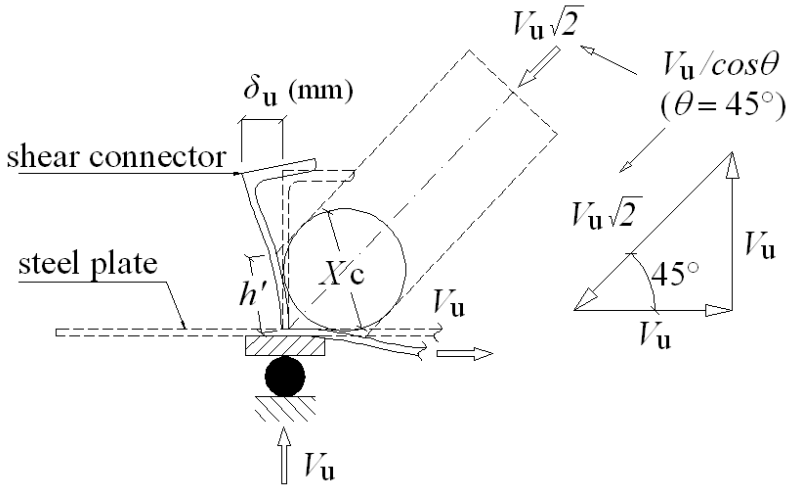

Figure IV.1. 5 Model of L-shape shear connector subjected to strut compressive force ($\boldsymbol{\theta = 45^o}$)

Fig.IV.1.5 gives the model of L-shape shear connector subjected to strut compressive force with strut angle $\theta = 45^o$. It has been observed that at split failure the relative displacement of the shear connector reached its ultimate value δ_u, and the height confining concrete against the shear connector was h'. Meanwhile, the width of the compressive strut was X_c. It is assumed that at split failure the behavior of the concrete in front of the shear connector was the same as that in the cylinder with diameter X_c in the split tensile strength test. Moreover, splitting crack occurred when the principal tensile stress exit the tensile strength of the concrete which can be expressed as followings:

$$f_t = \frac{2 \times \sqrt{2} \times V_u}{\pi \times X_c \times b_{sc}}$$

$$=> V_u = \frac{\pi}{2 \times \sqrt{2}} \times f_t \times b_{sc} \times X_c \qquad \text{Eq. IV. 1}$$

With $X_c = h'\sqrt{2}$ and $f_t = 0.44\sqrt{f_c'}$, JSCE (2005)[25] Eq.IV.1 can be given as followings:

$$V_u = 0.22 \times \pi \times h' \times b_{sc} \times \sqrt{f_c'}$$

Or $V_u = k_1 \times \sqrt{f_c'} \times b_{sc} \times h_{sc}$

That $k_1 = 0.22 \times \pi \times \frac{h'}{h_{sc}}$ *or* $k_1 = \frac{V_u}{\sqrt{f_c'} \times b_{sc} \times h_{sc}}$ Eq. IV. 2

Moreover, k_1 is a constant representing the effects of other factors. Meanwhile, the value of k_1 can be calculated by means of Eq.IV.2 where V_{u} is the ultimate shear force of the shear connector obtained from the experimental results, **Table IV.1.1**. Additionally, it has been known that the strength of the shear connector is highly influenced by its thickness to height ratio $t_{1,sc}/h_{sc}$. Therefore, the relationships between k_1 and $t_{1,sc}/h_{sc}$ were observed. It can be seen in **Fig.IV.1.6** that the values of k linearly increased with the values of $t_{1,sc}/h_{sc}$ and the relationships can be expressed as follows:

$$k_1 = 19.56 \times \left(\frac{t_{1,\mathrm{sc}}}{h_{\mathrm{sc}}}\right) + 0.494 \qquad \text{Eq. IV. 3}$$

Therefore, the ultimate shear force at split failure occurrence can be expressed as followings:

$$V_{\mathrm{u}} = k_1 \times \sqrt{f_c'} \times b_{\mathrm{sc}} \times h_{sc} \qquad \text{Eq. IV. 4}$$

Where,

V_{u} : ultimate shear force at splitting crack (N)

b_{sc} : width of shear connector (mm)

h_{sc} : height of shear connector (mm)

$t_{1,sc}$: thickness of shear connector (mm)

f_c' : concrete compressive strength (N/mm^2)

Table IV.1. 1 Ultimate shear forces and k_1 values obtained from experimental results

Specimens	$t_{1,sc}$ (mm)	h_{sc} (mm)	$\frac{t_{1,sc}}{h_{sc}}$	b_{sc} (mm)	f_c' (N/mm^2)	$V_{u.exp}$ (kN)	k_1
S-600-200-9-38.0-45	9	200	0.045	150	38.0	266	1.438
S-600-200-9-25.3-45	9	200	0.045	150	25.3	200	1.325
S-450-150-9-23.6-45	9	150	0.06	150	23.6	180	1.647
S-300-100-9-25.1-45	9	100	0.09	150	25.1	170	2.262

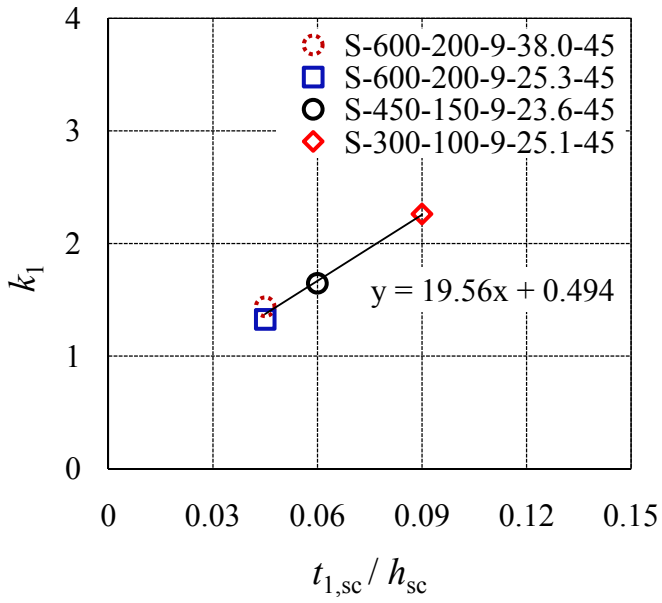

Figure IV.1. 6 Relationship between $\boldsymbol{k_1}$ and $\boldsymbol{t_{1,sc}/h_{sc}}$.

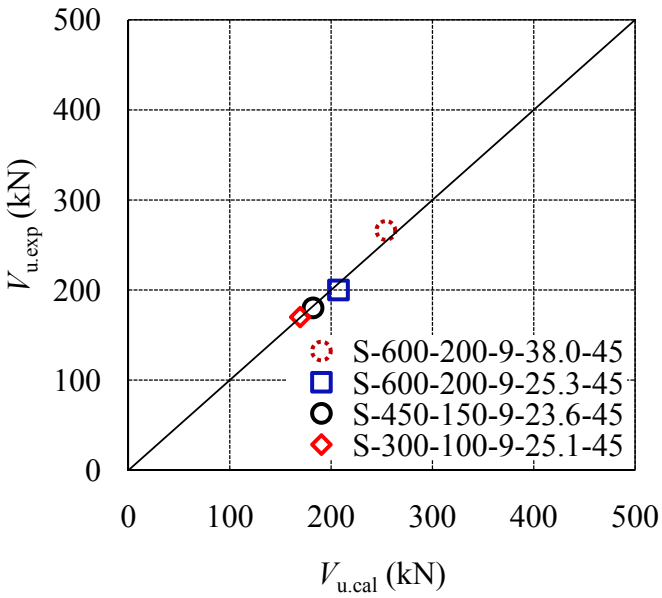

Figure IV.1. 7 The comparison between ultimate shear force from experiments and calculations

The ultimate shear forces of the shear connectors calculated by means of Eq.IV.4 $V_{u.cal}$ were compared with those obtained from the experiment $V_{u.exp}$. As shown in **Fig.IV.1.7**, the calculated ultimate shear forces $V_{u.cal}$ agreed well with the experimental results $V_{u.exp}$. Moreover, it can be said that Eq.IV.4 can precisely predict the ultimate shear force of L-shape shear connector at split failure with $V_{u.exp}$ to $V_{u.cal}$ ratios varied from 0.96 to 1.05, **Table IV.1.2**. However, Eq.IV.4 is applicable for the case that strut angle $\theta = 45^o$.

Table IV.1. 2 Ultimate Shear force of shear connector from experiments and calculations

Specimens	$V_{u.exp}$ (kN)	$V_{u.cal}$ (kN)	$\frac{V_{u.exp}}{V_{u.cal}}$
S-600-200-9-38.0-45	266	254	1.05
S-600-200-9-25.3-45	200	207	0.96
S-450-150-9-23.6-45	180	182	0.98
S-300-100-9-25.1-45	170	169	1.00

IV.1.4 Shear Force-Slip Relationship of L-shape Shear Connector

The average values obtained from the displacement transducers LD1-LD4 were determined as slip between the concrete and the steel plate in front of the shear connector. **Fig.IV.1.8** gives shear force-slip relationships of the shear connectors of 1st test series specimens. It can be observed that concrete-skin plate slip of L-shape shear connector subjected to strut compressive force appeared even at low load levels. These similar behaviors were also found by Kiyomiya et al. (1986) [6], Ueda et al. (1989) [10], and Chuah et al. (1991) [9].

It can be seen that the curves of the relationships in S-600-200-9-38.0-45, S-600-200-9-25.3-45, and S-450-150-9-23.6-45 were almost the same; therefore, no effects of concrete strength and height of shear connector on the shear force-slip relationships were observed. However, the experimental results showed that for the same size shear connector, the shear connector with higher concrete strength failed at greater values of ultimate slip as compared to the shear connector with lower concrete strength. Meanwhile, the shear connectors with the same concrete strength and strut angle were found to fail at similar value of the ultimate slips. In short, it can be said that concrete strength did not affect the shear force-slip relationships' curves but the ultimate shear force of the shear connector and the ultimate value of concrete-skin plate slip.

Moreover, it can be observed in S-600-200-9-25.3-45 and S-300-100-9-25.1-45 that after crack took place in the concrete starting from the head of the shear connector, the shear connectors were found to resist against the shear force with the values of slips almost constant until splitting crack occurred in the concrete in front of the shear connector. These behaviors indicated the development of the principal tensile stress in the concrete in front of the shear connector.

Meanwhile, it can be said that the stress in the concrete rapidly increased after crack appeared from the head of the shear connector leading to splitting crack occurrence.

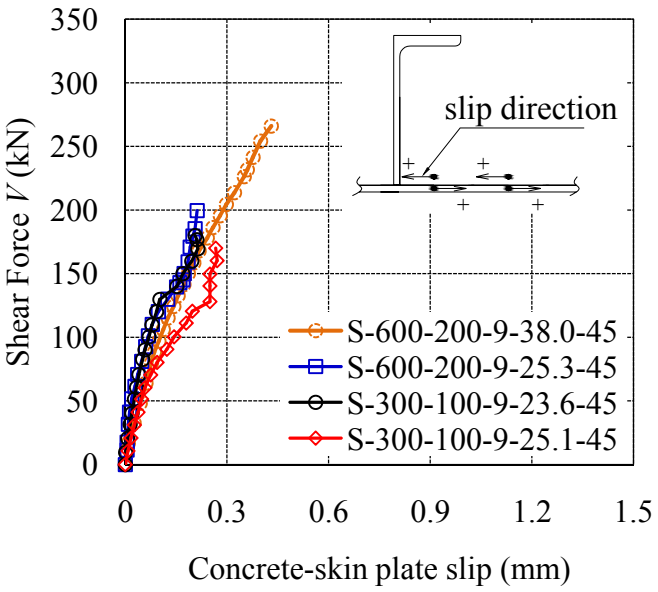

Figure IV.1. 8 Shear force-slip relationships $\boldsymbol{\theta = 45^o}$

More importantly, the experimental results showed that shear force-slip relationship is not applicable to fully explain the partial interaction mechanisms of L-shape shear connector since this relationship cannot be clearly observed at the ultimate state of the shear connector.

IV.1.5 Shear Force-Relative Displacement Relationships ($\boldsymbol{\theta = 45^o}$)

Since the relationships between shear force and relative displacement could be observed only in S-600-200-9-25.3-45 and S-300-100-9-25.1-45, the discussions were accordingly conducted. **Fig.IV.1.9** give the relationship between shear force and relative displacement of S-600-200-9-25.3-45 before the occurrence of crack from the head of the shear connector. It can be seen that the relative displacements of the shear connector were detected negatively when the levels of shear force were less than 150kN. The negative values of the relative displacement indicated the forward movement of the head of the shear connector. Similar behaviors were also observed in the steel-concrete sandwich beams by Makabe et al. (1991) [11] that when the load level was than 100kN, the head of the shear connector moved forward (negative); conversely, when load level was greater than 100kN, it moved backward (positive). However, it has been observed

during the experiment that at 150kN crack started to appeared in the concrete starting from the head of the shear connector; therefore, it seemed that the occurrence of this crack induced backward movement of the head of the shear connector.

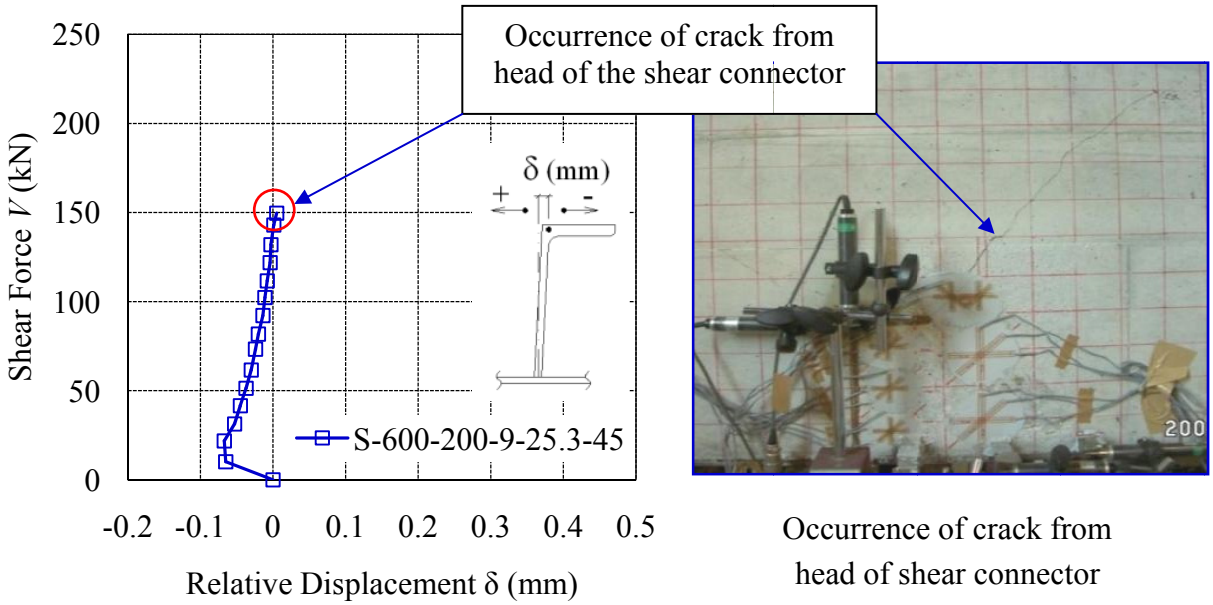

Figure IV.1. 9 Shear force-relative displacement relationship before the occurrence of crack from the head of the shear connector

Furthermore, it can be observed in **Fig.IV.1.10** that the relative displacements of the shear connectors were very small for both S-600-200-9-25.3-45 and S-300-100-9-25.1-45 before the occurrences of crack in the concrete starting from the head of the shear connectors. On the other hand, the sudden increment of the relative displacement at low level of shear force in S-300-100-9-25.1 was due to the unexpected sudden rotation of the inserted steel plate before it fully touched the steel plate of the specimen. Moreover, after the occurrence of the crack in the concrete from the head of the shear connector, big increments of the relative displacements with small increments of shear force were observed until failure of the shear connector. Similar behaviors were also observed in steel-concrete sandwich beam by Saidi et al. (1998 [12], 1999 [13], and 2008 [14]). Moreover, it was observed that larger size L-shape shear connector failed at greater value of ultimate shear force and ultimate relative displacement than the smaller size L-shape shear connector.

Additionally, the shapes of shear force-relative displacement relationships' curves of L-shape shear connector subjected to strut compressive force were clearly observed in the interval of the occurrence of crack from the head of the shear connector and failure of the shear connector. *More importantly, it can be observed that shear force-relative displacement is suitable to use to explain the partial interaction mechanisms of L-shape shear connector subjected to strut compressive force at its ultimate state. The ultimate relative displacement corresponding to the ultimate shear force of the shear connector can be clearly observed from the experimental results. Therefore, it is important to identify the equations of shear force-relative displacement relationship of the shear connector in this interval.*

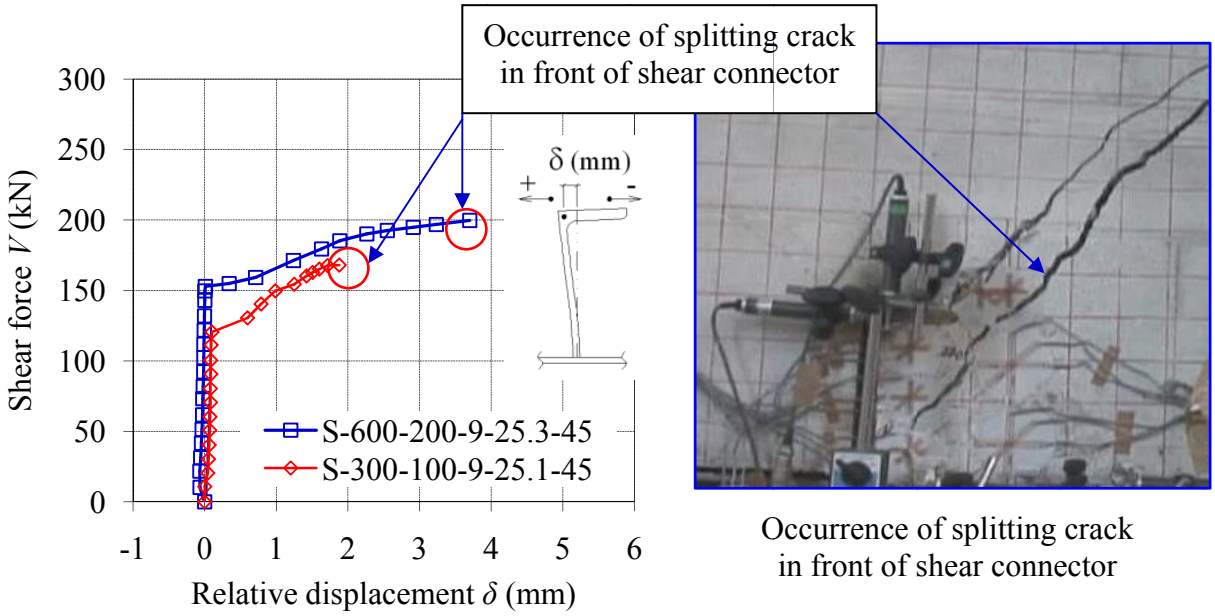

Figure IV.1. 10 Shear force-relative displacement relationship $\boldsymbol{\theta = 45^o}$

IV.1.6 FEM Analyses for Shear Force-Relative Displacement Relationships ($\boldsymbol{\theta = 45^o}$)

Finite element analyses were conducted to verify the experimental results. There were three material types for the element: plain concrete, steel and bond link or joint element. Based on elasto-plastic and fracture model, Okamura and Maekawa (1997) [26] a constitutive model for the concrete before cracking was constructed. Meanwhile, a constitutive model of cracked concrete consisted of tension stiffening, compression and shear transfer model. A two-dimensional failure criterion in tension-tension and compression-tension was applied to the analyses. Since steel plates and shear connectors were in elastic ranges until failure of the

specimens, elastic plate was selected and assumed to be steel plate and shear connector in the analyses. On the other hand, bond link element was originated from a linear bond stress-slip relationship. It was applied along the contact between the steel and the concrete. Bond link element's normal stiffness in compression direction was maintained a great value, 300 times greater than the shear stiffness in order to avoid element overlap. Meanwhile, the stiffness in tension was maintained a low value for easy parting between the steel elements and the concrete elements. The detail of bond link element is available in **APPENDIX IV.3**.

As mentions in the previous subchapter, the shape of the shear force-relative displacement relationships' curves were clearly observed after the occurrence of crack from the head of the shear connector. Therefore, FEM analyses were according conducted. **Fig.IV.1.11** illustrates the development of FEM mesh of beam type specimen after the occurrence of flexural crack and crack from the head of the shear connector. As shown in **Fig.IV.1.11**, in the analyses, the flexural crack and the crack in the concrete starting from the head of the shear connector were accordingly introduced to make it agree with the conditions of the specimens in the experiments.

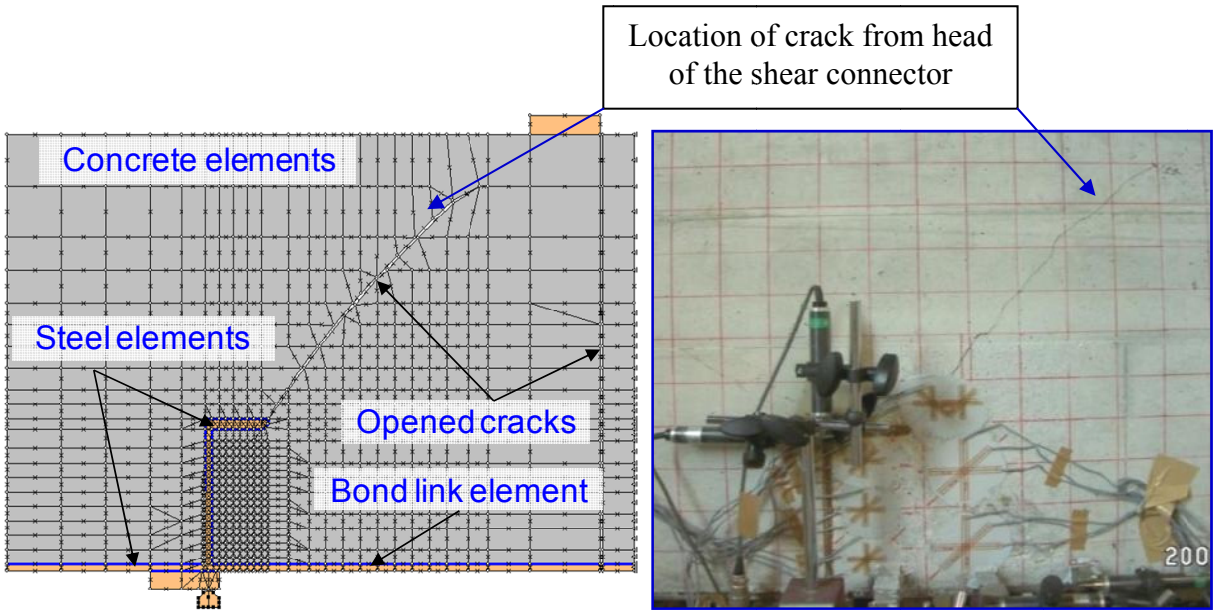

(a) FEM Mesh of beam type specimen

(b) Beam type specimen at the occurrence of crack from head of shear connector

Figure IV.1. 11 Development of FEM Mesh of beam type specimen

Fig.IV.1.12 shows the comparison between the failure mode observed in the FEM analyses and the experimental results. It can be seen that good agreements between the analyses results and the experimental results were observed in terms of the deformations of L-shape shear connector at failure and the crack distributions. Furthermore, as shown in **Fig.IV.1.12 (b)**, the locations and the directions of splitting cracks appeared in the FEM mesh were found to be the same as those appeared in beam type specimens.

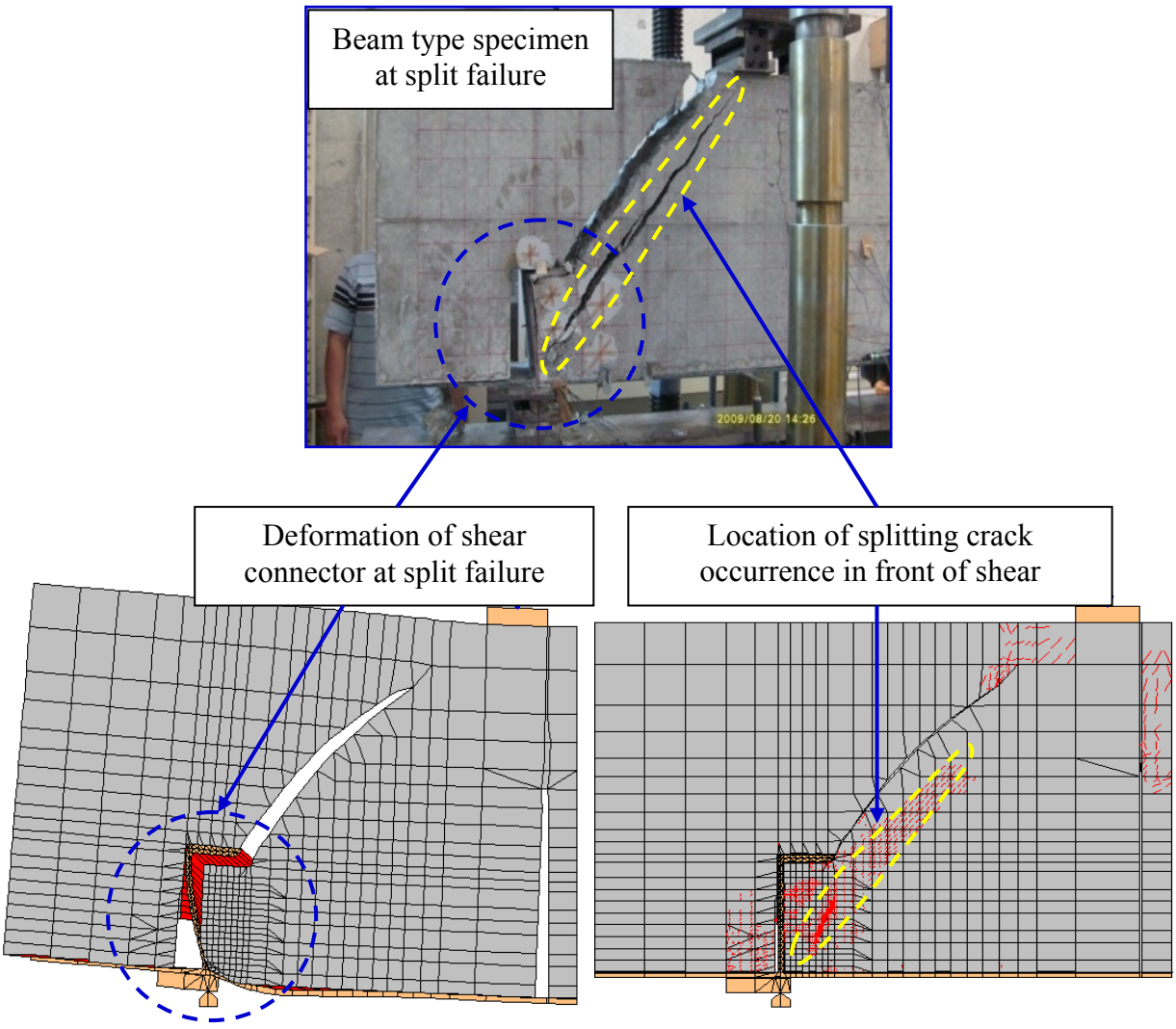

(a) Deformation of shear connector at failure (b) Crack distribution in FEM mesh at failure

Figure IV.1. 12 Failure mode of shear connector in FEM analysis and beam type specimen

Moreover, the experimental results and FEM analyses results were also compared for S-600-200-9-25.3-45 and S-300-100-9-25.1-45 in **Fig.IV.1.13** and **Fig.IV.1.14**, respectively. It can be seen

that the FEM analyses results agreed well with the experimental results in terms of ultimate shear force of L-shape shear connector, ultimate relative displacement, shear force-relative displacement relationships, and load-deflection relationships. Additionally, the stiffness of L-shape shear connectors in the FEM analyses were found a little smaller than those in the experiments due to the fact that flexural crack and crack from the head of the shear connector were initially introduced. However, most similar behaviors of L-shape shear connector subjected to strut compressive force were observed between the FEM analyses results and the experimental results.

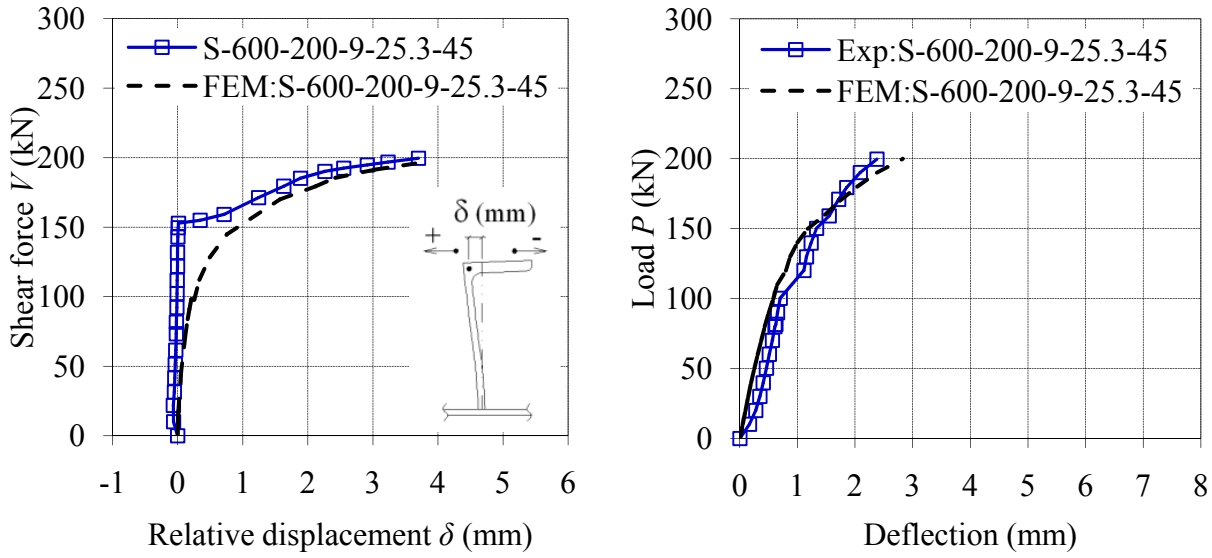

Figure IV.1. 13 Experimental Results and FEM analyses results S-600-200-9-25.3-45

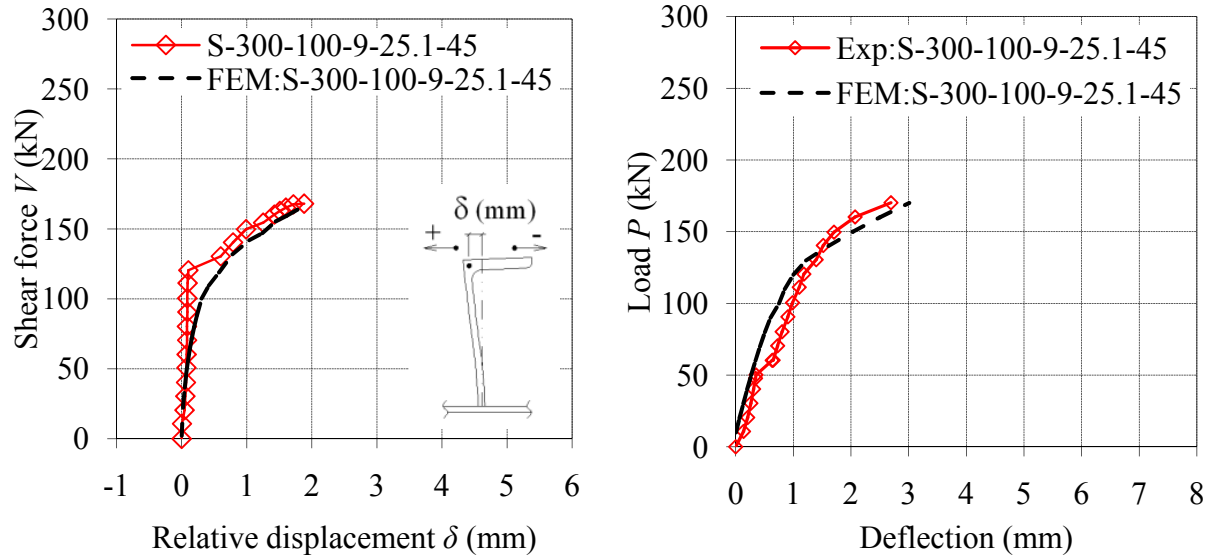

Figure IV.1. 14 Experimental Results and FEM analyses results S-300-100-9-25.1-45

It has been known that FEM Analyses with different sizes of element mesh division may give different results. However, according to this study the concrete element in front of the shear connector was divided into small meshes, 10 mm to 20 mm. The analyses results showed that the opened crack in concrete element in front of the shear connector occurred at the same location and direction of the splitting crack in the test specimens, and at the same level of ultimate shear force. Moreover, by means of joint element in steel-concrete element interface, steel-concrete interaction was set to zero in tension direction. It was observed that shear force-relative displacement relationships of shear connectors obtained from FEM analyses agreed well with experimental results.

Since FEM analyses results were found to agree with experimental results, it can be said that the results of FEM analyses are reliable. Therefore, the formulation for shear force-relative displacement of L-shape shear connector subjected to strut compressive force with strut direction 45^o will be developed by means of FEM analyses together with the experimental results. The formulation will be applicable for the case after the occurrence of crack from the head of the shear connector until failure of the shear connector, split failure.

IV.1.7 FEM Analyses for Eq.IV.4 Verification

a) Verifications of Ultimate Shear Force by Means of Eq.IV.4

A series of FEM analyses were conducted on the beam type specimens meshes with different sizes of L-shape shear connectors and concrete strengths but the same strut angle $\theta = 45^o$ in case the flexural crack and the crack in the concrete starting from the head of the shear connector already existed. These analyses were conducted to verify the ultimate shear force of shear connector given by Eq.IV.4 and also to formulate an equation for shear force-relative displacement relationships of the shear connector.

The FEM meshes were symbolized as F-h-h_{sc}-$t_{1,sc}$-f_c' and the characteristics of the meshes are given in **Table IV.1.3**. In the FEM analyses the ultimate shear forces $V_{u.FEM}$ were decided when the block of concrete element in front of the shear connector failed. Also the calculations of all specimens in FEM analyses stopped when opened cracks in the concrete elements in front of shear connector reached the loading point. Meanwhile, the opened cracks took place along the compressive strut's axis identically to the splitting cracks in the tested specimens. **Table IV.1.3** lists of the ultimate shear forces obtained from the FEM analyses $V_{u.FEM}$ and the those calculated

by means of Eq.(4) $V_{u.Eq4}$. It has been observed that $V_{u.FEM}$ agreed well with $V_{u.Eq4}$ that $V_{u.FEM}$ to $V_{u.Eq4}$ ratios varied from 0.92 to 1.06. Additionally, as shown in **Fig.IV.1.15** Eq.IV.4 can precisely predict the ultimate shear force of L-shape shear connector when $\theta = 45^o$.

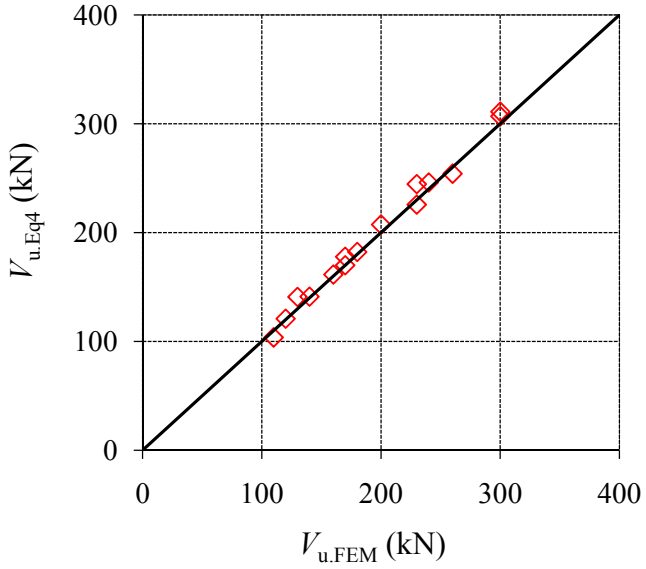

Figure IV.1. 15 The comparison between $\boldsymbol{V_{u.Eq4}}$ and $\boldsymbol{V_{u.FEM}}$

Table IV.1. 3 Ultimate shear forces from FEM analyses and calculation by means of Eq.IV.4

No	Specimens	h (mm)	h_{sc} (mm)	b_{sc} (mm)	t_{sc1} (mm)	t_f (mm)	f_c' (N/mm^2)	$V_{u.FEM}$ (kN)	$V_{u.Eq.4}$ (kN)	$\frac{V_{u.FEM}}{V_{u.Eq.4}}$
1	F-300-100-9-25.3	300	100	150	9	9	25.3	170	170	1.00
2	F-450-150-9-23.6	450	150	150	9	9	23.6	180	182	0.99
3	F-600-200-9-25.3	600	200	150	9	9	25.3	200	207	0.97
4	F-600-200-9-30	600	200	150	9	9	30	230	225	1.02
5	F-600-200-9-38	600	200	150	9	9	38	260	254	1.02
6	F-300-100-4.5-25.3	300	100	150	4.5	4.5	25.3	110	104	1.06
7	F-600-200-7-25.3	600	200	150	7	7	25.3	170	177	0.96
8	F-600-200-4.5-25.3	600	200	150	4.5	4.5	25.3	130	141	0.92
9	F-900-300-13.5-25.3	900	300	150	13.5	13.5	25.3	300	311	0.96
10	F-450-150-5-30	600	150	150	5	9	30	140	141	0.99
11	F-600-200-5-30	600	200	150	5	9	30	160	161	0.99
12	F-300-100-5-30	600	100	150	5	9	30	120	121	0.99
13	F-900-300-9-25.3	900	300	150	9	9	25.3	230	244	0.94
14	F-1200-400-9-30	1200	400	150	9	9	30	300	307	0.98
15	F-750-250-9-30	750	250	150	9	9	30	240	246	0.97

Moreover, the FEM analyses were also conducted to examine the applicable ranges of the proposed equation Eq.IV.4 in case of the sizes of the surrounding concrete are different. It can be observed in Table IV.1.4 that the increase of size of surrounding concrete does not effect on the shear capacity of the shear connector.

Table IV.1. 4 FEM analyses and calculations for size of surrounding concrete effects

No	Specimens	a' (mm)	h (mm)	h_{sc} (mm)	b_{sc} (mm)	t_{sc1} (mm)	t_f (mm)	f_c' (N/mm^2)	$V_{u.FEM}$ (kN)	$V_{u.Eq.4}$ (kN)	$\frac{V_{u.FEM}}{V_{u.Eq.4}}$
1	F-200-9-25.3	300	600	200	150	9	9	25.3	200	207	0.97
2	F-200-9-25.3	400	600	200	150	9	9	25.3	200	207	0.97
3	F-200-9-25.3	500	600	200	150	9	9	25.3	200	207	0.97
4	F-200-9-25.3	300	500	200	150	9	9	25.3	200	207	0.97
5	F-200-9-25.3	300	800	200	150	9	9	25.3	200	207	0.97

b) Shear Force-Relative Displacement Relationships ($\theta = 45^o$)

The relationships between shear force and relative displacement of the shear connectors were also observed. As shown in **Fig.IV.1.16**, the behaviors of the shear connectors with respect to shear forces observed in the FEM analyses are similar to those observed in the experiments.

Furthermore, it can be seen that the curves of shear force-relative displacement relationships are different with sizes of shear connectors and concrete strengths especially the ultimate shear force and the ultimate relative displacements.

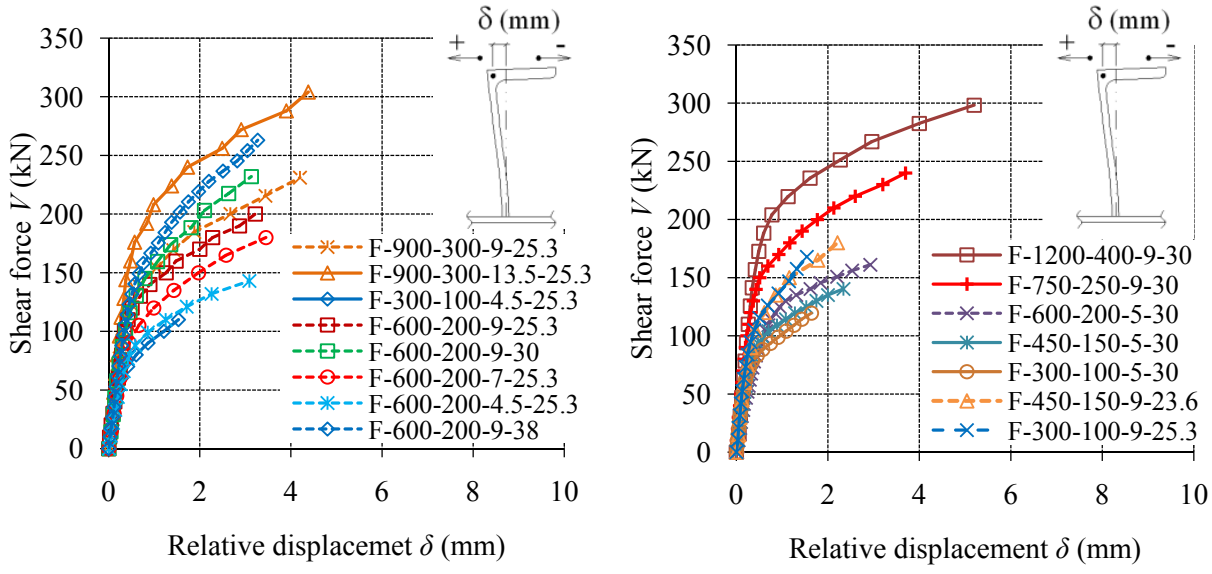

Figure IV.1. 16 Shear force-relative displacement relationship observed in FEM analyses

IV.1.8 Formulation for Shear Force-Relative Displacement Relationships ($\theta = 45^o$)

Since the results obtained from the FEM analyses agreed well with those obtained from the experiments, it can be said that the results of the FEM analyses are reliable. Therefore, the equation for the shear force-relative displacement relationship in case $\theta = 45^o$ was developed from the results of FEM analyses.

First of all, the observations were made on shear force-horizontal relative displacement relationships in F-300-100-4.5-25.3, F-600-200-9-25.3, and F-900-300-13.5-25.3 whose concrete strength and thickness to height ratios of the shear connectors are the same. Also, the thicknesses of the steel skin plates are the same as the thicknesses of the shear connectors. It can be observed in **Fig.IV.1.17** that the ultimate shear force of the shear connector and the ultimate relative displacement seems to proportionally increase with size of shear connector. Also, the shapes of shear force-relative displacement relationships' curves of the shear connector are similar.

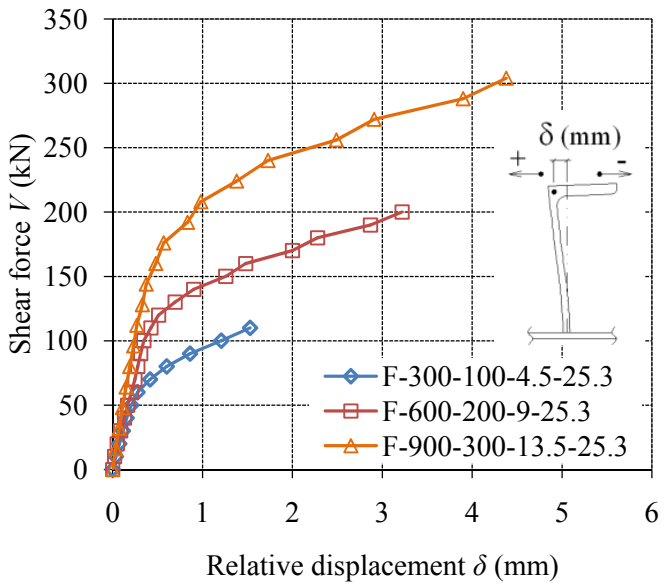

Figure IV.1. 17 $V - \delta$ relationships for the same size proportion shear connectors

Moreover, when the shear force was normalized by the ultimate shear force V/V_u and the relative displacement by the height of the shear connector δ/h_{sc} the curves of the relationships became unique as shown in **Fig.IV.1.18**. This results indicated that the relationship between shear force V and relative displacement δ can be represented by that between $V/V_{max.FEM}$ and

δ/h_{sc}. More importantly, the curves fitting analyses have been conducted and an equation representing the relationships' enveloped curve can be expressed as followings:

$$\frac{V}{V_u} = \left(1 - e^{-180\frac{\delta}{h_{sc}}}\right)^{0.6} \qquad \text{Eq.IV.5}$$

Where,

V_u : ultimate shear force of shear connector (N)

δ : relative displacement of the shear connector (mm)

h_{sc} : height of shear connector (mm)

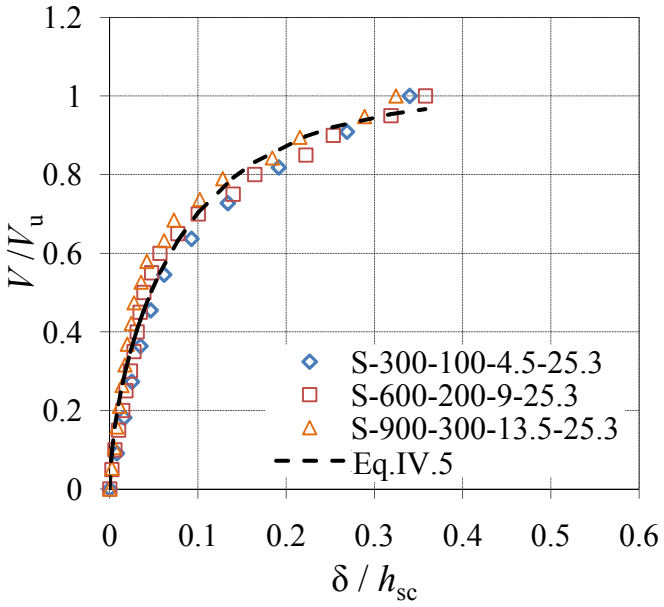

Figure IV.1. 18 $V/V_u - \delta/h_{sc}$ relationships for the same size proportion shear connectors

It can be seen in **Fig.IV.1.18** that Eq.IV.5 can precisely predict the enveloped curve of the shear force-relative displacement relationships of L-shape shear connector subjected to strut compressive force with $\theta = 45^o$.

a) Effects of $t_{1,sc}$ on Shear Force-Relative Displacement Relationships

The effect of the thickness of the shear connector $t_{1,sc}$ on shear force V and relative displacement δ relationships was also observed. **Fig.IV.1.19** gives V and δ relationships of the shear connectors with different thickness $t_{1,sc}$ but the same heights of shear connector h_{sc} and concrete strength $f_c^{'}$. It can be seen that the thin shear connector has greater displacement than the thick shear connector when the same level of shear force were carried. This similar behavior was also found in plate shape shear connector by Chuah et al. (1991) [9]. Additionally, the same height shear connectors were found to have similar ultimate relative displacement despite different $t_{1,sc}$.

Moreover, as shown in **Fig.IV.1.20** a unique enveloped curve was also observed when the shear forces V were normalized by the ultimate shear force V_u and the relative displacements δ by the height of the shear connector h_{sc}. Meanwhile, the enveloped curve fitted best with the curve of the relationships between V/V_u and δ/h_{sc} calculated by means of Eq.IV.5. It means that Eq.IV.5 is also applicable fore different thickness of L-shape shear connector.

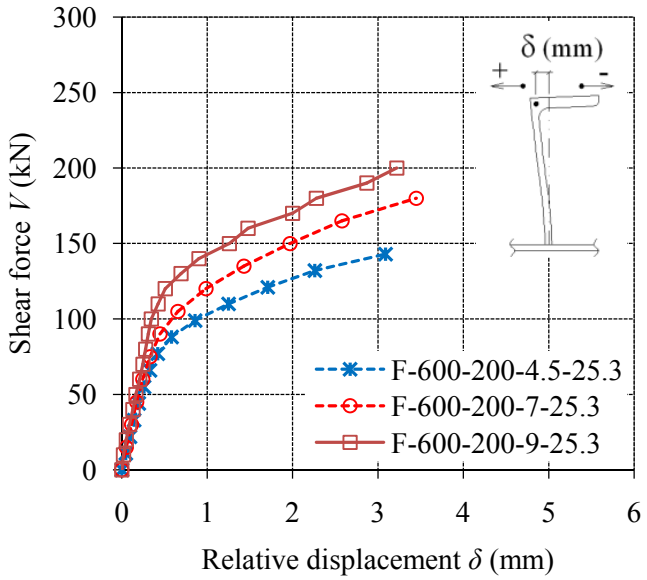

Figure IV.1. 19 $V-\delta$ relationships for different thickness of shear connectors

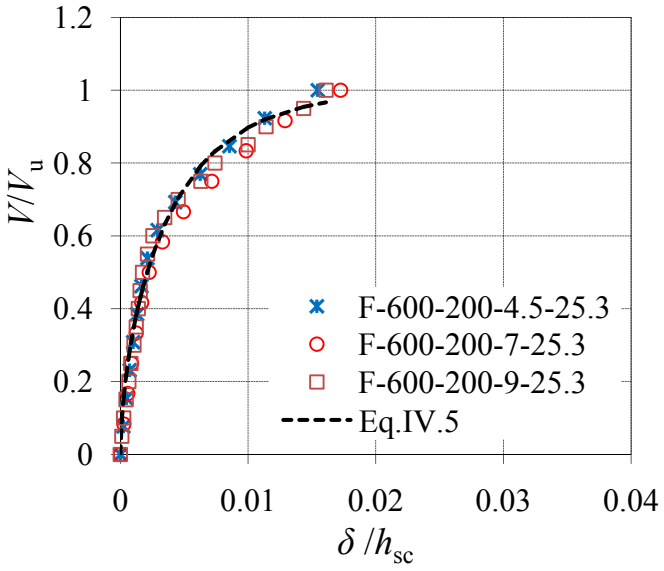

Figure IV.1. 20 $V/V_u - \delta/h_{sc}$ relationships for different thickness of shear connectors

b) Effects of f'_c on Shear Force-Relative Displacement Relationships

Furthermore, the effect of concrete strength f_c' on shear force V and horizontal relative displacement δ relationships was also observed. **Fig.IV.1.21** gives the relationships between shear force V and relative displacement δ of the same size shear connectors but different concrete strengths f_c'. It can be seen that when shear forces are less than approximately 120kN no effect of concrete strength on the relationships can be observed. However, when the level of shear force became higher, the shear connector with lower concrete strength displaced more as compared to the shear connector with higher concrete strength when the same level of shear force was carried. Also the ultimate relative displacements of the shear connectors were almost the same despite different levels of ultimate shear forces. These results show that there is no effect concrete strength on the ultimate relative displacement but the ultimate shear force of the shear connector.

Regardless of concrete strength, a unique enveloped curve was also observed for the relationships between V/V_u and δ/h_{sc} as given in **Fig.IV.1.22**. Moreover, the calculation results by means of Eq.IV.5 agreed well with the normalized curves. Therefore, it can be said that Eq.IV.5 is applicable fore V/V_u and δ/h_{sc} relationship of the connectors with different concrete strength.

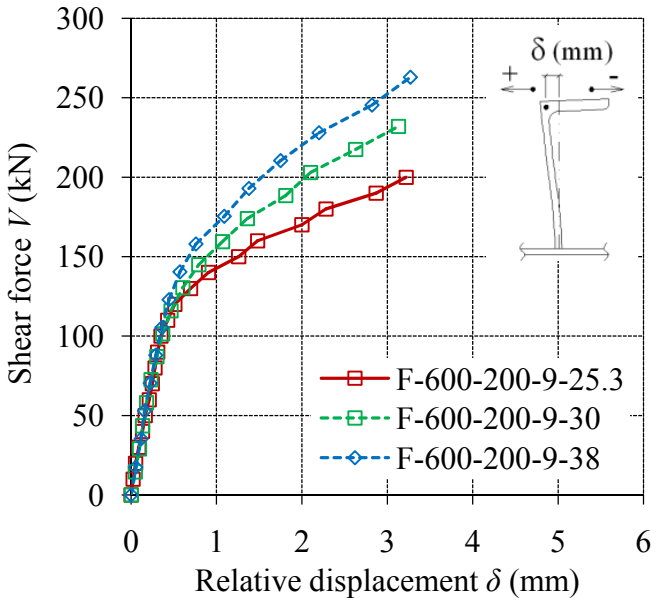

Figure IV.1. 21 $V-\delta$ relationships for different concrete strength

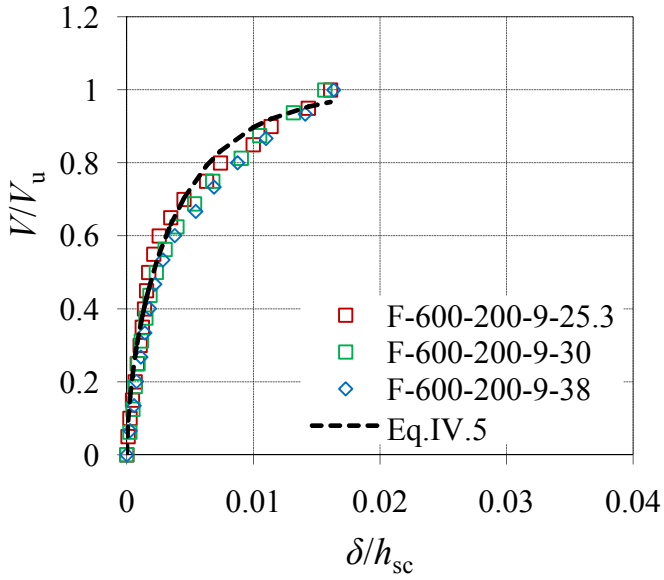

Figure IV.1. 22 $V/V_u-\delta/h_{sc}$ relationships for different concrete strength

c) Effects of h_{sc} on Shear Force-Relative Displacement Relationships

Moreover, the effect of height of shear connector h_{sc} on shear force $V$and horizontal relative displacement δ relationships can be observed in **Fig.IV.1.23**. It can be observed that with same

thickness of shear connector $t_{1,sc}$ and the same concrete strength f_c', the greater height shear connectors failed at higher level of ultimate shear force V_u and also at greater value of ultimate relative displacements δ_u as compared to the smaller height shear connectors. However, the shear connectors were found to have similar stiffness even thought the height of the shear connector h_{sc}were different.

Again, as shown in **Fig.IV.1.24**, when shear forces V were normalized by the ultimate shear force V/V_u and relative displacement δ by the height of the shear connector h_{sc}, δ/h_{sc}, a unique enveloped curve was obtained. Fortunately, the results obtained from the calculations by means of Eq.IV.5 fitted best with the data. Therefore, it means that Eq.IV.5 is also applicable for the prediction of shear force-relative displacement relationship of different height shear connectors.

In short, Eq.IV.5 was found to be applicable to predict shear force-relative displacement relationships of different size of shear connectors and also different concrete strength. However, the equation is applicable only in case that strut angle is equal to 45°, $\theta = 45^o$.

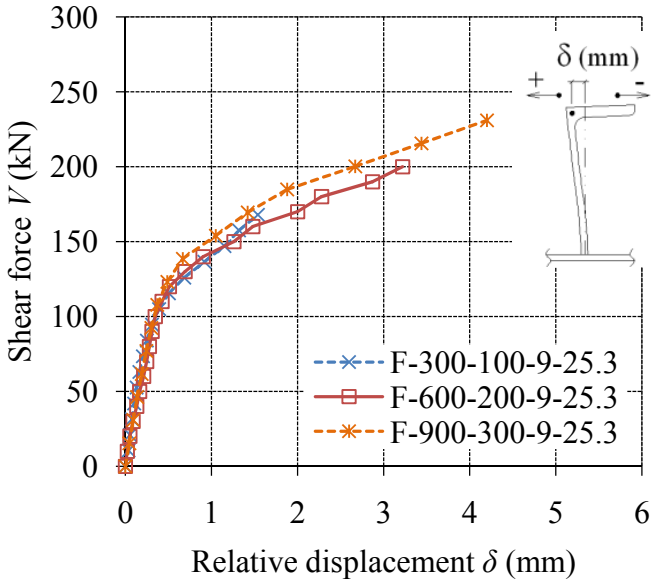

Figure IV.1. 23 $V-\delta$ relationships for different height of shear connectors

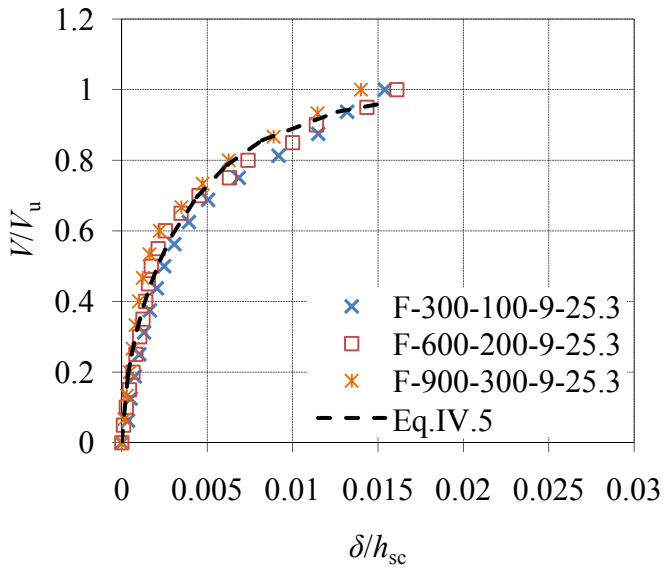

Figure IV.1. 24 $V/V_u - \delta/h_{sc}$ relationships for different height of shear connector

c) Experimental Results and Calculation Results by Means of Eq.IV.5 Comparison

The relationships between V/V_u and δ/h_{sc} calculated by means of Eq.IV.5 were compared with those obtained from the experimental results, shown in **Fig.IV.1.25**. It can be observed that the calculated relationships agreed well with those obtained from the experimental results from the occurrence of crack in the concrete starting from the head of the shear connector to the occurrence of split failure of the shear connector.

Furthermore, the relationships between ultimate shear forces V_u and the maximum values of δ/h_{sc} obtained from the FEM analyses can be observed in **Fig.IV.1.26**. It can be seen that the values of δ_u/h_{sc} varied from 0.014 to 0.017 regardless of the size of the shear connector and the concrete strength. On the other hand, as shown in **Fig.IV.1.25** the experimental results showed that the ultimate relative displacements of the shear connector were approximately 0.02 times the height of the shear connector.

However, the equations for the ultimate shear force Eq.IV.4 and the relationship between V/V_u and δ/h_{sc} Eq.IV.5 were found only for the case that strut angle was 45° ($\theta = 45^o$) and the shear connector failed by split failure mode. Therefore, the formulations for the ultimate shear force and the shear force-relative displacement relationships of L-shape shear connector for the case

that strut angle smaller than 45° ($\theta < 45^o$) are necessary. The following subchapter discussed the results of 2nd test series shear connectors whose strut angle smaller than 45° ($\theta < 45^o$).

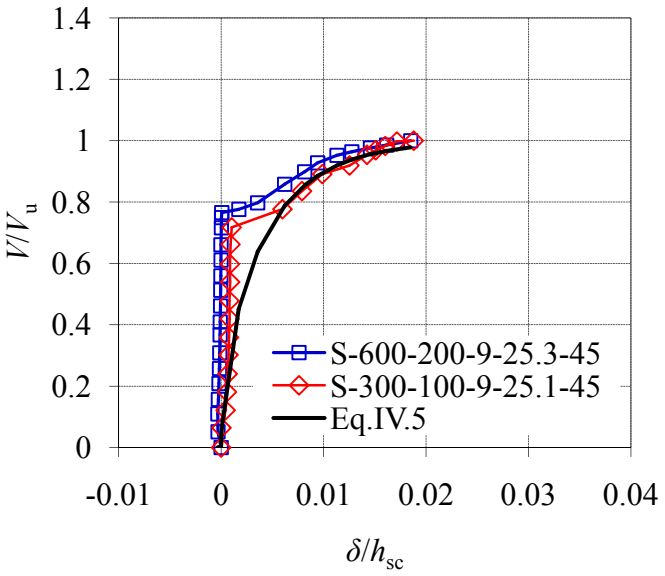

Figure IV.1. 25 $\boldsymbol{V/V_u - \delta/h_{sc}}$ relationships from experimental results and Eq.IV.5

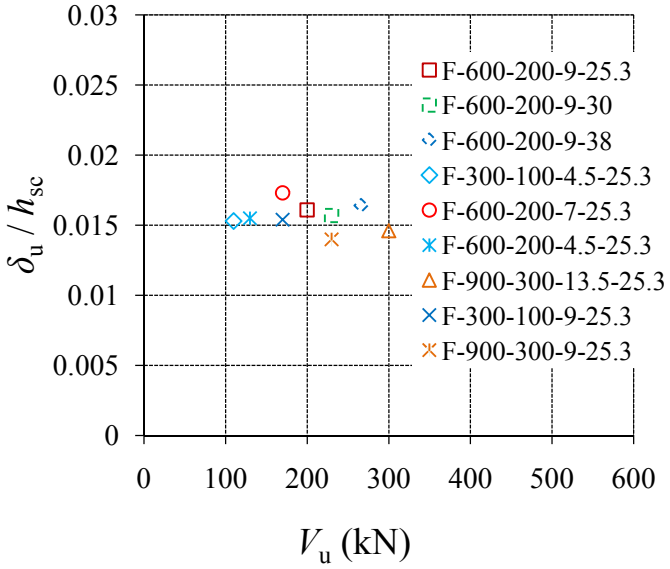

Figure IV.1. 26 Relationships between $\boldsymbol{\delta_u/h_{sc}}$ and $\boldsymbol{V_u}$

IV.2 L-Shape Shear Connector under Strut Compressive Force with Strut Angle Smaller Than 45 Degrees (2nd Test Series Specimens)

IV.2.1 General

The 2nd test series consists of six specimens whose strut angle $\theta < 45^o$. The focused parameters of the 2nd test series specimens were performed by means of a pre-study through FEM analyses. Based on 1st test series results and finite element analyses (FEM) results described in the previous subchapter, when strut angle is equal to 45° (θ = 45°) splitting crack occurrence in the concrete in front of the shear connector occurred (split failure) regardless of size of shear connector and concrete strength. Moreover, good agreements between the experimental results and the FEM analyses results in terms of the final failure mode, the ultimate shear force V_u, and the shear force-relative displacement relationships of the shear connectors were observed.

Therefore, prior to the selection of the focused parameters for 2nd test series specimens, the effects of strut angle, concrete strength, and size of shear connector on the performance of the shear connectors were examined by means of FEM analyses as given in the following subchapter.

IV.2.2 FEM Analyses for Parameter Selection for 2nd Test Series Specimens

Based on FEM analyses study, different final failure modes, split failure and shear failure of L-shape shear connector which is dependent on the strut angle and the size of the shear connector were observed. More importantly, as shown in **Fig.IV.2.1**, the critical strut angle θ_o representing the border between split failure and concrete crush was found to vary with thickness to height ratio of the shear connector $t_{1,sc}/h_{sc}$. The criteria of shear failure and split failure are respectively illustrated in **Fig.IV.2.2** and **Fig.IV.2.3**. More details of these two different failure modes are given in the following subchapter.

The selection of the strut angle and the size of the shear connector for 2nd test series specimens were according made in order to clarify the performance of L-shape shear connectors observed in the test preparation study. As given in **Fig.IV.2.1**, three specimens were expected to fail in split failure mode while three others were expected to fail in shear failure mode. The next subchapter describes and discusses every detail of the 2nd test series results.

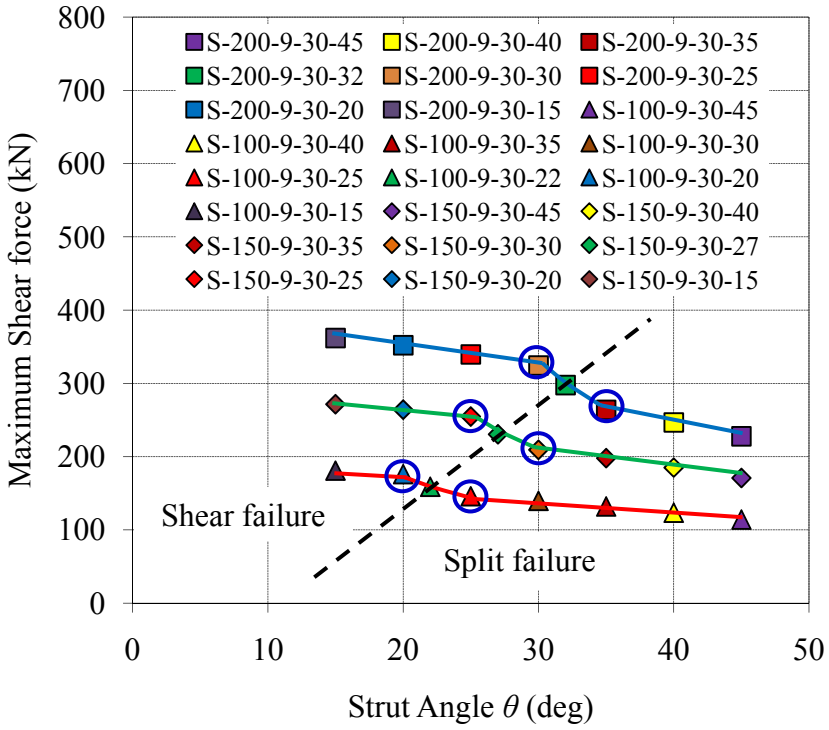

Figure IV.2.1 Ultimate shear force and strut angle

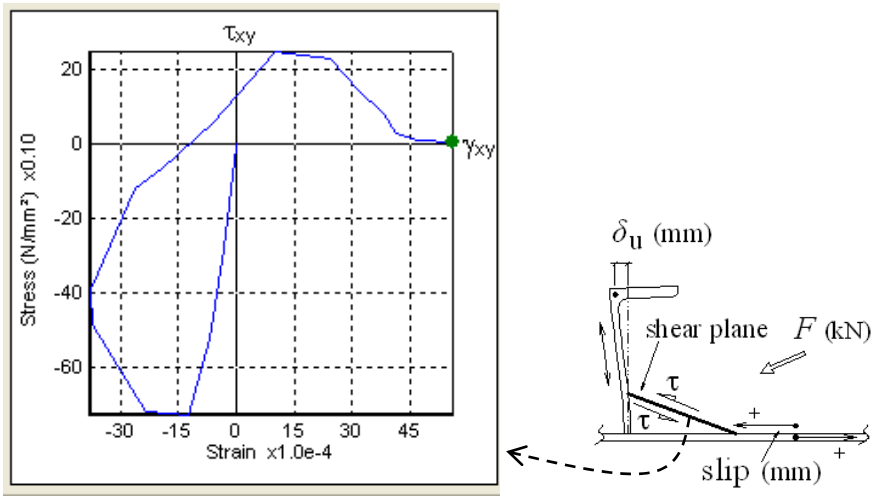

Figure IV.2.2 Shear failure criteria

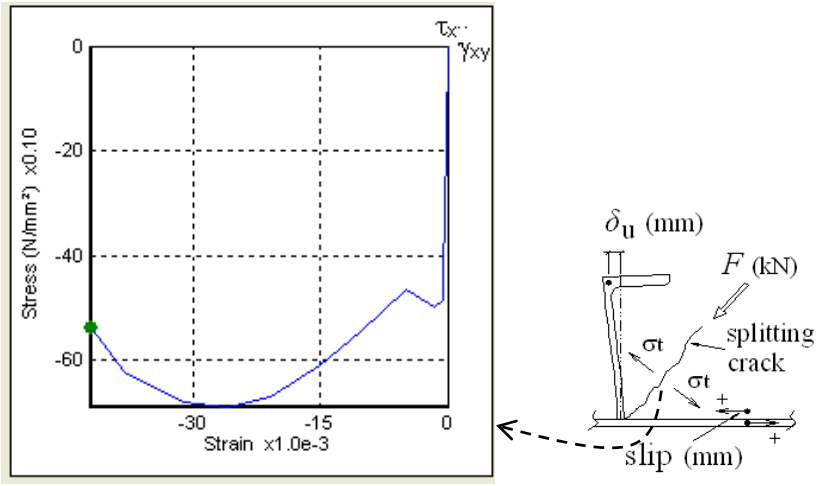

Figure IV.2.3 Split failure criteria

IV.2.3 Failure Mode of 2nd Test Series Shear Connectors ($\theta < 45^o$)

a) Failure Mode

Since only left size shear connectors failed, the discussions are accordingly made in this study. The conditions of the shear connectors at failures observed in 2nd test series specimens are illustrated in **Fig.IV.2.4**. Different failure modes of the shear connectors, split failure, shear-split failure, concrete crush, and shear failure were identified. Meanwhile, crack patterns of the specimens failed in split failure mode and in non-split failure mode are given in **Fig.IV.2.5** and **Fig.IV.2.6**, respectively. The numbers in the figures represent load P for 1st series specimens and $2P$ for 2nd series specimens.

As shown in **Fig.IV.2.5**, the shear connectors were found to fail in split failure mode in S-450-150-9-43-30 and S-300-100-9-41.5-25. However, S-450-150-9-43-30 was found to have a sudden split failure at the same time with the occurrence of crack from the head of the shear connector; this indicated that the level of load carrying capacity at splitting crack in front of the shear connector in this specimen was lower than that at the occurrence of crack from the head of the shear connector. Therefore, the ultimate shear force V_u in this specimen cannot be discussed with those in other specimens whose split failure order occurred after the occurrence of cracks from the head of the shear connectors. Moreover, break of shear connector was observed only in S-600-200-9-43-30, **Fig.IV.2.6(a)** after small crush of concrete appeared. However, the breaking part was at welding liquid-skin plate interface which was due to low welding quality. Therefore,

the ultimate shear force V_u observed in S-600-200-9-43-30 also cannot be discussed with those of other specimens.

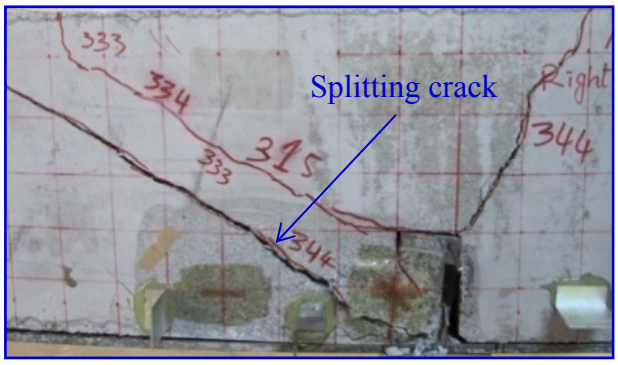

(a) Split failure S-300-100-9-41.5-25

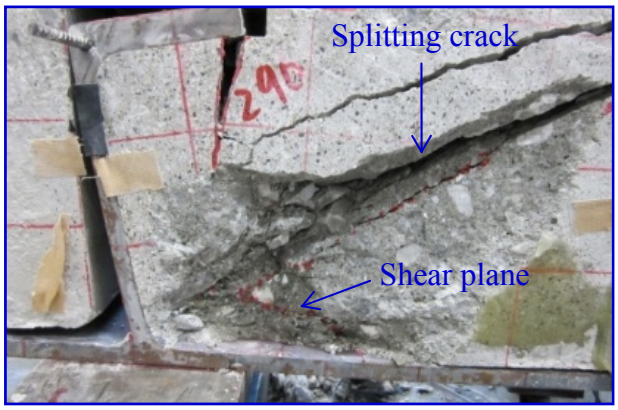

(b) Shear-split failure S-450-150-9-43-25

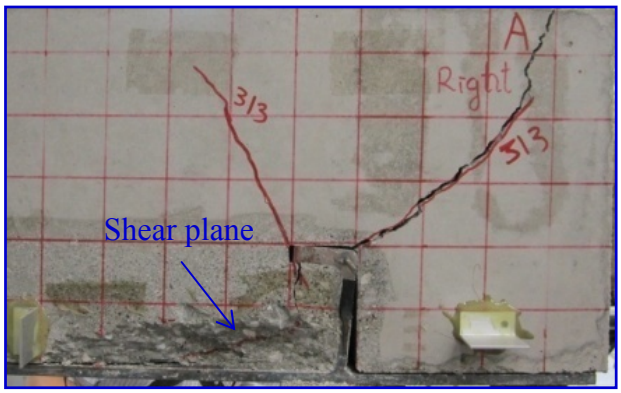

(c) Shear failure S-300-100-9-42.7-20

Figure IV.2. 4 Different failure modes of shear connectors in 2nd test series specimens.

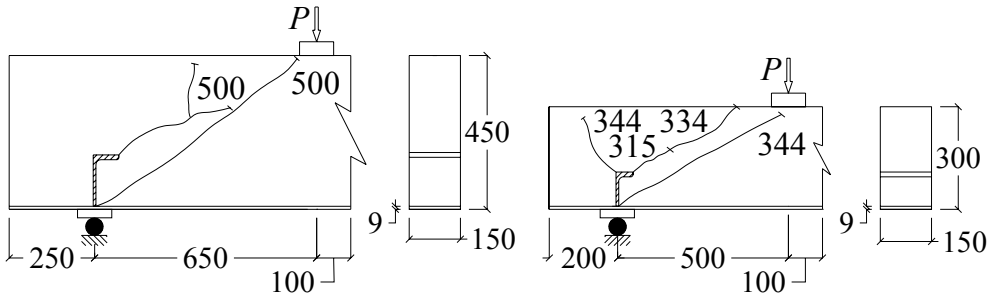

(a) S-450-150-9-43-30 (b) S-300-100-9-41.5-25

Figure IV.2. 5 Crack patterns of specimens failed in split failure mode.

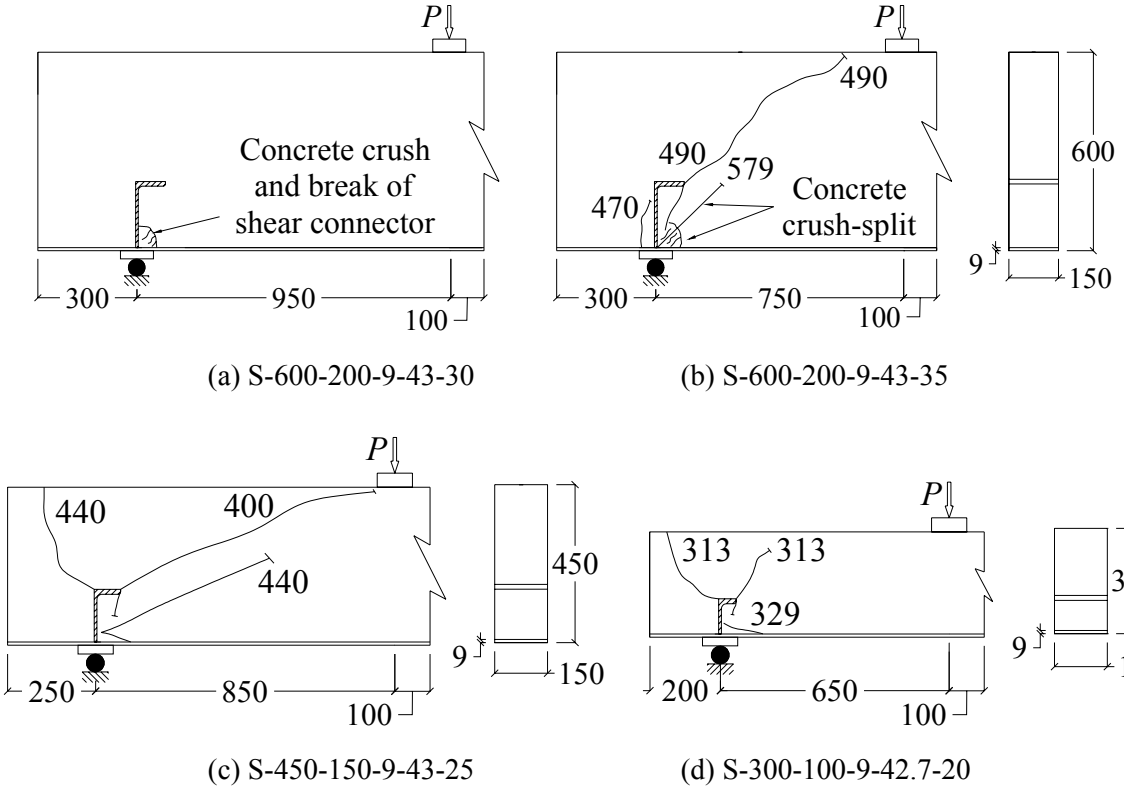

(a) S-600-200-9-43-30 (b) S-600-200-9-43-35

(c) S-450-150-9-43-25 (d) S-300-100-9-42.7-20

Figure IV.2. 6 Crack patterns of specimens failed in concrete crush and shear failure mode.

More importantly, the experimental results showed that the possibility of split failure, concrete crush or shear failure occurrences depend on the strut angle θ and the size of the shear connector. It can be seen in S-300-100-9-41.5-25 and S-300-100-9-42.7-20 whose concrete strength and size of shear connector are the same that the shear connector failed in split failure mode and in shear failure mode when strut angle θ is equal to 25^{o} and 20^{o}, respectively. Meanwhile, shear-split failure mode and split failure mode appeared when h_{sc} = 150 mm and h_{sc} = 100 mm,

respectively despite the same concrete strength and strut angle, S-450-150-9-43-25 and S-300-100-9-41.5-25.

a) Border Line between Split Failure Mode and Concrete Crush or Shear Failure Mode

It was found that the strut angle θ and the size of the shear connector influenced not only the failure modes of the shear connectors, but also the shear resisting mechanism. **Fig.IV.2.7** gives the relationships between shear force and strain in the vertical part of the shear connectors in 2nd test series specimens. It can be seen that for the same size shear connectors, tensile strains in the shear connectors with smaller strut angle were found much greater value than those with bigger strut angle. It means that the shear connectors with smaller strut angle or the shear connectors which failed in concrete crush or shear failures modes resisted against an uplifting mechanism.

Furthermore, as shown in **Fig.IV.2.7(a)**, when $t_{1,sc}/h_{sc}$ is equal to 0.09, the shear connectors were found to have different shear resisting mechanism and were found to fail in shear failure mode and split failure mode between strut angle $\theta = 20^{o}$ and $\theta = 25^{o}$. These results indicated that the border of split failure modes and shear failure modes of L-shape shear connector subjected to strut compressive force located between 20^{o} and 25^{o} of strut angle when $t_{1,sc}/h_{sc} = 0.09$. Similarly, for S-450-150-9-43-25 and S-450-150-9-43-30 shown in **Fig.IV.2.7(b)**, shear-split failure mode and split failure mode occurred when the strut angle $\theta = 25^{o}$ and $\theta = 30^{o}$, respectively. It would mean that the border of split failure mode and shear failure mode located between 25^{o} and 30^{o} of strut angle when $t_{1,sc}/h_{sc} = 0.06$. Additionally, concrete crush and concrete crush with splitting crack were observed in S-600-200-9-43-30 and S-600-200-9-43-35, respectively. These different failure modes and different shear resisting mechanisms of the shear connectors shown in **Fig.IV.2.7(c)** also indicated that the border line between split failure mode and shear failure modes is reasonably located between the strut angle of 30^{o} and 35^{o} when $t_{1,sc}/h_{sc} = 0.045$. These experimental results showed that thickness to height ratio of the shear connector $t_{1,sc}/h_{sc}$ and strut angle θ controlled the final failure mode of L-shape shear connector subjected to strut compressive force. It also means that the experimental results of 2nd test series specimens confirmed the border line between split failure zone and concrete crush or shear failure zone observed in the FEM analyses during the experimental preparation.

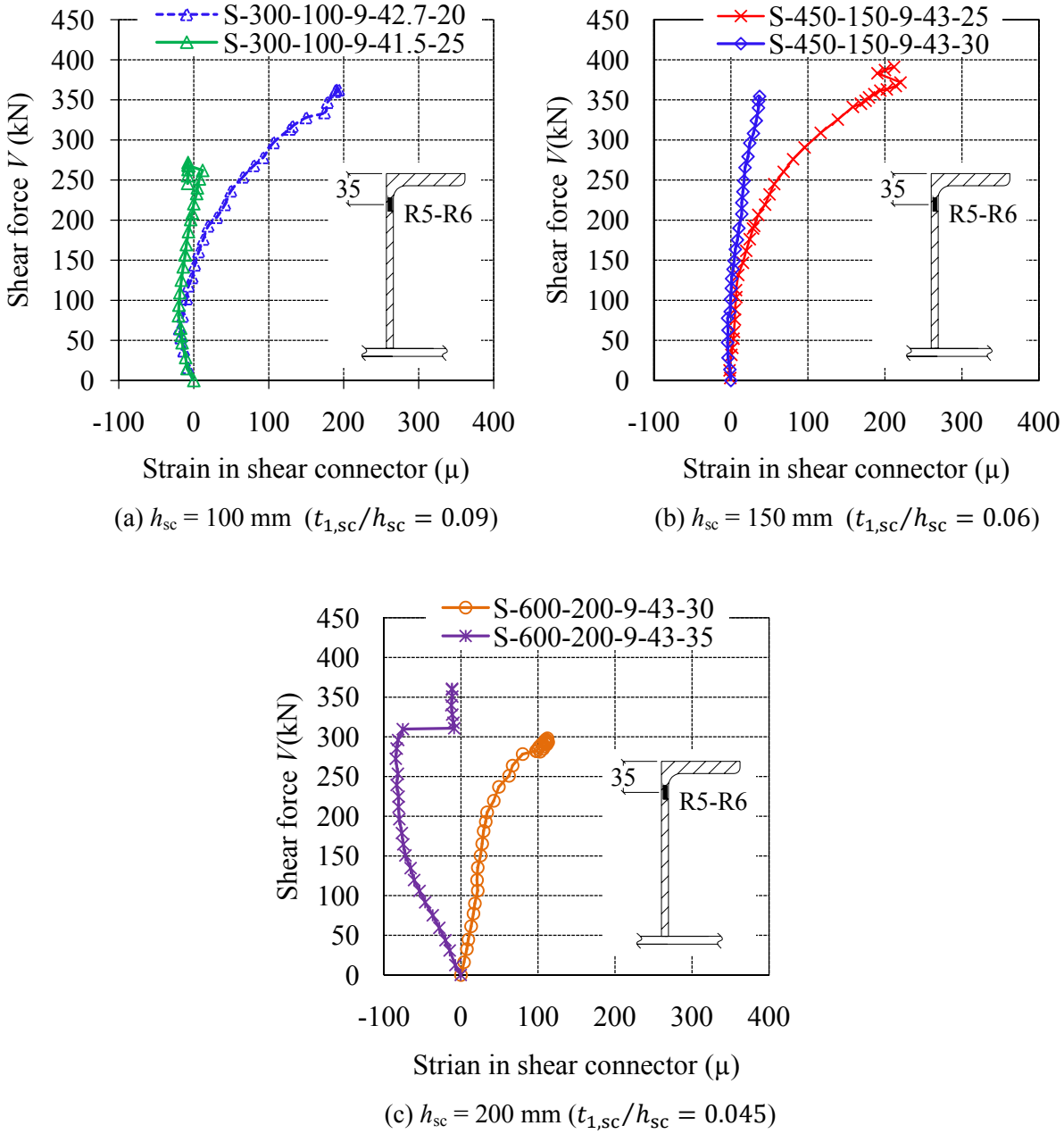

(a) h_{sc} = 100 mm $(t_{1,sc}/h_{sc} = 0.09)$ (b) h_{sc} = 150 mm $(t_{1,sc}/h_{sc} = 0.06)$

(c) h_{sc} = 200 mm $(t_{1,sc}/h_{sc} = 0.045)$

Figure IV.2. 7 Relationships between shear force and strain in the vertical part of the shear connectors in 2nd series specimens.

Therefore, an equation for a critical strut angle θ_o representing the border between split failure modes and concrete crush or shear failure modes can be reasonably developed from the experimental results of 2nd test series specimens which is a function of $t_{1,sc}/h_{sc}$. The relationships between θ and $t_{1,sc}/h_{sc}$ are given in **Fig.IV.2.8**. The equation of the critical strut angle $\theta_o$can be given as follows:

$$\theta_o = -210\left(\frac{t_{1,sc}}{h_{sc}}\right) + 41 \qquad \text{Eq. IV. 6}$$

Where,

θ_o : critical strut angle (degree),

$t_{1,sc}$: thickness of the shear connector (mm),

h_{sc} : height of the shear connector (mm).

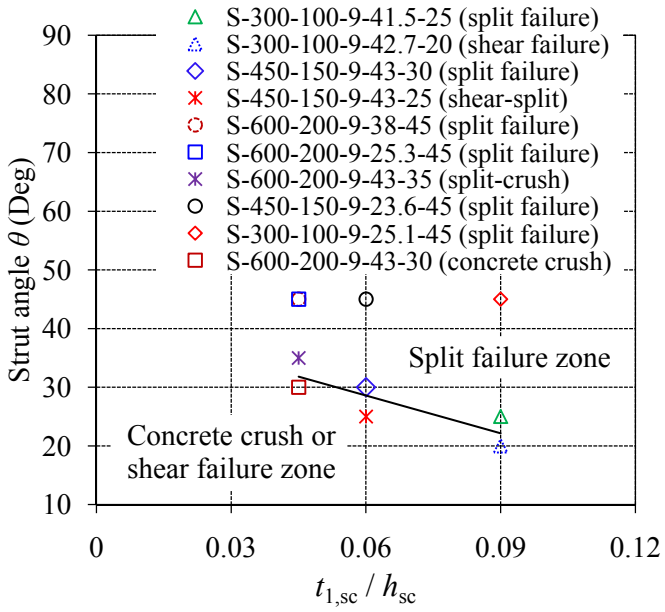

Figure IV.2. 8 Relationships between shear force and strain in the vertical

It means that split failure mode and concrete crush or shear failure mode of L-shape shear connector occurred when strut angle $\theta > \theta_o$ and $\theta \leq \theta_o$, respectively.

Additionally, the different performance of L-shape shear connectors failed in split failure mode and in concrete crush or shear failure mode can be simply illustrated by **Fig.IV.2.9** and **Fig.IV.2.9**, respectively. As shown in **Fig.IV.2.8(a)**, when $\theta > \theta_o$ the concrete in front of the shear connector seemed to resist against multi-direction stresses; and the release of the principal tensile stress σ_t of the concrete depended on the relative displacement of the shear connector. Then, when the relative displacement reached its ultimate value δ_u, splitting crack took place in the concrete along the compressive strut axis perpendicular to the principal tensile stress

direction, **Fig.IV.2.9(b)**. Differently, as shown in **Fig.IV.2.10(a)**, when $\theta \leq \theta_o$ the concrete in front of the shear connector tried to escape from the crushing point along the direction of the principal tensile stress σ_t. This mechanism induced vertical confinement of concrete in front of the shear connector and resulted in high tensile stress or tensile strain in the vertical part of the shear connector shown in **Fig.IV.2.7**. Furthermore, due to the vertical confinement upon the concrete in front of the shear connector, due to the relative displacement of the shear connector, and due to the strut compressive force with $\theta \leq \theta_o$, the concrete in front of the shear connector failed in concrete crush or shear failure mode at ultimate relative displacement $\delta_u$of the shear connector and at a shear compressive stress τ forming a shear plane as shown in **Fig.IV.2.4(b), Fig.IV.2.4(c),** and **Fig.IV.2.10(b)**.

Additionally, it is not easy to distinguish split failure mode from shear-split failure mode. However, these two failure modes can be distinguished by observing the appearance of the shear crack at the toe of the shear connector as shown in **Fig.IV.2.4(b) & (c)** and **Fig.IV.2.6(c) & (d)**. The appearance of shear plane indicated the changing of failure mode of the concrete in front of the shear connector due to the decrease of strut angle. Moreover, the differences in tensile strain in the vertical part of the shear connector as shown in **Fig.IV.2.7** also showed the changing of shear resisting mechanisms of the shear connectors. When the strut angle was small enough e.g. S-300-100-42.7-20 ($\theta = 20^o$), only shear plane appeared in front of the shear connector as shown in **Fig.IV.2.4(c)** and **Fig.IV.2.6(d)** and this shear failure mode is quite different from split failure mode shown in **Fig.IV.2.4(a)** and **Fig.IV.2.5**.

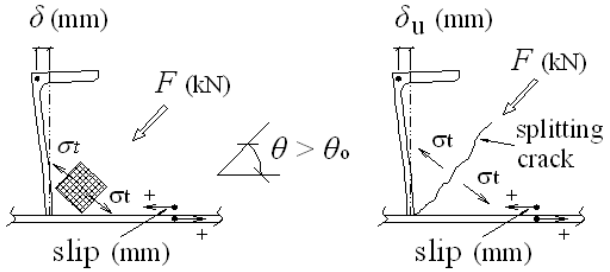

(a) Before split failure (b) At split failure

Figure IV.2. 9 L-shape shear connector with ($\theta > \theta_o$).

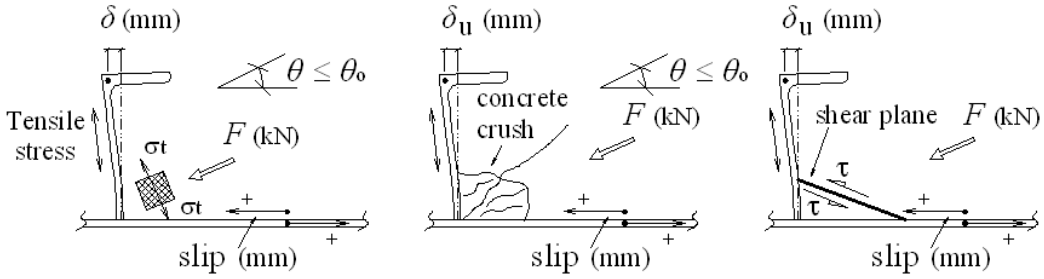

(a) Before shear failure (b) At concrete crush or shear failure

Figure IV.2. 10 L-shape shear connector with ($\theta \leq \theta_o$).

IV.2.4 Ultimate Shear Force of L-shape Shear Connector ($\boldsymbol{\theta \leq 45^o}$)

Table IV.2.1 gives the summary of the ultimate shear forces $V_{u.exp}$ obtained from the experimental results and the calculation results V_{sc1} by means of the guidelines for performance verification of steel-concrete hybrid structures of JSCE (2006) [1] with all safety factors 1.0. Meanwhile, since there is only one shear connector in the shear span, the spacing of the shear connector used to calculate V_{sc1} was infinite. It can be observed that V_{sc1} agreed with $V_{u.exp}$ by chance for 1st series shear connectors with $V_{u.exp}$ to V_{sc1} ratios varied from 1.02 to 1.11. However, $V_{u.exp}$ to V_{sc1} varied from 1.37 to 1.69 for 2nd series shear connectors whose strut angles were small. These results showed that the formula given by the guidelines for performance verification of steel-concrete hybrid structures of JSCE (2006) [1] can conservatively predict the shear capacity of the shear connector.

However, the value of $V_{u.exp}$ to V_{sc1} ratio is up to 1.69 which means that the shear capacity of L-shape shear connector calculated by means of the formula given by JSCE (2006) [1] is too conservative when the strut angle is small. Therefore, new formulas for the ultimate shear forces of L-shape shear connectors V_u failed in split failure mode and in concrete crush or shear failure mode are necessary.

Table IV.2. 1 Ultimate shear force of shear connector obtained from experiment and calculation results.

Specimens	Final failure mode	$V_{u.exp}$ (kN)	V_{sc1} (kN)	$V_{u.exp} / V_{sc1}$
S-600-200-9-38-45	Split failure	266	240	1.11
S-600-200-9-25.3-45	Split failure	200	195	1.02
S-450-150-9-23.6-45	Split failure	182	171	1.06
S-300-100-9-25.1-45	Split failure	170	154	1.11
S-600-200-9-43-35	Split-concrete crush failure	362	254	1.42
S-450-150-9-43-30	Split failure	357	231	1.54
S-450-150-9-43-25	Shear-split failure	391	231	1.69
S-300-100-9-41.5-25	Split failure	272	198	1.37
S-300-100-9-42.7-20	Shear failure	360	202	1.63

IV.2.5 Ultimate Shear Force of Shear Connector, Split Failure Mode ($\theta_o < \theta \leq 45^o$)

The ultimate shear force V_u of L-shape shear connector at split failure occurrence was previously proposed based on the experimental results of 1st test series specimens mentioned in the previous subchapter that the concrete in which splitting crack occurred was assumed to behave like a cylinder in the split tensile strength test, Eq.IV.4.

It can be seen in **Table IV.2.2** that Eq.IV.4 can precisely predict the ultimate shear forces only in case $\theta = 45^o$. However, this equation was found to underestimate the ultimate shear force when $\theta < 45^o$, S-300-100-9-41.5-25 that $V_{u.exp}$ to $V_{u.Eq4}$ ratio was equal to 1.25.

Table IV.2. 2 Ultimate shear forces obtained from experiments and calculations by means of Eq.IV.4 and Eq.IV.7.

Specimens	θ (deg)	f_c' (N/mm^2)	$V_{u.exp}$ (kN)	$V_{u.Eq4}$ (kN)	$V_{u.exp} / V_{u.Eq4}$	$V_{u.Eq7}$ (kN)	$V_{u.exp} / V_{u.Eq7}$
S-600-200-9-38-45	45	38	266	254	1.05	256	1.04
S-600-200-9-25.3-45	45	25.3	200	207	0.96	209	0.96
S-450-150-9-23.6-45	45	23.6	180	182	0.98	184	0.98
S-300-100-9-25.1-45	45	25.1	170	169	1.00	171	0.99
S-300-100-9-41.5-25	25	41.5	272	218	1.25	282	0.97

Therefore, the revision of Eq.IV.4 is necessary. It can be observed in the previous model of (Ros and Shima, 2010 [20]), **Fig.IV.2.11(a)** that the strut compressive force on the shear connector was equal to $V_u\sqrt{2}$ which is equal to $(V_u/\cos 45)$. It means that $\cos 45$ was included in the equation of k_1, Eq.IV.3. That is why Eq.IV.2 cannot predict the ultimate shear forces of the shear connector when the strut angle $\theta < 45^o$. Therefore, the authors decided to remove $\cos 45$ from the equation of k_1, Eq.IV.3 and keep $\cos\theta$ in Eq.IV.4, **Fig.IV.2.11(b)**. Eq.IV.4 and Eq.IV.3 can be replaced by Eq.IV.7 and Eq.IV.8, respectively.

$$V_u = k_1 \times \sqrt{f_c'} \times b_{sc} \times h_{sc} \times \cos\theta \qquad \text{Eq.IV.7}$$

$$k_1 = 28 \times \left(\frac{t_{1,sc}}{h_{sc}}\right) + 0.70 \qquad \text{Eq. IV. 8}$$

Where,

V_u : ultimate shear force in split failure mode (N),

b_{sc} : width of shear connector (mm),

h_{sc} : height of shear connector (mm),

$t_{1,sc}$: thickness of shear connector (mm),

f_c' : concrete compressive strength (N/mm^2),

θ : strut angle ($\theta > \theta_o$) (degree)

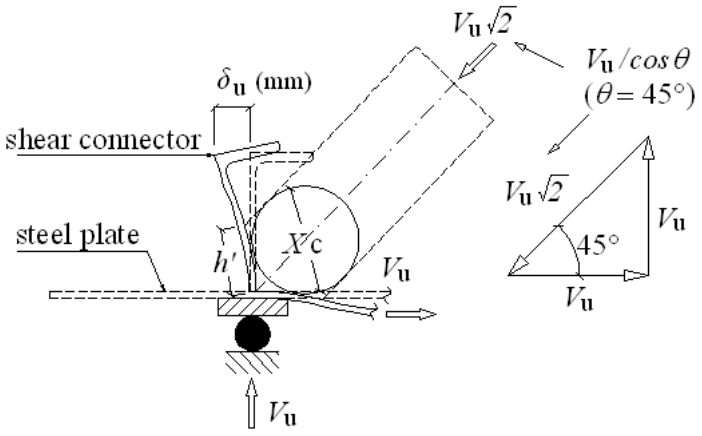

a) Previous consideration with $\theta = 45^o$

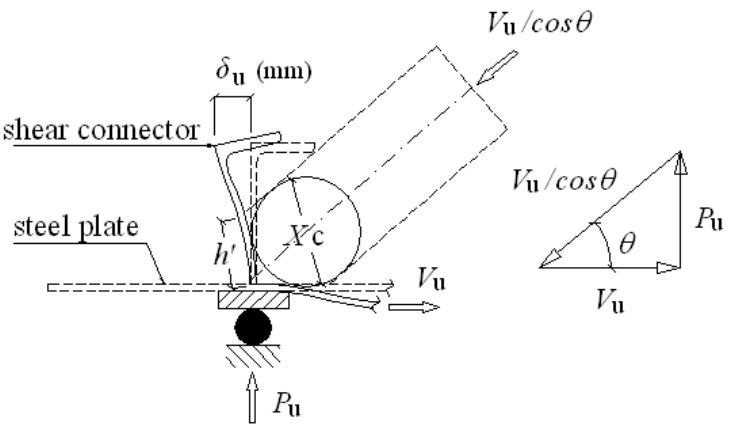

b) New consideration with $\theta_o < \theta \leq 45^o$

Figure IV.2. 11 Model of L-shape shear connector failed in split failure mode.

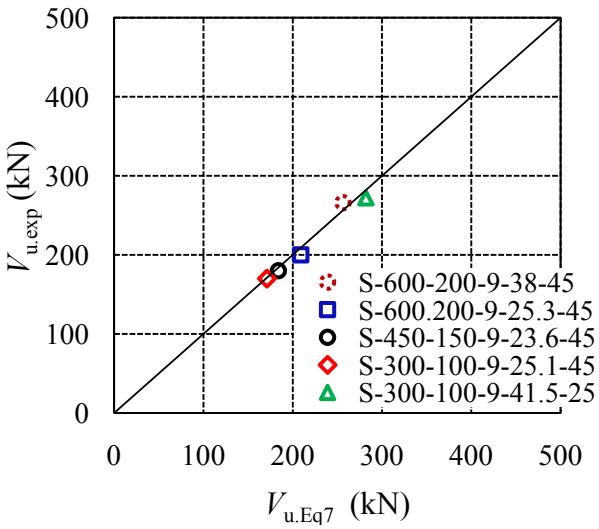

Figure IV.2. 12 Ultimate shear force of shear connectors in split failure mode.

As shown in **Table IV.2.2** and **Fig.IV.2.12**, Eq.7 can precisely predict the ultimate shear forces of L-shape shear connector at split failure occurrence under different strut angle with $V_{u.exp}$ to $V_{u.Eq7}$ ratio varied from 0.96 to 1.04. However, when $\theta \leq \theta_o$ the shear connectors were found to fail in concrete crush or shear failure modes. Therefore, another formula for ultimate shear force of L-shape shear connector at concrete crush or shear failure mode is necessary.

IV.2.6 Ultimate Shear Force of Shear Connector in Concrete Crush/Shear Failure Mode

Three specimens of the 2nd test series were found to fail in concrete crush or shear failure modes, **Fig.IV.2.4**. A shear plane was clearly observed in front of the shear connector, **Fig.IV.2.13(b)**; also the shear connectors were found to resist against an uplifting mechanism. Therefore, a simplified model of L-shape shear connector in shear failure mode was developed as illustrated in **Fig.IV.2.13(a)**. At failure, shear plane resisted against the shear compressive stress τ, ($\tau = 1.25\sqrt{f_c'}$, JSCE, 2006 [1]) and the ultimate shear force at shear failure occurrence can be expressed as followings:

$$V_1 - V_2 = \tau \times b_{sc} \times l \qquad \text{Eq.IV.9}$$

Where,

τ: shear compressive stress (N/mm^2),
l: length of shear plane (mm), $l = h''/\sin i$,
b_{sc}: width of the shear connector (mm).

Since $V_1 = F_1 \times \cos i$, $V_2 = F_2 \times \sin i$, $F_1 = F \times \cos\theta$, and $F_2 = F \times \sin\theta$, **Fig.IV.2.13(a)** Eq.IV.9 can be expressed as followings:

$$F \times (\cos\theta \times \cos i - \sin\theta \times \sin i) = 1.25\sqrt{f_c'} \times b_{sc} \times \frac{h''}{\sin i}$$

Or $$F \times \cos(\theta + i) = 1.25\sqrt{f_c'} \times b_{sc} \times \frac{h''}{\sin i} \qquad \text{Eq. IV. 10}$$

Since $h'' = h_{sc} \times (\tan i/\tan j)$ and $F = V_u/\cos\theta$, Eq.IV.10 can be given as followings:

$$V_u = \frac{1}{\cos i \times \cos(\theta + i) \times \tan j} \times 1.25\sqrt{f_c'} \times b_{sc} \times h_{sc} \times \cos\theta$$

Or $$V_u = k_2 \times \sqrt{f_c'} \times b_{sc} \times h_{sc} \times \cos\theta \qquad \text{Eq.IV.11}$$

That k_2 is the constant representing other controlling factors which can be calculated by Eq.IV.12.

$$k_2 = \frac{V_u}{\sqrt{f_c'} \times b_{sc} \times h_{sc} \times \cos\theta} \qquad \text{Eq. IV. 12}$$

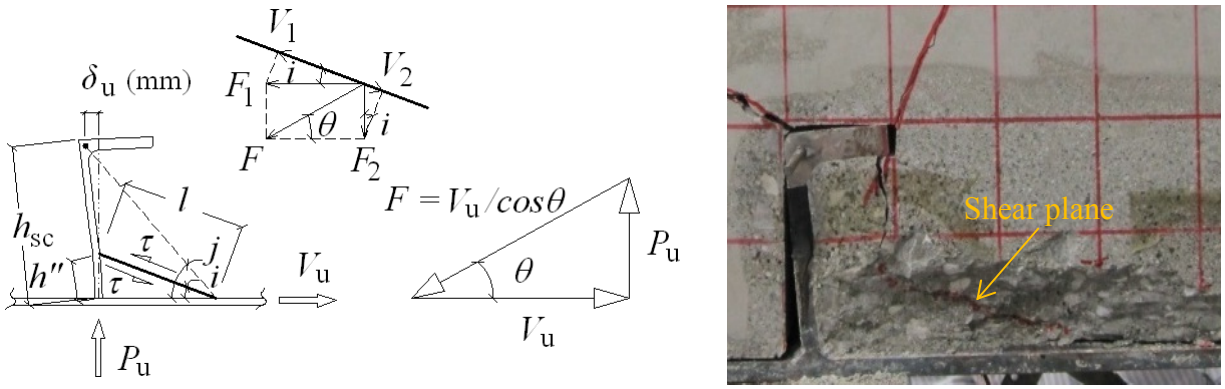

(a) Model of shear connector in shear failure mode (b) Tested specimen in shear failure mode

Figure IV.2. 13 L-shape shear connector in shear failure mode.

Table IV.2.3 gives the values of k_2 obtained from Eq.IV.9 where V_u is the ultimate shear force of shear connector failed in shear failure modes or by concrete crush observed during the experiments. Moreover, it has been known that the strength of the shear connector is highly influenced by its thickness to height ratio $t_{1,sc}/h_{sc}$. Meanwhile, the angle i and j varied depending on the $t_{1,sc}/h_{sc}$. Therefore, the values of k_2 are reasonably influenced by the values of $t_{1,sc}/h_{sc}$. The relationships between k_2 and $t_{1,sc}/h_{sc}$ of the shear connectors failed in shear failure mode or by concrete crush were plotted against those between k_1 and $t_{1,sc}/h_{sc}$ of shear connectors failed in split failure mode as given in **Fig.IV.2.14**. It can be seen two different lines of k_1 and k_2 which represent the two different failure modes mentioned in the previous subchapter. Particularly, the values of k_2 linearly increases with the values of $t_{1,sc}/h_{sc}$ whose equation can be expressed as follows:

$$k_2 = 36 \times \left(\frac{t_{1,sc}}{h_{sc}}\right) + 0.66 \qquad \text{Eq. IV. 13}$$

Table IV.2. 3 The values of k_2 obtained from Eq.IV.12.

Specimens	$t_{1,sc}$ (mm)	h_{sc} (mm)	$t_{1,sc}/h_{sc}$	θ (deg)	f_c' (N/mm^2)	V_u (kN)	k_2
S-600-200-9-43-30	9	200	0.045	35	43.0	362	2.25
S-450-150-9-43-25	9	150	0.06	25	43.0	391	2.92
S-300-100-9-42.7-20	9	100	0.09	20	42.7	360	3.91

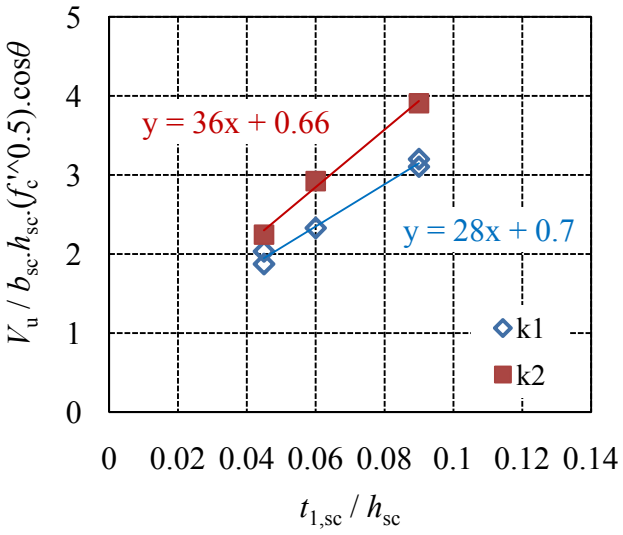

Figure IV.2. 14 Relationship between k_2 and $t_{1,sc}/h_{sc}$.

Therefore, the ultimate shear force of L-shape shear connector at concrete crush or shear failure mode can be given as followings:

$$V_u = k_2 \times \sqrt{f_c'} \times b_{sc} \times h_{sc} \times \cos\theta \qquad \text{Eq.IV.14}$$

$$k_2 = 36 \times \left(\frac{t_{1,sc}}{h_{sc}}\right) + 0.66$$

Where,

V_u : ultimate shear force in shear failure mode or by concrete crush (N),
b_{sc} : width of shear connector (mm),
h_{sc} : height of shear connector (mm),
$t_{1,sc}$: thickness of shear connector (mm),
f_c' : concrete compressive strength (N/mm^2),
θ : strut angle ($\theta \leq \theta_o$) (degree).

Table IV.2.4 gives the values of the ultimate shear forces obtained from the experimental results $V_{u.exp}$ and those calculated by means of Eq.IV.14 $V_{u.Eq14}$. As shown in **Fig.IV.2.15** and **Table IV.2.4**, Eq.IV.14 can precisely predict the ultimate shear force with $V_{u.exp}$ to $V_{u.Eq14}$ ratio 0.99 to 1.04.

Table IV.2. 4 Calculated ultimate shear force $V_{u.exp}$ and $V_{u.Eq14}$.

Specimens	$V_{u.exp}$ (kN)	$V_{u.Eq14}$ (kN)	$V_{u.exp} / V_{u.Eq14}$
S-600-200-9-43-35	362	367	0.99
S-450-150-9-43-25	391	377	1.04
S-300-100-9-42.7-20	360	359	1.00

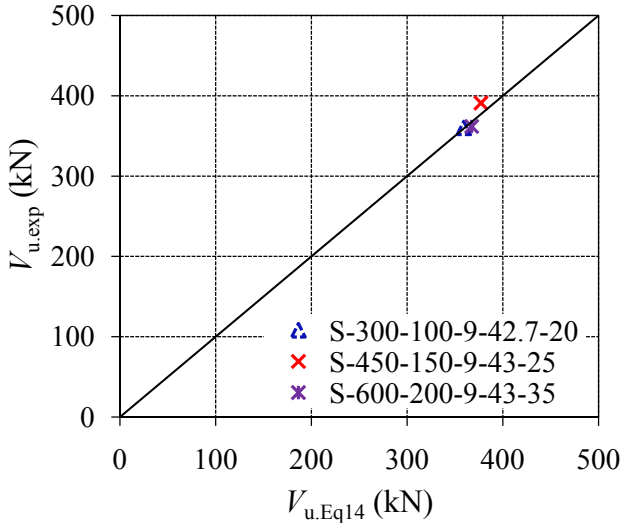

Figure IV.2. 15 Comparison between $V_{u.Eq14}$ and $V_{u.exp}$.

Therefore, the ultimate shear capacity of shear connector in split failure mode and in concrete crush or shear failure mode can be predicted through Eq.IV.7 and Eq.IV.14, respectively. However, it is difficult to determine the strut angle in the design work for a real structure; therefore, the strut angle which gives conservative strength of the shear connector should be selected. Since, the applicable ranges of the proposed equations are in the interval of strut angle ($20^o \leq \theta \leq 45^o$), the strut angle of 45° is recommended for conservative strength. In additions, the maximum height of shear connector applicable for the proposed equation was h_{sc} = 400mm which is large enough for L-shape shear connector sizes available on market.

Additionally, the equation of V_u can be expressed as follows:

$$V_{\mathrm{u}} = \begin{cases} \left(28t_{1,sc} + 0.70h_{sc}\right) \times \sqrt{f_{\mathrm{c}}'} \times b_{\mathrm{sc}} \times \cos\theta & (Split\ failure) \\ \left(36t_{1,sc} + 0.66h_{sc}\right) \times \sqrt{f_{\mathrm{c}}'} \times b_{\mathrm{sc}} \times \cos\theta & (Shear\ failure) \end{cases} \quad \text{Eq.IV.15}$$

Based on these expressions, the effect of thickness $t_{1,\mathrm{sc}}$ and height h_{sc} of shear connector on its shear capacity can be clearly observed. $t_{1,\mathrm{sc}}$ was found to have much higher effect on the shear capacity than h_{sc}.

Furthermore, only the ultimate shear capacity of the shear connector is not enough to fully understand the performance of the shear connector. Therefore, shear force-slip relationships and shear force-relative displacement relationships of the shear connector are also discussed in the following sub-chapters.

IV.2.7 Shear Force-Slip Relationship of L-shape Shear Connector ($\theta \leq 45^o$)

The relationships between shear force and concrete-skin plate slip in front of the shear connector of 1st and 2nd test series specimens are given in **Fig.IV.2.16**. The experimental results showed that the stiffness of the same size shear connectors was the same despite different concrete strength and different strut angle. However, the shear connectors with smaller strut angle were found to be capable to resist against higher level of shear forces and gave greater ultimate slip values as compared to those with greater strut angle even though the concrete strengths and the size of shear connectors are the same. Additionally, it can be said that the shear connectors which failed in concrete crush or shear failure modes gave greater values of ultimate slip than those failed in split failure modes.

Moreover, L-shape shear connectors in beam type specimens were found to have shear resistance even crack already appeared in the concrete from the head of the shear connector. These results proved the advantage of the test method as compared to push-out and pull-out test methods. Based on the experimental results of Kiyomiya et al. (1986) [6], Ueda et al. (1989) [10], and Chuah et al. (1991) [9], in push-out and pull-out tests the shear connectors were found to gradually lose their shear resisting ability after crack took place in the concrete from the head of the shear connectors. However, they also found similar behaviors of the shear connectors that the slip between concrete and skin plate in front of the shear connector occurred even under low load levels.

Furthermore, as shown in **Fig.IV.2.17**, no an effect of the height of the shear connector on shear force-slip relationships of the shear connector was observed. However, based on the

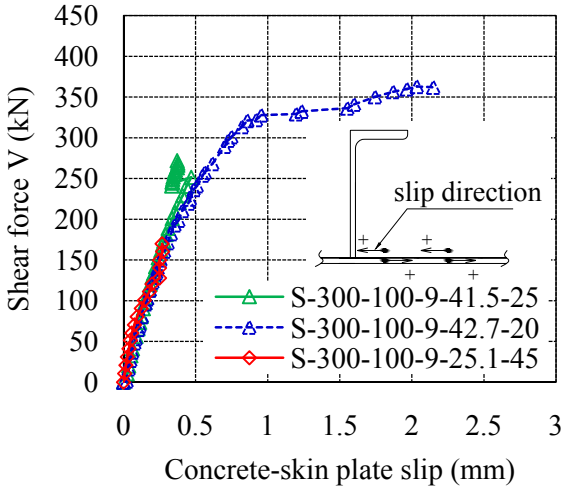

(a) h_{sc} = 100 mm

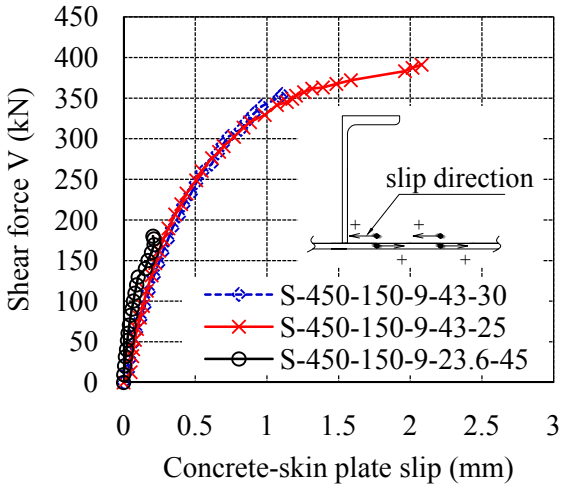

(b) h_{sc} = 150 mm

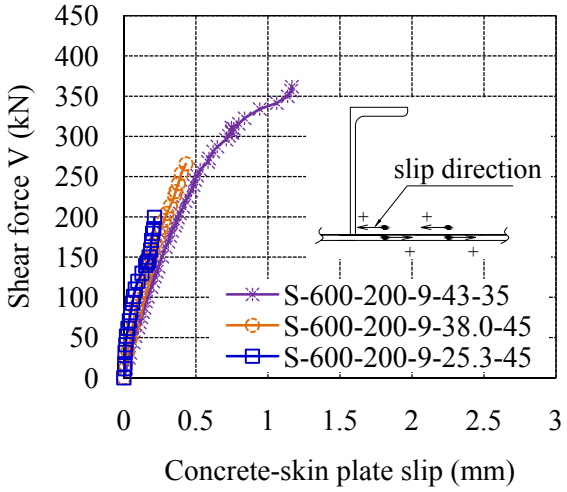

(c) h_{sc} = 200mm

Figure IV.2. 16 Shear force-slip relationships of 1st and 2nd test series shear connectors.

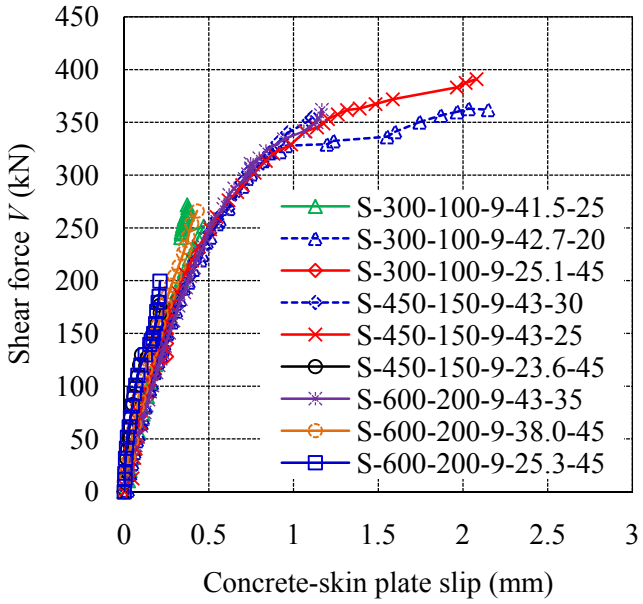

Figure IV.2.17 Shear force-slip relationships of shear connectors.

experimental results, the final failure mode of the shear connector and the strut angle were found to have effect on the ultimate shear force V_u and the ultimate concrete-skin plate slip in front of the shear connector.

IV.2.8 Shear Force-Relative Displacement Relationships ($\theta \leq 45^o$)

The relationships between shear force and relative displacement obtained from the 1st and 2nd test series specimens were compared and discussed. Shear force-relative displacement relationships of the shear connectors with h_{sc} = 100 mm and with h_{sc} = 200 mm are given in **Fig.IV.2.18** and **Fig.IV.2.19**, respectively. Big increments of relative displacement with small increments of shear force were observed after crack took place from the head of the shear connector. These showed that the stiffness of the shear connectors suddenly reduced when the first diagonal crack occurred. These similar behaviors were also found for L-shape shear connector in steel-concrete sandwich beam by (Saidi et al. 1998 [12], 1999 [13], 2008 [14]). However, differently from the steel concrete sandwich beam test, the ultimate relative displacements δ_u and the ultimate shear force V_u of L-shape shear connectors could be observed in the beam type test method.

Moreover, it can be observed in S-300-100-9-41.5-25 and S-300-100-9-42.7-20 that at the same value of relative displacement, the shear connector with smaller strut angle could resist higher level of shear force than that with greater strut angle. However, the same size shear connectors

gave similar values of ultimate relative displacement despite different strut angle, concrete strength, and final failure mode. Therefore, it can be said that the strut angle, the concrete strength, and the final failure mode were found to have no effect on the ultimate relative displacement δ_u of the shear connector but the shear resisting ability. Moreover, as shown in **Fig.IV.2.20**, the height of the shear connector was found to have effect on the ultimate relative displacement δ_u. It can be seen that the specimens with larger size shear connectors failed at greater values of ultimate relative displacements δ_u regardless of the strut angle, the concrete strength, and the final failure mode.

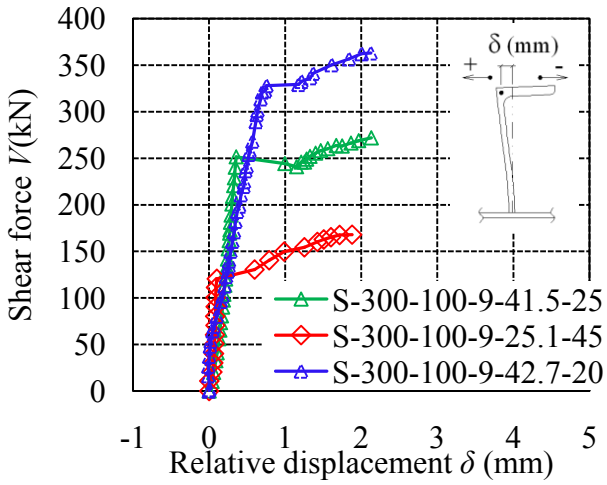

Figure IV.2. 18 $V-\delta$ relationships for $h_{sc} = 100$ mm.

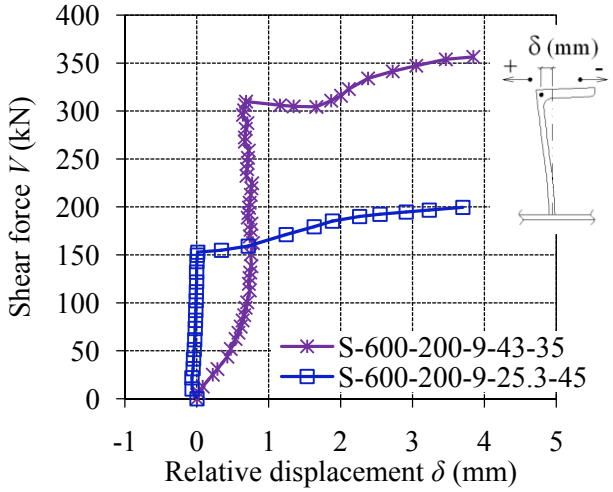

Figure IV.2. 19 $\boldsymbol{V-\delta}$ relationships for $\boldsymbol{h_{sc} = 200}$ **mm**.

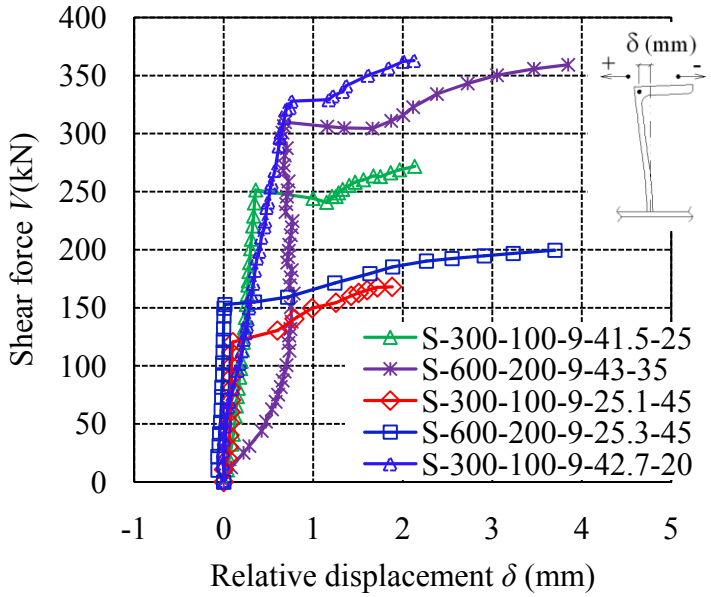

Figure IV.2. 20 $\boldsymbol{V-\delta}$ relationships of 1st and 2nd test series shear connectors.

Even though shear force-relative displacement relationships of L-shape shear connectors were clearly understood from the experimental results, the formula to predict the enveloped curve of the relationships also plays a vital role in the design. Therefore, the following sub-chapter discussed the formulation for the enveloped curve of shear force-relative displacement relationships of the shear connectors.

IV.2.9 Formulation for Shear Force-Relative Displacement Relationships ($\boldsymbol{\theta \leq 45^o}$)

The formula for shear force-relative displacement relationship of L-shape shear connector proposed in previous subchapter by means of the results from 1st test series specimens and FEM analyses for the case that strut angle θ approximately 45° and splitting crack in front of the shear connector controlled the final failure modes, Eq.IV.5. The formula was given as followings:

$$\frac{V}{V_{\mathrm{u}}} = \left(1 - e^{-180\frac{\delta}{h_{\mathrm{sc}}}}\right)^{0.6} \qquad \text{Eq. IV. 5}$$

Additionally, Eq.IV.5 was proposed for the case after the occurrence of crack from the head of the shear connector until failure of the shear connector where the shapes of the curves were clearly observed. The calculated results by means of Eq.IV.5 were compared with those obtained

CHAPTER V

CONCLUSIONS

Based on the experimental results, analyses, and discussions in the previous chapter, the followings conclusions can be obtained.

1. L-shape shear connectors subjected to strut compressive force in steel-concrete composite structures were found to have two different failure modes, split failure mode and concrete crush/shear failure mode. Meanwhile, the failure criterion of L-shape shear connector was determined by the failure criterion of concrete element in front of the shear connector.

2. The strut angle and the thickness to height ratio of the shear connector $t_{1,sc}/h_{sc}$ were found to control the final failure mode of the shear connector.

3. There existed a critical strut angle θ_o representing the border between split failure mode and concrete crush/shear failure mode of L-shape shear connector subjected to strut compressive force. Accordingly, an equation to predict the critical strut angle θ_o was developed and proposed. The equation was found to be a function of the thickness to height ratio of the shear connector which is expressed as followings:

$$\theta_o = -210\left(\frac{t_{1,sc}}{h_{sc}}\right) + 41$$

   Split failure and concrete crush/shear failure would occur when the strut angle $\theta > \theta_o$ and $\theta \leq \theta_o$, respectively.

4. The equation to predict the ultimate shear capacity V_u of L-shape shear connector subjected to strut compressive force in steel-concrete composite structures was developed and proposed for two cases of failure modes, split failure mode and concrete crush/shear failure mode. The equation was a function of the concrete strength, the width and the height of the shear connector, the strut angle, and a constant k; while the equation of constant k was a function of thickness to height ratio of the shear connector. The selection of constant k depends on the strut angle θ used comparing to the critical strut angle θ_o. The equations are expressed as followings:

$$V_{\mathrm{u}} = k \times f_t \times b_{\mathrm{sc}} \times h_{\mathrm{sc}} \times \cos\theta$$

$$k = 63 \times \left(\frac{t_{1,\mathrm{sc}}}{h_{\mathrm{sc}}}\right) + 1.60 \qquad (\text{for } \theta > \theta_o)$$

$$k = 81 \times \left(\frac{t_{1,sc}}{h_{sc}}\right) + 1.50 \qquad (\text{for } \theta \leq \theta_o)$$

The applicable ranges of the proposed equations are in the interval of strut angle ($20^o \leq \theta \leq 45^o$).

5. When the relationship between shear force V and relative displacement δ represented by the relationships between V/V_{u} and δ/h_{sc}, a unique enveloped curve of the relationships was observed regardless of the size of the shear connector, the concrete strength, and the strut angle for the case after the occurrence of crack from the head of the shear connector until failure of the shear connector.

6. An equation to predict the enveloped curved of the relationships between V/V_{u} and δ/h_{sc} of L-shape shear connector subjected to strut compressive force in steel-concrete composite structure was developed and proposed as followings:

$$\frac{V}{V_{\mathrm{u}}} = \left(1 - e^{-180\frac{\delta}{h_{\mathrm{sc}}}}\right)^{0.6}$$

The enveloped curved was proposed for the case after the occurrence of crack from the head of the shear connector until failure of the shear connector.

7. The ultimate relative displacements δ_{u} of L-shape shear connectors were found approximately 0.02 times the height of the shear connector regardless of the concrete strength and the strut angle.

The equation to predict the enveloped curve of the shear force-relative displacement relationship of the shear connector was proposed only after the occurrence of crack from the head of the shear connector. However, by means of this equation, the ultimate state of partial interaction mechanism of the shear connector which is important for the design can be understood. Additionally, the performances and the formulations for L-shape shear connector found in this study were found only for the shear connector whose direction is opposite of the direction of shear force. Therefore, further study should be taken into account the effects of the direction of the shear connector.

REFERENCES

1) JSCE, (2006). "Guideline for performance verification of steel-concrete hybrid structures." Hybrid Structure Series 2, Japan Society of Civil Engineers.
2) Japanese Society of Civil Engineer (2009). "Standard specifications for hybrid structure", JSCE. (in Japanese)
3) JSCE Research Subcommittee on Steel-Concrete Sandwich Structures (1992). "Design code for steel-concrete sandwich structures – Draft", Concrete Library of JSCE, No. 20, 1-21.
4) Sakai, F., Yabe, J., Ohgaki, K., Hashimoto, Y. and Tomoda, T. (1995). "A study on three dimensional characteristics of composite bridges with two plate girders. *Journal of Structure Engineering*, JSCE, Vol.41A.
5) Sakai, F., Yabe, J., Ohgaki, K. and Hashimoto, Y. (1997). "A study on positioning of cross beam in composite two-plate-girder bridges", *Bridge and Foundation*, Vol.31, No.3, 31-38.
6) Kiyomiya, O. and Yokota, H. (1986). "Strength of shear connector by shape steel in composite member with steel and concrete", *Proc. of Symposium on Research and Application of Composite Constructions, JSCE*, 113-118.
7) Kimura, H., Kojima, K., and Kiyomiya, O. (1993). "Influence of Test Methods to Ultimate Strength of Shaped Steel Shear connector", Proc. of The 48th Annual Conference of The Japan Society of Civil Engineers, V, 20-21. (in Japanese).
8) Chin, C. K. and Ueda, T. (1989). "Experimental study on plate shear connector for composite construction", *Proc. of The Second East Asia-Pacific Conference on Structural Engineering and Construction*, Vol.1, 651-656.
9) Chuah, C.L., Shima, H., and Virach, R. (1991). "Load-displacement relationship of plate shear connector in steel-concrete composite structure." *Proc. of JSCE*, No. 433/V-15, 223-229.
10) Ueda, T. and Chin, C.K. (1989). "Strength of steel plate shear connector." *Proc. Of Second Symposium on Research and Application of Composite Constructions, JSCE*, 149-156. (in Japanese)
11) Makabe, T., Malek, N., Mutsuyoshi, H. and Machida, A. (1992). "Experimental Study on Mechanical Properties of Steel and Concrete Sandwich Beam", *J. of Structural Div., JCI*, Vol.14, 729-733.
12) Saidi, T., Furuuchi, H., and Ueda, T. (1998). "Relationship between transferred shear force and relative displacement of shear connector in steel-concrete sandwich beam." *Journal of*

Structural Engineering, JSCE, 44 (A), 1537-1545.

13) Saidi, T., Furuuchi, H. and Ueda, T. (1999). "Effect of shape and location of shear connector on its transferred shear force and relative displacement relationship in steel-concrete sandwich beam." *Journal of Structural Engineering, JSCE,* 45 (A), 1451-1459.

14) Saidi, T., Furuuchi, H., and Ueda, T. (2008). "The transfer shear force-relative displacement relationship of the shear connector in steel-concrete sandwich beam and its model." *Doboku Gakkai Ronbunshuu, E, JSCE,* Vol.64, No.1, 122-141.

15) Ollgaard, J., Slutter, R. and Fisher, J. (1971). "Shear strength of stud connectors in lightweight and normal-weight concrete", AISC Engineering Journal, 55-64.

16) Shima, H. and Watanabe, S. (2009). "Formulation for Load-Slip Relationships of Headed Stud Connector, *Proc. Of fib2009*, 22-24, London.

17) Ros, S. and Shima, H. (2009): "New beam type test method for load-slip relationship of L-shape shear connector," *Proc. of 8th Symposium on Research and Application of Hybrid and Composite Structures JSCE,* Tokyo, Japan.

18) Ros, S. and Shima, H. (2009): "Finite Element Analyses for Performance of L-shape Shear Connector Subjected to Strut Compressive Force in Beam Type Specimen" AIJ Shikoku Chapter Architectural Research Meeting, No.10, Kochi.

19) Ros, S. and Shima, H. (2010). "Behaviors of L-shape shear connector subjected to strut compressive force in beam type test specimens." *Proceeding of the Japan Concrete Institute, JCI,* Vol.32, No.2, 1195-1200.

20) Ros, S. and Shima, H. (2010). "Shear force-horizontal relative displacement relationship of L-shape shear connector subjected to strut compressive force in steel-concrete composite structures." *Doboku Gakkai Ronbunshuu A, JSCE*, Vol. 66, No.4, 767-782.

21) Ros, S. and Shima, H. (2010): "Formulation for maximum shear force of L-shape shear connector subjected to strut compressive force at splitting crack occurrence in steel-concrete composite structures," The Twelfth East Asia-Pacific Conference on Structural Engineering and Construction, *EASEC-12.*

22) Ros, S. and Shima, H. (2011). "Effect of strut angle on the behavior of L-shape shear connector subjected to strut compressive force in steel-concrete composite structures." *Journal of Structural Engineering, JSCE,* Vol. 57A, 987-995.

23) Ros, S. and Shima, H. (2010). "Formulation for shear force-relative displacement relationship of L-shape shear connector in steel-concrete composite structures." *Journal of Advanced Concrete Technology, ACT.* (Accepted May-2011)

24) Ros, S. and Shima, H. (2011). "Shear force-relative displacement relationship of L-shape shear connector." Annual Join Convention, *JCI,* Vol.33, No.2, 1219-1224.

25) JSCE Committee on Revision of the Standard Specification for Concrete Structure: Standard Specification for concrete Structures-2002, "Material and Construction", *JSCE Guideline for Concrete*, No.6, pp.64, November 2005.

26) Okamura, H. and Maekawa, K. "Nonlinear Analysis and Constitutive Models of Reinforced Concrete", January 1997. (in Japanese)

APPENDIX III.1

Stress-strain relationships of the steels used in the experiments

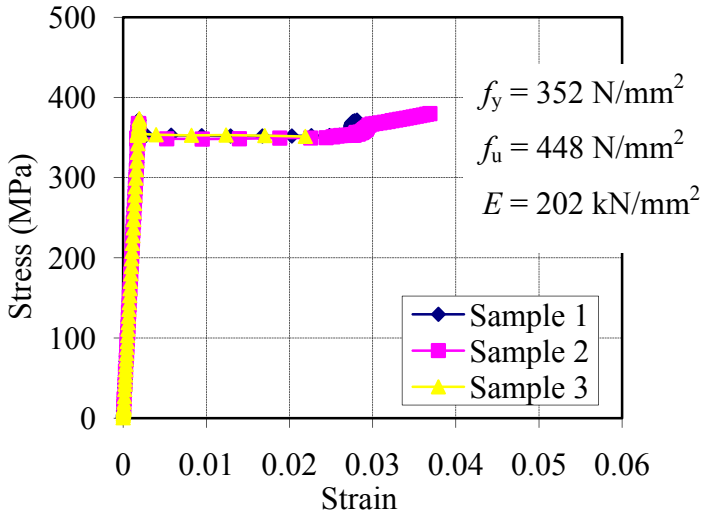

Fig.A.III.1 Stress-strain relationship of L-shape shear connector SS400

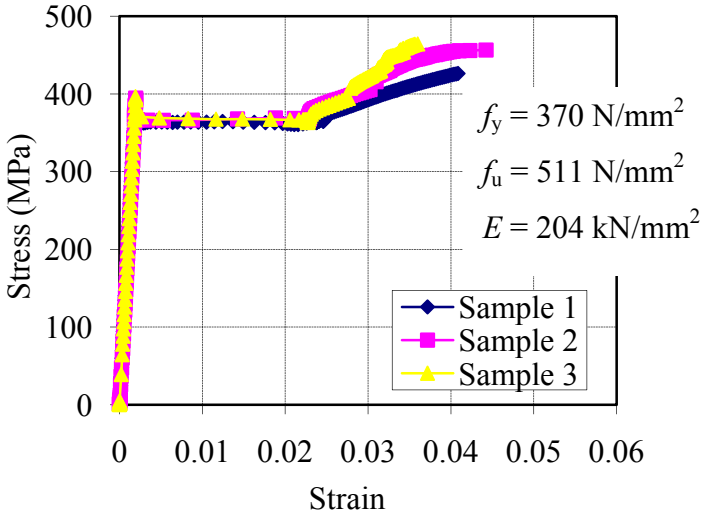

Fig.A.III.2 Stress-strain relationship of steel skin plate SM490

APPEXDIX III.2

The activities of concrete work, form work and experimental set-up

Fig.A.III.3 Concrete work, form work, and experimental set-up

APPENDIX IV.1

Conditions of 1st series specimens at failure

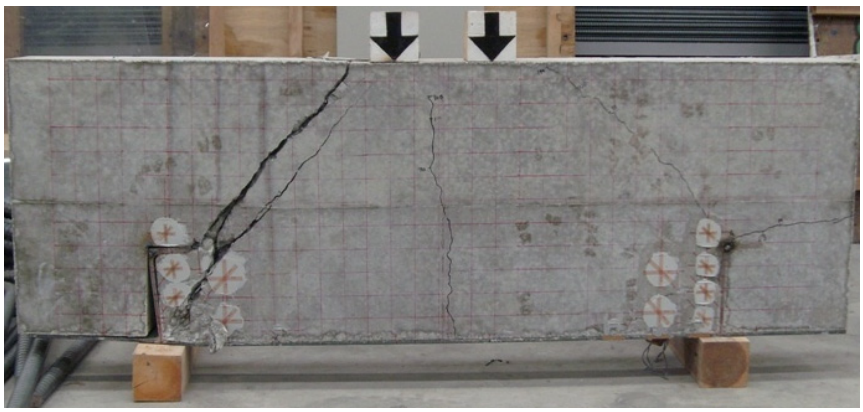

Fig.A.IV.1 Specimen S-600-200-9-38-45 at failure

Fig.A.IV.2 Specimen S-600-200-9-25.3-45 at failure

Fig.A.IV.3 Specimen S-450-150-9-23.6-45 at failure

Fig.A.IV.4 Specimen S-300-100-9-25.1-45 at failure

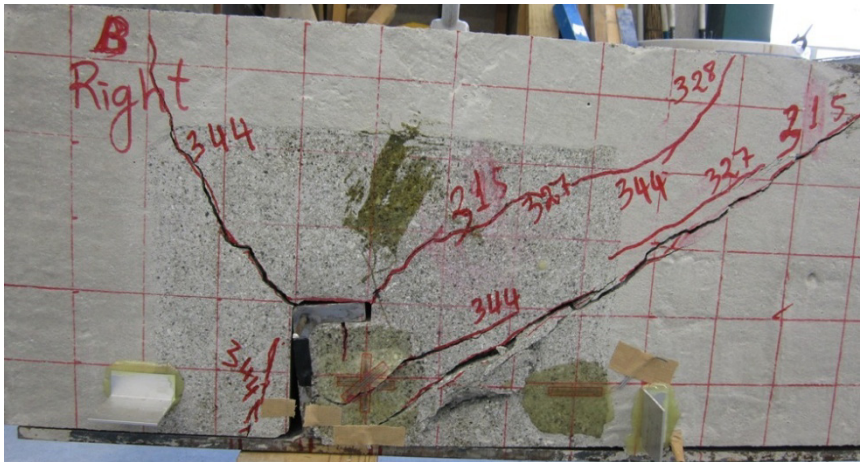

Fig.A.IV.5 Specimen S-300-100-9-41.5-25 at failure

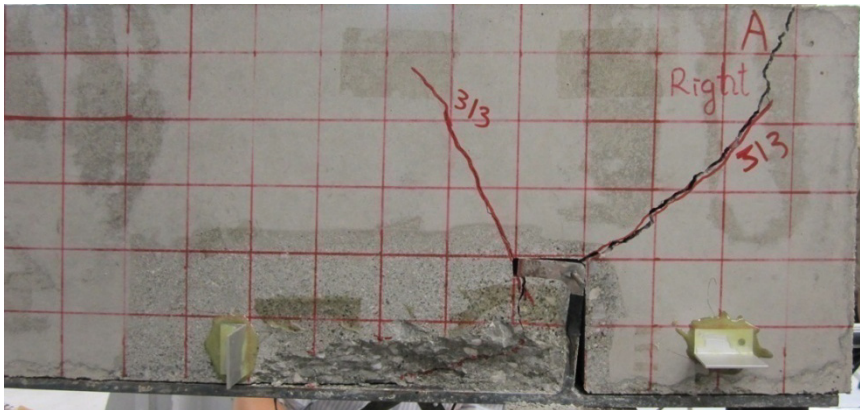

Fig.A.IV.6 Specimen S-300-100-9-42.7-20 at failure

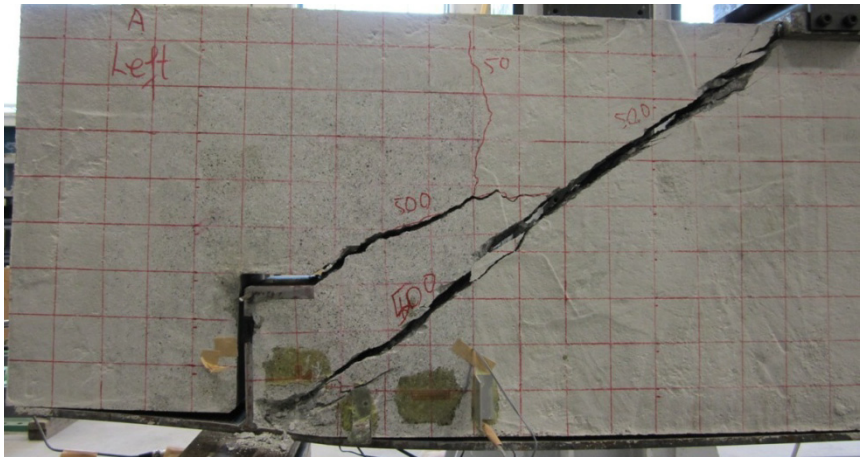

Fig.A.IV.7 Specimen S-450-150-9-43-30 at failure

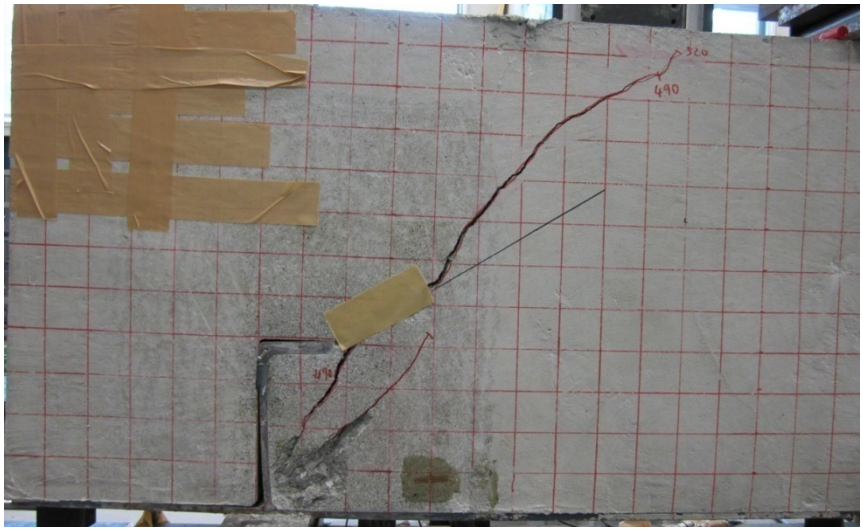

Fig.A.IV.8 Specimen S-600-200-9-43-35 at failure

APPENDIX IV.2

Linear relationships between load P (kN) and tensile strain in the skin plate show that the steel plate was still in elastic range. The lists of strain data are given in **Table A.IV.1** and **A.IV.2**.

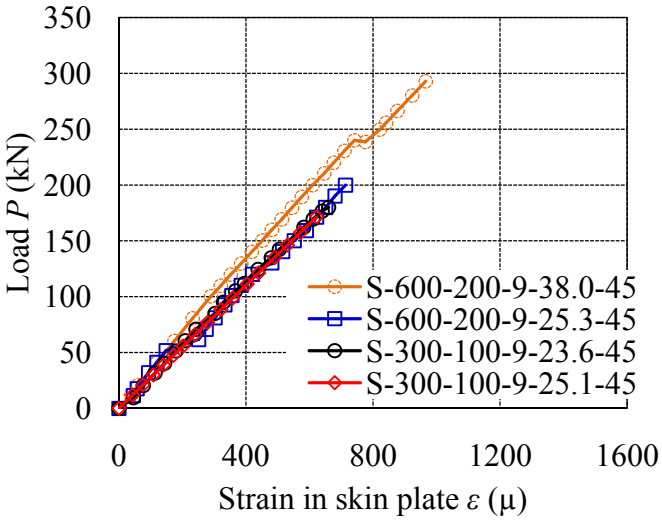

Fig.A.IV.9 Load-strain in skin plate relationship of 1st test series specimens

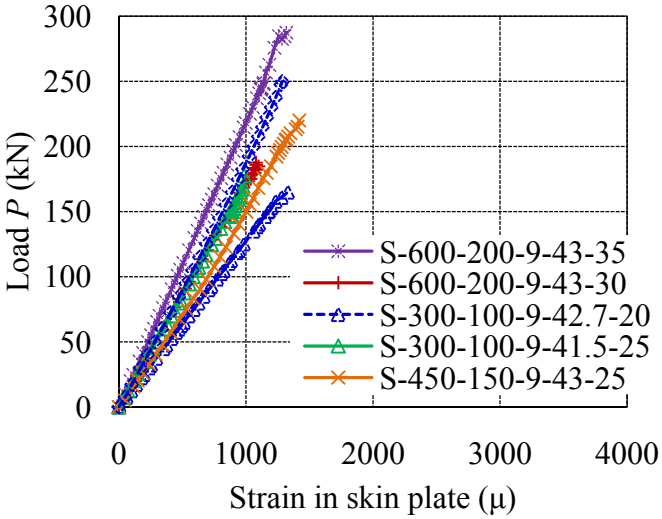

Fig.A.IV.10 Load-strain in skin plate relationship of 2st test series specimens

Table A.IV.1 Load-average strain in steel plate data 1st test series specimens

S-600-200-9-38-45		S-600-200-9-25.3-45		S-300-100-9-23.6-45		S-300-100-9-25.1-45	
Load P (kN)	Strain (μ)	Load P (kN)	Strain (μ)	Load P (kN)	Strain (μ)	Load P (kN)	Strain (μ)
0	0.000	0	0	0	0	0	0
12	37.736	12	45	10	46	12	43
21	61.321	18	58	20	77	21	76
41	118.868	32	93	32	114	30	109
60	175.000	41	120	40	144	39	141
81	232.547	52	149	51	180	48	173
100	290.095	62	251	61	209	56	202
110	321.226	71	275	71	242	66	240
120	352.359	81	303	85	303	77	279
130	385.377	93	334	95	329	88	321
140	418.396	101	356	105	367	99	358
150	451.415	110	385	112	395	111	404
160	482.076	120	421	125	439	121	440
169	513.208	130	481	135	479	135	491
180	544.811	140	516	142	506	146	531
189	575.472	150	552	162	582	157	572
200	609.906	159	590	170	611	172	623
210	646.699	171	622	177	640		
220	676.415	180	651	180	660		
231	710.378	190	680				
240	741.982	200	714				
239	775.944						
250	821.699						
256	841.038						
266	876.887						
280	923.113						
293	966.039						

Table A.IV.2 Load-average strain in steel plate data 2nd test series specimens

S-600-200-9-43-35		S-300-100-9-42.7-20		S-300-100-9-41.5-25	
Load P (kN)	Strain (μ)	Load P (kN)	Strain (μ)	Load P (kN)	Strain (μ)
0	0.764	0	0.000	0	0.00
10	46.618	1	5.240	7	37.50
20	91.707	8	60.264	12	72.64
25	113.869	13	98.257	20	118.16
35	161.250	17	136.249	26	149.06
42	190.291	23	176.862	35	204.01
50	229.266	25	196.513	41	237.50
55	252.957	30	237.126	45	266.75
60	275.883	32	254.158	50	293.16
66	300.338	38	294.771	55	327.59
70	320.208	45	352.415	60	354.72
76	348.484	48	374.686	64	377.12
81	369.118	53	413.989	70	412.50
90	414.207	57	450.672	74	436.79
96	439.427	60	471.633	80	469.34
101	462.353	63	492.595	82	482.78
105	482.985	65	512.246	88	514.62
111	506.679	70	550.238	95	554.48
121	552.530	75	589.541	100	586.56
130	595.329	80	627.534	105	615.57
135	620.545	85	668.146	107	628.54
141	646.530	90	707.449	112	658.02
146	669.458	93	728.411	117	685.85
151	693.147	98	772.954	125	729.25
155	709.961	103	805.705	130	758.73
159	730.592	105	824.045	137	800.71
164	749.702	110	867.280	142	831.37
170	779.506	113	884.316	150	872.41
176	804.726	119	931.479	157	912.97
180	824.592	120	944.578	147	886.79
186	852.869	125	983.876	146	874.29
192	878.089	135	1061.174	150	892.69
197	901.779	139	1088.685	150	892.45
201	921.649	141	1104.408	152	904.01
207	949.161	146	1150.259	155	914.86

215	983.553	150	1177.770	158	927.36
218	999.601	150	1181.699	160	937.27
225	1031.697	153	1202.664	162	945.05
230	1054.625	158	1233.292	165	957.08
237	1085.955	161	1282.154	165	955.19
241	1103.534	165	1331.015	167	966.75
245	1123.405			170	976.18
248	1136.395			178	987.03
245	1122.639				
244	1118.056				
244	1116.525				
249	1140.218				
257	1158.357				
263	1183.917				
276	1225.223				
285	1258.383				
283	1284.219				
285	1304.524				
288	1317.840				

Table A.IV.3 Load-average strain in steel plate data 2nd test series specimens

S-600-200-9-43-30		S-450-150-9-43-25		S-450-150-9-43-30	
Load P (kN)	Strain (μ)	Load P (kN)	Strain (μ)	Load P (kN)	Strain (μ)
0	0.000	0	0	0	0.000
5	33.019	5	46	8	49.764
13	75.000	16	117	17	102.830
25	143.396	20	149	30	171.934
38	215.095	26	190	40	228.066
50	285.378	33	238	50	282.312
65	374.528	41	289	60	339.859
76	434.434	48	342	72	406.840
83	473.113	58	410	85	474.292
91	522.170	68	478	95	527.830
96	552.830	75	533	105	580.896
100	580.189	83	588	115	636.793
107	614.623	90	640	125	690.094
113	653.774	98	689	135	743.632
120	696.699	108	750	145	792.689
129	742.453	115	797	155	843.161
132	759.906	123	844	165	892.453
138	801.415	133	903	175	939.859
143	834.434	140	946	183	975.472
150	876.415	150	1003	192	1025.470
157	914.151	156	1031	200	1063.443
164	955.189	160	1055	208	1099.055
168	981.605	168	1097	215	1131.135
173	1020.754	176	1138	222	1165.565
175	1038.209	180	1163	230	1200.470
180	1069.339	185	1195	238	1234.668
182	1083.018	192	1239	248	1276.418
185	1100.470	195	1254	250	1286.793
188	1080.188	197	1267		
186	1081.605	200	1282		
183	1062.262	202	1298		
183	1069.813	205	1313		
179	1043.395	206	1318		
		208	1334		
		210	1350		
		213	1391		
		215	1406		
		220	1420		

APPENDIX IV.3

Bound link element was the universal joints may be defined in the joint plane between different material elements, such as a RC element and a soil element. By introducing universal joints, the shear slip and gap opening can be considered between two material boundary planes.

Contact stiffness K_n (kN/mm^2/mm) represents the resistance property to gap closure in a normal direction to a joint plane. This value is defined as a property per unit length. A large value for K_n for gap closure is theoretically better and it is set to 10 (kN/mm^2/mm) in basic mode to prevent overlapping. The stiffness is effective for gap closure and would reduce for gap opening, generally it should be set to 0.0 for opening.

Note that the contact closure stiffness never controls the structural behavior. So do not be nervous with this value. However if a large value is entered, there may be a danger of a rounding error or a divergence. If the stiffness can be presumed, for instance in an experimental specimen etc., you can use an optional value in advanced mode.

Shear Stiffness
Universal joints may be defined in the joint plane between different material elements, such as a RC element and a soil element. By introducing universal joints, the shear slip and gap opening can be considered between the two material boundary planes Shear stiffness K_s (kN/mm2/mm) represents the resistance property to slip along the joint plane, this value is defined as a property per unit length. The stiffness is effective when the joint is closed, and it would decrease when the joint is open. Generally it should be set to 0.0 for opening and the value of Ks for closing recommended as 0.1 (kN/mm2/mm) through the numerical verifications in the past in basic mode.

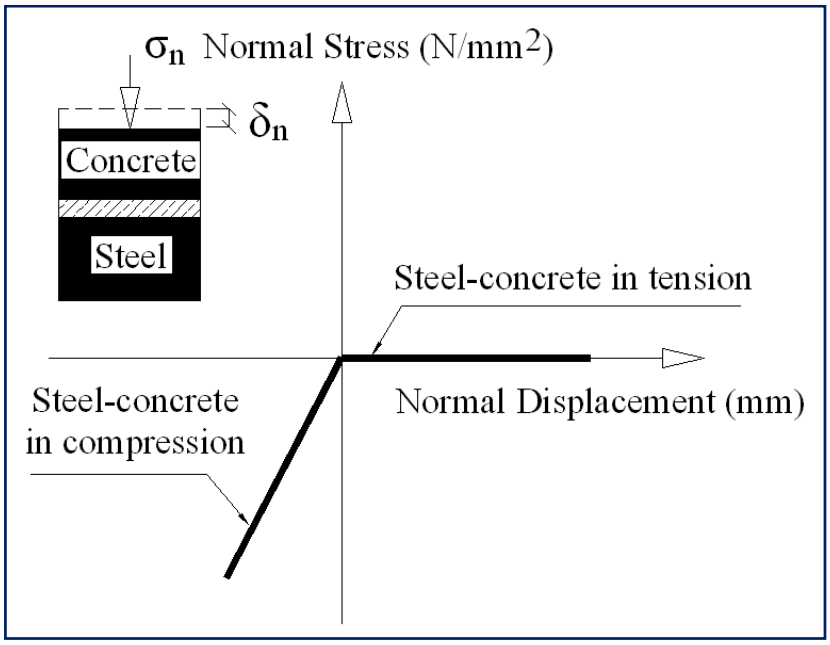

Fig.A.IV.11 Function of bond link element

APPENDIX IV.4

Table. A.IV.4 Shear Force-Slip Data 1st Test Series Specimens

S-600-200-9-38-45		S-600-200-9-25.3-45		S-300-100-9-23.6-45		S-300-100-9-25.1-45	
Shear Force V (kN)	Slip (mm)	Shear Force V (kN)	Slip (mm)	Shear Force V (kN)	Slip (mm)	Shear Force V (kN)	Slip (mm)
0	0.000	0	0.000	0	0.000	0	0
10	0.003	12	0.005	10	0.001	11	0.008
17	0.009	18	0.005	20	0.007	21	0.017
33	0.026	32	0.009	32	0.014	31	0.027
48	0.044	41	0.013	40	0.020	41	0.038
64	0.061	52	0.019	51	0.027	51	0.048
80	0.077	62	0.029	61	0.033	60	0.058
88	0.086	71	0.037	71	0.040	70	0.075
97	0.099	81	0.048	83	0.051	80	0.094
106	0.112	93	0.060	90	0.058	91	0.123
115	0.126	101	0.068	100	0.070	100	0.144
124	0.143	110	0.080	110	0.079	111	0.18
133	0.156	120	0.098	120	0.092	120	0.198
141	0.173	130	0.125	130	0.102	128	0.25
150	0.186	140	0.151	140	0.152	140	0.25
158	0.202	143	0.161	150	0.170	150	0.25
168	0.218	145	0.170	160	0.196	160	0.271
178	0.242	150	0.174	170	0.214	170	0.267
186	0.259	159	0.185	177	0.211		
196	0.280	171	0.192	180	0.206		
204	0.298	179	0.200				
214	0.322	185	0.206				
226	0.351	200	0.212				
232	0.360						
241	0.377						
254	0.399						
266	0.431						

Table A.IV.5 Shear Force-Relative Displacement Data of 1st Test Series Specimens

S-600-200-9-25.3-45		S-300-100-9-25.1-45	
Shear Force V (kN)	Relative Displacement δ (mm)	Shear Force V (kN)	Relative Displacement δ (mm)
0	0.000	0	0
10	-0.065	11	0.003
22	-0.067	20	0.044
31	-0.053	30	0.056
42	-0.045	40	0.064
51	-0.037	51	0.072
62	-0.030	60	0.076
73	-0.024	70	0.082
82	-0.020	80	0.081
92	-0.014	91	0.087
102	-0.011	100	0.085
112	-0.008	111	0.091
122	-0.004	120	0.102
132	-0.003	130	0.598
143	0.001	140	0.789
150	0.005	150	0.987
153	0.012	154	1.252
155	0.342	160	1.423
159	0.713	163	1.507
171	1.241	165	1.601
179	1.631	168	1.716
185	1.885	170	1.88
190	2.263		
192	2.549		
195	2.911		
197	3.232		
200	3.699		

Table A.IV.6 Shear Force-Slip Data 2st Test Series Specimens

S-600-200-9-43-35		S-300-100-9-42.7-20		S-300-100-9-41.5-25	
Shear Force V (kN)	Slip (mm)	Shear Force V (kN)	Slip (mm)	Shear Force V (kN)	Slip (mm)
0	-0.001	0	0.000	0	0.000
13	0.015	1	0.023	10	0.026
25	0.034	16	0.037	20	0.035
31	0.045	27	0.048	33	0.051
44	0.068	37	0.061	41	0.062
52	0.081	48	0.076	56	0.086
63	0.101	54	0.086	65	0.100
69	0.109	65	0.103	73	0.112
75	0.121	69	0.112	81	0.123
82	0.132	80	0.128	90	0.137
87	0.143	96	0.154	98	0.149
95	0.153	102	0.166	104	0.158
101	0.167	113	0.184	114	0.174
113	0.191	123	0.202	120	0.186
120	0.203	129	0.219	129	0.200
126	0.215	134	0.229	133	0.207
132	0.227	140	0.238	142	0.222
138	0.241	150	0.258	153	0.241
151	0.266	161	0.283	162	0.259
162	0.291	171	0.307	170	0.273
169	0.309	182	0.330	173	0.280
176	0.321	193	0.355	181	0.295
183	0.335	199	0.382	189	0.310
189	0.355	211	0.409	201	0.338
194	0.365	220	0.450	209	0.355
199	0.375	225	0.462	221	0.386
204	0.389	237	0.488	229	0.410
213	0.412	241	0.509	240	0.435
219	0.428	254	0.550	251	0.470
225	0.445	258	0.564	244	0.338
233	0.468	268	0.617	241	0.335
239	0.483	289	0.701	246	0.338
246	0.495	297	0.726	246	0.339

251	0.509	301	0.749	249	0.341
259	0.530	314	0.822	252	0.345
268	0.585	321	0.859	255	0.351
273	0.591	322	0.920	258	0.355
281	0.620	328	0.956	260	0.360
288	0.649	329	1.198	264	0.368
296	0.711	333	1.237	263	0.373
301	0.730	336	1.554	266	0.376
306	0.749	341	1.600	269	0.376
310	0.762	350	1.745	272	0.372
306	0.750	357	1.870		
305	0.751	360	1.967		
304	0.751	363	2.035		
311	0.747	362	2.1495		
316	0.797				
323	0.837				
334	0.943				
342	1.061				
350	1.136				
357	1.161				
362	1.167				

Table A.IV.7 Shear Force-Slip Data 2st Test Series Specimens

S-600-200-9-43-30		S-450-150-9-43-25		S-450-150-9-43-30	
Shear Force V (kN)	Slip (mm)	Shear Force V (kN)	Slip (mm)	Shear Force V (kN)	Slip (mm)
0	0.000	0	0.000	0	0.000
9	0.010	13	0.050	14	0.032
21	0.014	32	0.060	28	0.045
39	0.045	41	0.067	47	0.066
59	0.081	52	0.079	63	0.089
79	0.122	66	0.094	78	0.117
103	0.171	80	0.115	94	0.146
120	0.209	94	0.135	112	0.176
130	0.232	113	0.163	131	0.212
144	0.264	132	0.196	145	0.243
152	0.286	147	0.221	160	0.272
160	0.306	162	0.249	175	0.310
169	0.330	176	0.277	190	0.341
180	0.369	190	0.313	205	0.387
192	0.405	207	0.360	218	0.419
204	0.447	219	0.402	232	0.471
209	0.480	232	0.439	246	0.508
221	0.521	249	0.508	259	0.550
230	0.559	260	0.545	269	0.614
241	0.619	276	0.616	282	0.659
252	0.693	284	0.667	293	0.694
263	0.768	291	0.698	303	0.735
270	0.835	302	0.771	312	0.820
281	0.983	314	0.837	321	0.859
286	1.194	320	0.882	331	0.908
294	1.310	329	0.986	340	0.965
298	1.411	341	1.070	352	1.093
303	1.611	345	1.139	354	1.108
297	1.841	349	1.177		
298	2.045	353	1.203		
293	2.212	357	1.260		
295	2.450	362	1.315		
287	2.648	363	1.390		
		367	1.484		
		372	1.585		
		383	1.963		
		387	2.015		
		391	2.080		

Table A.IV.8 Shear Force-Relative Displacement Data 2st Test Series Specimens

S-600-200-9-43-35		S-300-100-9-42.7-20		S-300-100-9-41.5-25	
Shear Force V (kN)	R.D δ (mm)	Shear Force V (kN)	R.D δ (mm)	Shear Force V (kN)	R.D δ (mm)
0	0.000	0	0.000	0	0.000
13	0.081	1	0.008	10	0.041
25	0.221	16	-0.007	20	0.059
31	0.286	27	-0.007	33	0.090
44	0.423	37	0.002	41	0.106
52	0.471	48	0.013	56	0.130
63	0.537	54	0.021	65	0.141
69	0.578	65	0.048	73	0.151
75	0.608	69	0.064	81	0.162
82	0.635	80	0.101	90	0.178
87	0.657	96	0.157	98	0.188
95	0.678	102	0.179	104	0.195
101	0.701	113	0.205	114	0.208
113	0.735	123	0.227	120	0.218
120	0.722	129	0.249	129	0.228
126	0.731	134	0.259	133	0.232
132	0.743	140	0.267	142	0.240
138	0.757	150	0.285	153	0.251
151	0.751	161	0.309	162	0.263
162	0.780	171	0.332	170	0.270
169	0.735	182	0.349	173	0.274
176	0.746	193	0.371	181	0.281
183	0.759	199	0.399	189	0.289
189	0.710	211	0.419	201	0.300
194	0.718	220	0.455	209	0.308
199	0.725	225	0.464	221	0.323
204	0.733	237	0.480	229	0.334
213	0.749	241	0.497	240	0.343
219	0.759	254	0.524	251	0.357
225	0.769	258	0.535	244	0.997
233	0.689	268	0.571	241	1.149
239	0.699	289	0.616	246	1.210
246	0.706	297	0.627	246	1.255

251	0.712	301	0.639	249	1.282
259	0.723	314	0.679	252	1.327
268	0.667	321	0.699	255	1.401
273	0.670	322	0.738	258	1.467
281	0.681	328	0.757	260	1.560
288	0.703	329	1.176	264	1.671
296	0.640	333	1.218	263	1.750
301	0.655	336	1.330	266	1.864
306	0.672	341	1.368	269	1.965
310	0.685	350	1.613	272	2.133
306	1.157	357	1.839		
305	1.346	362	2.007		
304	1.663	363	2.126		
311	1.870				
316	2.004				
323	2.115				
334	2.381				
342	2.724				
350	3.051				
357	3.464				
362	3.847				

Table A.IV.9 Shear Force-Relative Displacement Data (FEM Analyses $\theta = 45^{o}$)

F-300-100-9-25.3		S-450-150-9-25.3		S-600-200-9-25.3	
Shear Force V (kN)	R.D δ (mm)	Shear Force V (kN)	R.D δ (mm)	Shear Force V (kN)	R.D δ (mm)
0	0.000	0	0.001	0	0.000
10	0.022	15	0.052	10	0.002
20	0.046	30	0.081	20	0.004
30	0.070	45	0.125	30	0.006
40	0.096	60	0.178	40	0.007
50	0.124	75	0.241	50	0.009
60	0.153	90	0.314	60	0.010
70	0.189	105	0.415	70	0.047
80	0.233	120	0.612	80	0.112
90	0.305	135	0.860	90	0.153
100	0.417	150	1.160	100	0.180
110	0.573	165	1.780	110	0.209
120	0.780	180	2.210	120	0.253
130	1.037			130	0.333
140	1.237			140	0.493
150	1.444			150	0.756
160	1.618			160	1.570
170	1.785			170	2.120
				180	2.420
				190	3.040
				200	3.400

Table A.IV.10 Shear Force-Relative Displacement Data (FEM Analyses $\theta = 45^{o}$)

S-600-200-9-30		F-600-200-9-38		F-300-100-4.5-25.3	
Shear Force V (kN)	R.D δ (mm)	Shear Force V (kN)	R.D δ (mm)	Shear Force V (kN)	R.D δ (mm)
0	0.001	0	0.000	0	0.000
15	0.048	18	0.054	10	0.037
29	0.096	35	0.118	20	0.075
44	0.132	53	0.156	30	0.114
58	0.179	70	0.223	40	0.157
73	0.232	88	0.288	50	0.209
87	0.302	105	0.359	60	0.278
102	0.369	123	0.444	70	0.417
116	0.466	140	0.572	80	0.603
131	0.605	158	0.759	90	0.862
145	0.793	175	1.090	100	1.210
160	1.070	193	1.380	110	1.530
174	1.360	210	1.750		
189	1.810	228	2.200		
203	2.100	245	2.820		
218	2.630	263	3.270		
232	3.130				

Table A.IV.10 Shear Force-Relative Displacement Data (FEM Analyses $\theta = 45^{o}$)

F-600-200-7-25.3		F-600-200-4.5-25.3		F-900-300-13.5-25.3	
Shear Force V (kN)	R.D δ (mm)	Shear Force V (kN)	R.D δ (mm)	Shear Force V (kN)	R.D δ (mm)
0	0.001	0	0.001	0	0.000
15	0.053	11	0.047	16	0.034
30	0.114	22	0.095	32	0.072
45	0.174	33	0.144	48	0.109
60	0.246	44	0.199	64	0.150
75	0.332	55	0.261	80	0.190
90	0.449	66	0.331	96	0.233
105	0.659	77	0.422	112	0.270
120	0.986	88	0.583	128	0.332
135	1.430	99	0.858	144	0.374
150	1.970	110	1.250	160	0.481
165	2.580	121	1.710	176	0.569
180	3.450	132	2.260	192	0.834
		143	3.090	208	0.982
				224	1.380
				240	1.730
				256	2.490
				272	2.910
				288	3.900
				304	4.380

Table A.IV.11 Shear Force-Relative Displacement Data (FEM Analyses $\theta = 45^{o}$)

F-450-150-5-30		F-600-200-5-30		F-300-100-5-30	
Shear Force V (kN)	R.D δ (mm)	Shear Force V (kN)	R.D δ (mm)	Shear Force V (kN)	R.D δ (mm)
0	0.000	0	0.001	0	0.000
5	0.016	5	0.019	5	0.014
10	0.033	10	0.037	10	0.026
16	0.050	16	0.055	16	0.039
21	0.067	21	0.073	21	0.053
26	0.084	26	0.091	26	0.067
31	0.101	31	0.110	31	0.081
36	0.119	36	0.128	36	0.096
42	0.137	42	0.148	42	0.112
47	0.156	47	0.168	47	0.130
52	0.176	52	0.190	52	0.150
57	0.196	57	0.213	57	0.172
62	0.219	62	0.237	62	0.199
68	0.244	68	0.262	68	0.235
73	0.273	73	0.292	73	0.285
78	0.306	78	0.319	78	0.352
83	0.342	83	0.348	83	0.456
88	0.394	88	0.380	88	0.579
94	0.473	94	0.416	94	0.747
99	0.580	99	0.462	99	0.912
104	0.703	104	0.5411	104	1.090
109	0.888	109	0.6684	109	1.260
114	1.080	114	0.8204	114	1.430
120	1.280	120	0.9834	120	1.640
125	1.530	125	1.1614		
130	1.750	130	1.424		
135	2.000	135	1.467		
140	2.340	140	1.673		
		146	1.882		
		151	2.096		
		156	2.725		
		161	3.163		

Table A.IV.12 Shear Force-Relative Displacement Data (FEM Analyses $\theta = 45^{o}$)

F-900-300-9-25.3		F-1200-400-9-30		F-750-250-9-30	
Shear Force V (kN)	R.D δ (mm)	Shear Force V (kN)	R.D δ (mm)	Shear Force V (kN)	R.D δ (mm)
0	0.000	0	0.000	0	0.000
15	0.047	16	0.059	10	0.001
31	0.091	31	0.090	20	0.030
46	0.138	47	0.121	30	0.047
62	0.189	63	0.154	40	0.071
77	0.243	79	0.188	50	0.095
92	0.301	94	0.226	60	0.120
108	0.369	110	0.258	70	0.146
123	0.487	126	0.304	80	0.173
139	0.667	141	0.347	90	0.201
154	1.050	157	0.418	100	0.232
169	1.420	173	0.490	110	0.275
185	1.880	188	0.600	120	0.316
200	2.670	204	0.776	130	0.372
216	3.440	220	1.130	140	0.432
231	4.200	236	1.610	150	0.513
		251	2.270	160	0.691
		267	2.960	170	0.926
		283	4.000	180	1.170
		298	5.200	190	1.440
				200	1.770
				210	2.130
				220	2.600
				230	3.200
				240	3.700

Table A.IV.10 Shear Force-Relative Displacement Data (FEM Analyses $\theta = 45^{o}$)

S-600-200-9-30		F-600-200-9-38		F-300-100-4.5-25.3	
Shear Force V (kN)	R.D δ (mm)	Shear Force V (kN)	R.D δ (mm)	Shear Force V (kN)	R.D δ (mm)
0	0.001	0	0.000	0	0.000
15	0.048	18	0.054	10	0.037
29	0.096	35	0.118	20	0.075
44	0.132	53	0.156	30	0.114
58	0.179	70	0.223	40	0.157
73	0.232	88	0.288	50	0.209
87	0.302	105	0.359	60	0.278
102	0.369	123	0.444	70	0.417
116	0.466	140	0.572	80	0.603
131	0.605	158	0.759	90	0.862
145	0.793	175	1.090	100	1.210
160	1.070	193	1.380	110	1.530
174	1.360	210	1.750		
189	1.810	228	2.200		
203	2.100	245	2.820		
218	2.630	263	3.270		
232	3.130				

Table A.IV.10 Shear Force-Relative Displacement Data (FEM Analyses $\theta = 45^{o}$)

F-600-200-7-25.3		F-600-200-4.5-25.3		F-900-300-13.5-25.3	
Shear Force V (kN)	R.D δ (mm)	Shear Force V (kN)	R.D δ (mm)	Shear Force V (kN)	R.D δ (mm)
0	0.001	0	0.001	0	0.000
15	0.053	11	0.047	16	0.034
30	0.114	22	0.095	32	0.072
45	0.174	33	0.144	48	0.109
60	0.246	44	0.199	64	0.150
75	0.332	55	0.261	80	0.190
90	0.449	66	0.331	96	0.233
105	0.659	77	0.422	112	0.270
120	0.986	88	0.583	128	0.332
135	1.430	99	0.858	144	0.374
150	1.970	110	1.250	160	0.481
165	2.580	121	1.710	176	0.569
180	3.450	132	2.260	192	0.834
		143	3.090	208	0.982
				224	1.380
				240	1.730
				256	2.490
				272	2.910
				288	3.900
				304	4.380

Table A.IV.11 Shear Force-Relative Displacement Data (FEM Analyses $\theta = 45^{o}$)

F-450-150-5-30		F-600-200-5-30		F-300-100-5-30	
Shear Force V (kN)	R.D δ (mm)	Shear Force V (kN)	R.D δ (mm)	Shear Force V (kN)	R.D δ (mm)
0	0.000	0	0.001	0	0.000
5	0.016	5	0.019	5	0.014
10	0.033	10	0.037	10	0.026
16	0.050	16	0.055	16	0.039
21	0.067	21	0.073	21	0.053
26	0.084	26	0.091	26	0.067
31	0.101	31	0.110	31	0.081
36	0.119	36	0.128	36	0.096
42	0.137	42	0.148	42	0.112
47	0.156	47	0.168	47	0.130
52	0.176	52	0.190	52	0.150
57	0.196	57	0.213	57	0.172
62	0.219	62	0.237	62	0.199
68	0.244	68	0.262	68	0.235
73	0.273	73	0.292	73	0.285
78	0.306	78	0.319	78	0.352
83	0.342	83	0.348	83	0.456
88	0.394	88	0.380	88	0.579
94	0.473	94	0.416	94	0.747
99	0.580	99	0.462	99	0.912
104	0.703	104	0.5411	104	1.090
109	0.888	109	0.6684	109	1.260
114	1.080	114	0.8204	114	1.430
120	1.280	120	0.9834	120	1.640
125	1.530	125	1.1614		
130	1.750	130	1.424		
135	2.000	135	1.467		
140	2.340	140	1.673		
		146	1.882		
		151	2.096		
		156	2.725		
		161	3.163		

Table A.IV.12 Shear Force-Relative Displacement Data (FEM Analyses $\theta = 45^{o}$)

F-900-300-9-25.3		F-1200-400-9-30		F-750-250-9-30	
Shear Force V (kN)	R.D δ (mm)	Shear Force V (kN)	R.D δ (mm)	Shear Force V (kN)	R.D δ (mm)
0	0.000	0	0.000	0	0.000
15	0.047	16	0.059	10	0.001
31	0.091	31	0.090	20	0.030
46	0.138	47	0.121	30	0.047
62	0.189	63	0.154	40	0.071
77	0.243	79	0.188	50	0.095
92	0.301	94	0.226	60	0.120
108	0.369	110	0.258	70	0.146
123	0.487	126	0.304	80	0.173
139	0.667	141	0.347	90	0.201
154	1.050	157	0.418	100	0.232
169	1.420	173	0.490	110	0.275
185	1.880	188	0.600	120	0.316
200	2.670	204	0.776	130	0.372
216	3.440	220	1.130	140	0.432
231	4.200	236	1.610	150	0.513
		251	2.270	160	0.691
		267	2.960	170	0.926
		283	4.000	180	1.170
		298	5.200	190	1.440
				200	1.770
				210	2.130
				220	2.600
				230	3.200
				240	3.700